UBR5-mediated degradation of splicing and gene expression factors in normal and malignant states

Dissertation

Zur Erlangung des Grades

“Doktor der Naturwissenschaften”

(Dr. rer. nat.)

am Fachbereich Biologie

der Johannes-Gutenberg-Universität Mainz

Ekaterina Isaakova

Geboren am 11.09.1995 in Woronesch, Russland

Mainz, Oktober 2025

Dekan: Prof. Dr. Eckhard Thines

1. Berichterstatter: Retracted

2. Berichterstatter: Retracted

Tag der mündlichen Prüfung: 26.02.2026

Declaration of authorship

I, Ekaterina Isaakova, hereby declare that the work presented in this dissertation is my own original work. All sources of information and literature used have been properly cited. I gratefully acknowledge the following specific contributions: support for experimental design by my supervisor, retracted; Western blot experiments for Figure 16A performed by retracted; Western blot experiments for Figures 17E and 18D,E performed by retracted; EU-incorporation assay conducted by retracted; and generation and characterization of the AQR-APEX2-3×FLAG cell line by former Master's student retracted. The AQR endogenous proximity proteomics and the DIA-MS total proteome experiment were performed by retracted, and data analysis of the mRNA-seq dataset was carried out by retracted (Bioinformatics Core Facility, IMB). While some mass spectrometry experiments were conducted by colleagues, all MS data presented in this thesis were analyzed by me. I also gratefully acknowledge the technical support provided by the IMB core facilities especially retracted for producing OtUBD probe.

Abstract

Nuclear processes constitute the foundation of cellular function, orchestrated by macromolecular assemblies such as the transcriptional and splicing machineries as well as epigenetic regulatory complexes. However, fluctuations in gene expression and translation caused by endogenous or exogenous sources, such as genotoxic and proteotoxic stress, threaten cellular homeostasis if not efficiently cleared. Therefore, nuclear protein quality control is essential for preserving genomic stability by facilitating the recognition and degradation of aberrant or misfolded proteins within the nucleus.

UBR5 is an E3 ubiquitin ligase that has emerged as a systems-level regulator of nuclear protein homeostasis, coordinating orphan protein quality control. We systematically investigate the impact of UBR5 loss in malignant and non-malignant cellular contexts to identify conserved and context-specific UBR5-dependent quality control mechanisms. By integrating global proteomic and ubiquitylomic analyses, we demonstrate that UBR5 governs interconnected nuclear processes, including chromatin remodeling, transcriptional regulation, cell-cycle progression, and RNA metabolism. While UBR5 directly targets individual subunits, its predominant effect emerges at the level of multiprotein assemblies, where loss of UBR5 disrupts stoichiometric balance and induces coordinated protein-level shifts.

We identify the intron-binding complex as the most prominent target of conserved UBR5 quality control regulation. Specifically, we show that AQR, a central scaffold subunit required for intron-binding complex formation, is a direct substrate of UBR5. Together with TRIP12, UBR5 governs AQR turnover and secures correct complex recycling.

In summary, these findings advance our understanding of UBR5 as a central regulator of nuclear protein homeostasis in cancer and beyond, with direct involvement in quality control of the pre-mRNA splicing machinery through regulation of AQR.

Zusammenfassung

Nukleäre Prozesse bilden die Grundlage der Zellfunktion und werden durch makromolekulare Komplexe wie Transkriptions- und Spleißmaschinen sowie epigenetische Regulationskomplexe gesteuert. Schwankungen in Genexpression und Translation, hervorgerufen durch endogene oder exogene Ursachen wie genotoxischen und proteotoxischen Stress, gefährden jedoch die zelluläre Homöostase, wenn sie nicht effizient beseitigt werden. Daher ist die Qualitätskontrolle nukleärer Proteine entscheidend für die Aufrechterhaltung der genomischen Stabilität, da durch diese fehlgefalteten Proteine im Zellkern erkannt und abbaut werden.

UBR5 ist eine E3-Ubiquitin-Ligase, die als Regulator der nukleären Proteinhomöostase die Qualitätskontrolle von Orphan-Proteinen koordiniert. Wir untersuchen die Auswirkungen des Verlusts von UBR5 in malignen und nicht-malignen Kontexten, um konservierte und kontextspezifische UBR5-abhängige Mechanismen zu identifizieren. Durch globale Proteom- und Ubiquitylom-Analysen zeigen wir, dass UBR5 zentrale nukleäre Prozesse steuert, darunter Chromatin-Remodellierung, Transkriptionsregulation, Zellzyklusprogression und RNA-Stoffwechsel. Während UBR5 spezifische Untereinheiten einzelner Komplexe direkt adressiert, entfaltet sich seine Hauptwirkung bei der Zusammensetzung von Proteinkomplexen, wobei der Verlust von UBR5 das stöchiometrische Gleichgewicht stört und Veränderungen der Proteinlevel hervorruft.

Wir identifizieren den Intron-bindenden Komplex als wichtigstes Ziel der konservierten UBR5-Qualitätskontrolle und zeigen, dass AQR, eine zentrales Gerüstprotein, ein direktes Substrat von UBR5 ist. Zusammen mit TRIP12 reguliert UBR5 den Abbau von AQR und gewährleistet das Recycling des Komplexes.

Diese Ergebnisse erweitern das Verständnis von UBR5 als zentralen Regulator der nukleären Proteinhomöostase in Krebs und darüber hinaus, mit direkter Beteiligung an der Qualitätskontrolle des Spleißens von prä-mRNA durch Regulation von AQR.

Contents

1. Introduction

1.1 Ubiquitin-proteasome system: central arbiter of proteostasis

1.1.1 Ubiquitin modification

Ubiquitylation is a posttranslational modification (PTM) that is critical for maintaining cellular homeostasis. It is a tightly regulated process that revolves around ubiquitin (Ub), a highly conserved 76-amino-acid protein of approximately 8.5 kDa, that is present across eukaryotes — from yeast to humans [1] . Once believed to modify only lysine residues, multiple studies show that ubiquitylation can also occur on serine, threonine, cysteine, and even the protein N-terminus, broadening the spectrum of regulatory sites on the substrates [2], [3], [4], [5]. Ubiquitin itself has seven internal lysines (K6, K11, K27, K29, K33, K48 and K63) (Fig. 1A), which enable the formation of not only monoubiquitylation or multi-monoubiquitylation of the substrate, but also the formation of ubiquitin chains [6], [7]. All of these seven lysines and alternatively the amino terminal methionine (M1) are used by the cell for ubiquitin chain formation with varying length, topology, and linkages explored in detail in the next chapter [6], [7], [8], [9].

In addition to ubiquitin itself, a broader family of modifiers known as ubiquitin-like proteins (UBLs) [10]. The most studied examples of UBLs include NEDD8 (Neural precursor cell Expressed, Developmentally Down-regulated protein 8), SUMO1/2/3 (Small Ubiquitin-like Modifier) and ISG15 (Interferon-Stimulated Gene 15) [10], [11], [12], [13]. UBLs expand the regulatory potential of post-translational modifications by regulation of distinct substrates and/or target PTM sites on the substrates as well as by cross-talk with other post-translational modifications and ubiquitin itself [14], [15]. While structurally similar to ubiquitin, these proteins often differ in their amino acid sequences (e.g. SUMO). This structural similarity underlies a conserved conjugation paralleling that of the ubiquitin system [10], [16].

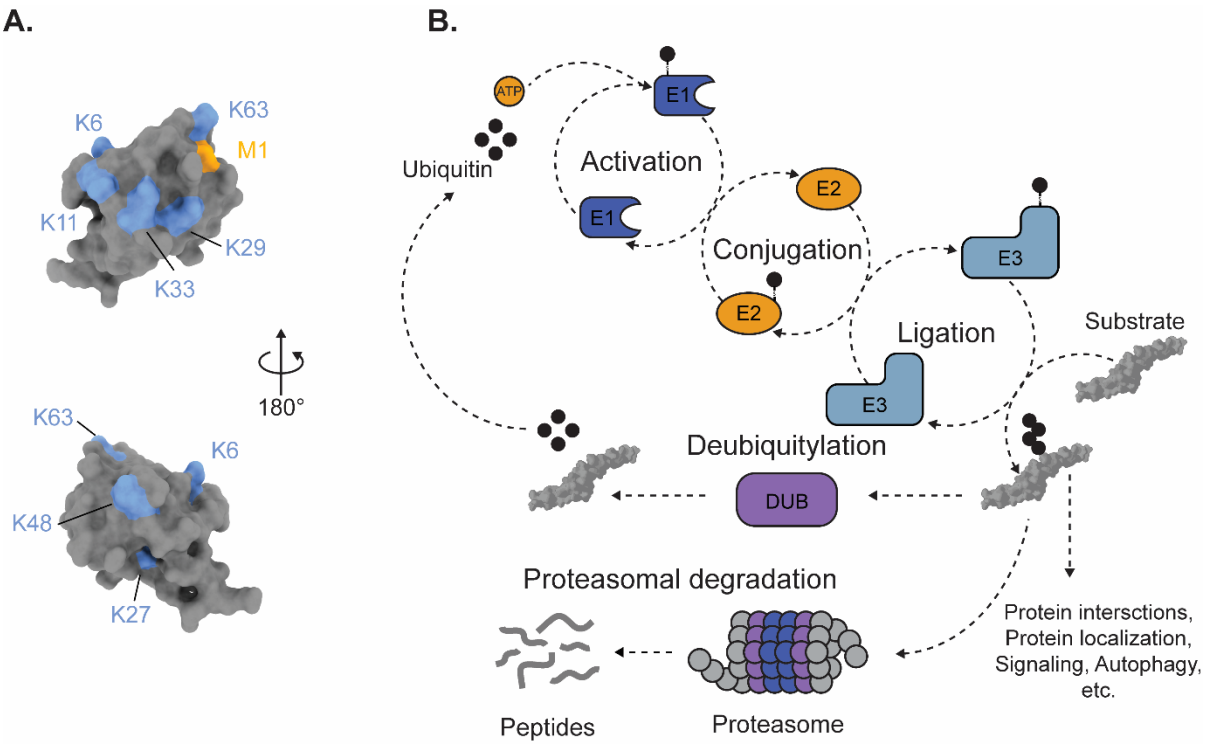

Figure 1 Ubiquitin signalling in cell.
A. Surface representation of the ubiquitin molecule. Acceptor sites for polyubiquitin chain assembly are highlighted: seven lysine residues (K6, K11, K27, K29, K33, K48, K63) in blue, and the N-terminal methionine (M1) in orange. **B** Enzymatic cascade of ubiquitin conjugation and substrate processing. Ubiquitin is first activated by an E1 enzyme in an ATP-dependent manner, transferred to an E2 conjugating enzyme, and subsequently ligated to substrates by E3 ligases. Ubiquitin chains serve as molecular signals that can direct proteasomal degradation, alter subcellular localization, regulate signaling pathways, or trigger autophagy. Conversely, deubiquitinases (DUBs) can edit or remove ubiquitin chains to modulate these outcomes.

1.1.2 Enzymatic cascade of ubiquitin conjugation

Ubiquitin conjugation is carried out through the sequential action of three enzyme classes: ubiquitin-activating enzymes (E1), ubiquitin-conjugating enzymes (E2), and ubiquitin ligases (E3) (Fig. 1B). In the canonical ubiquitin pathway in humans, the process begins with one of two E1 enzymes, which use ATP to form a high-energy thioester bond with ubiquitin [17], [18]. Subsequently, activated ubiquitin is transferred to one of approximately 40 E2s, setting the stage for further downstream modifications and substrate-specific ubiquitylation by over 600 ubiquitin ligases. E3 ligases are structurally diverse, ensuring precise substrate recognition and specificity [17]. Based on their E2-binding domains and mechanisms of

ubiquitin transfer, E3 ligases are classified into three major categories: HECT, RING, and RING-between-RING (RBR) [19], [20], [21].

Homologous to E6AP C-terminus or for short HECT-type E3 ligases are characterized by the presence of a conserved homologous to E6-AP carboxyl terminus (HECT) domain. This domain contains a catalytic cysteine residue that forms a thiol-based intermediate with ubiquitin, facilitating its transfer to a lysine residue on the substrate protein (Fig. 2A) [19]. Based on the content of their N-terminal domains, HECT E3 ligases are classified into three families: the Nedd4 family (9 members in humans), the HERC family (6 members in humans), and the Other HECTs (13 members in humans).

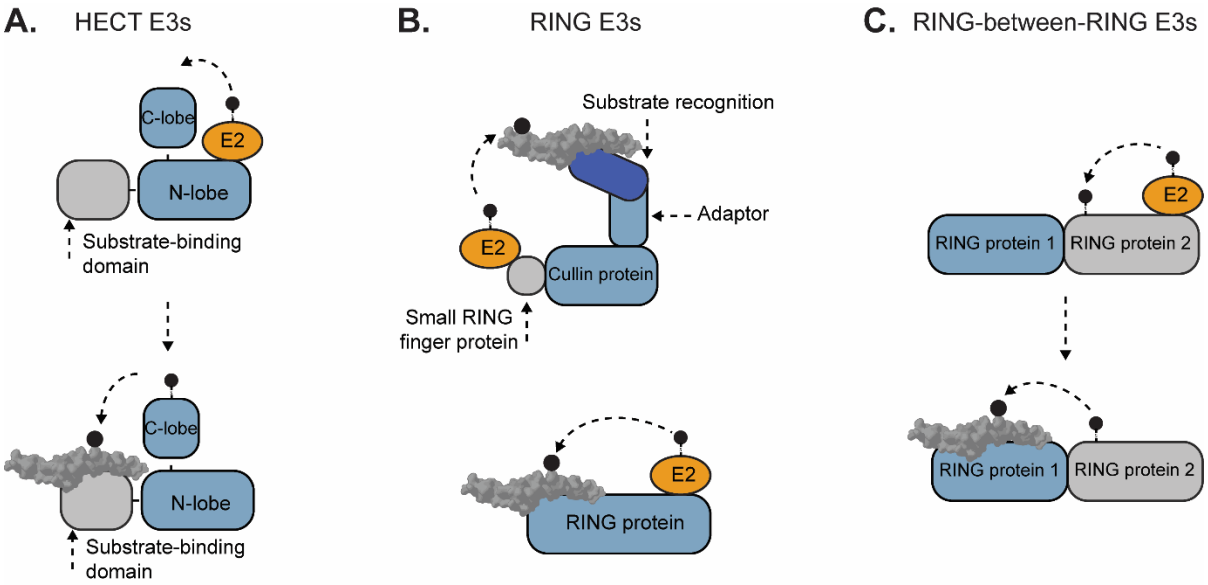

Figure 2 Major categories of E3 ligases.
A. HECT-type E3 ligases. The C-terminal HECT domain mediates a two-step ubiquitylation reaction: first, ubiquitin is transferred to the C-lobe of the catalytic domain, and then to the substrate. Substrate specificity is determined by additional protein-binding domains. **B.** RING-type E3 ligases. The E2 enzyme forms a complex with the E3 ligase and transfers ubiquitin directly to the substrate. Substrate specificity is determined either by intrinsic protein-binding domains or, alternatively, through substrate adaptors, as in the case of cullin–RING ligases (upper panel). **C.** RING-between-RING (RBR) E3 ligases. These ligases combine features of RING- and HECT-type mechanisms. A RING domain first recruits the ubiquitin-charged E2, after which ubiquitin is transferred to a catalytic cysteine in the RING2 domain and then onto the substrate. Substrate specificity is mediated by accessory protein-binding domains.

Members of the Nedd4 family possess WW domains and a C2 domain . The WW domains recognize short Pro-rich motifs of target proteins (PPxY or LPxY, where x denotes any amino acid) [22], while the N-terminal C2 domain binds membrane phospholipids in a calcium-dependent manner and mediates translocation of Nedd4-2 to the membrane [23]. These domains not only determine substrate specificity but also contribute to E3 ligase autoinhibition, which prevents autoubiquitylation and excessive ubiquitylation of substrates, as observed for WWP1, WWP2, and Itch [24].

The HERC family of HECT E3 ligases is defined by the presence of one or more regulator of chromosome condensation 1 (RCC1)-like domains [25]. Based on the number of these domains, HERCs are further subdivided into two large and four small HERC proteins. Despite their structural similarities, members of this family carry out distinct biological functions. For instance, the small HERC proteins HERC5 and HERC6 have been shown to act as E3 ligases not only for ubiquitin but also for the ubiquitin-like modifier ISG15 [26], [27].

In contrast to the Nedd4 and HERC families, the Other HECT E3 ligases lack conserved structural characteristics and instead contain a variety of protein–protein interaction domains, allowing them to influence a wide spectrum of cellular processes. For example, TRIP12 contains a variety of domains that allow it to interact with chromatin via its N-terminal chromatin-binding domain, while its WWE and ARM (Armadillo repeat) domains mediate protein-protein interactions [28]. Interestingly, the WWE domain of TRIP12 interacts with PARP1 in response to genotoxic stress [29]. Other notable members of Other HECTs group include HUWE1 and UBR5, which contain a UBA domain that binds to ubiquitin moieties on target proteins [30]. This interaction influences the efficiency, localization, or processivity of ubiquitylation, thereby affecting the fate of preubiquitylated substrates.

RING E3 ligases are a major class of E3 ligases, comprising approximately 600 members, and are defined by their RING domain. Unlike HECT-type E3 ligases, members of the RING family do not form an intermediate thioester bond with ubiquitin. Instead, they act as a scaffold that facilitates direct transfer of ubiquitin from the E2~Ub conjugate to the

substrate (Fig. 2B) [20]. Ubiquitylation catalysis arises from induced proximity of E2~Ub and substrate instead of covalent intermediate with Ub. These ligases can function as monomeric, dimeric, or large multi-subunit complexes [20].

The largest class of the RING family memers are the cullin-RING ligases (CRLs), a highly diverse group of ubiquitin ligases that share several common structural features [20]. A typical CRL complex consists of a cullin scaffold, with the RING-box protein (RBX) at the C-terminus, an adaptor protein, and a substrate receptor (SR) at the N-terminus [31]. The functional diversity of CRLs arises from the ability of the CUL–RBX module to interact with a wide range of protein partners—substrate-bound SRs and E2 enzymes carrying ubiquitin—with varying specificities.

A key step in CRL activation is the conjugation of the ubiquitin-like protein NEDD8. NEDD8 modification induces a conformational shift to an open, active state, enabling efficient substrate ubiquitylation [32]. NEDD8 serves as a structural nexus, linking different elements of the cullin scaffold to the RING-bound, ubiquitin-charged E2 enzyme (e.g., UBE2D) [33]. This modification facilitates both local remodeling of the NEDD8 site and large-scale rearrangements of CRL domains, thereby positioning the substrate in close proximity to the catalytic site and promoting ubiquitylation.

RING-between-RING (RBR) is a relatively recently discovered class of E3 ubiquitin ligases, comprising 14 members in humans [21]. These ligases are structurally characterized by the following domain structure: a RING1 domain, central in-between-RINGs (IBR), and a RING2 domain. The RING1 domain is responsible for recruiting the E2~Ub conjugate, while the RING2 domain contains a catalytic cysteine residue (Fig. 2C). Similar to HECT-type E3 ligases, RBR ligases mediate ubiquitination through a two-step reaction: ubiquitin is first transferred from the E2 enzyme to the catalytic cysteine of the RING2 domain, and subsequently to the substrate protein [21].

1.1.3 Deubiquitylating enzymes

Like other post-translational modifications (PTMs), ubiquitylation is reversible and can be removed by deubiquitylating enzymes (DUBs) (Fig. 1B). Based on sequence and structural similarities, DUBs are classified into seven families: Ubiquitin-specific proteases (USPs), Ubiquitin C-terminal hydrolases (UCHs), Machado–Joseph disease protein domain proteases (MJDs), Ovarian tumor proteases (OTUs), JAMM/MPN+ metalloproteases, Motif-interacting with ubiquitin-containing novel DUBs (MINDYs), and Zinc finger–containing ubiquitin peptidase 1 (ZUFSP) [34]. Six of these families are cysteine proteases, while the JAMM family belongs to the zinc-dependent metalloproteases and requires a zinc ion for catalytic activity.

DUBs generally operate via two modes of recognition: they either recognize a specific ubiquitin signal (such as chain type) in a target-agnostic manner, or they recognize specific target proteins independently of the ubiquitin signal [34]. This dual mode of recognition enables approximately 100 specialized DUBs in humans to effectively counteract the broad and complex ubiquitylation machinery, thereby ensuring balanced regulation of substrate fate.

1.1.4 Ubiquitin readers and functional consequences of ubiquitylation

The diverse array of ubiquitin signatures is recognized by specific cellular proteins, that mediate PTM functional outcomes. This recognition is carried out by specialized ubiquitin readers—proteins that contain dedicated ubiquitin-binding domains (UBDs) [35], [36]. Ultimately, ubiquitin readers determine the fate of the tagged proteins in the cell — from protein turnover to participation in signaling cascades (Fig. 1B).

Perhaps the most extensively studied function of ubiquitin is its role as a signal for proteasomal degradation [35], [36], [37]. The 26S proteasome is an ATP-dependent protease (ATPase) that maintains protein homeostasis (proteostasis) by selectively removing damaged, misfolded, or regulatory proteins [37]. It consists of two major subcomplexes: the 20S core particle and the 19S regulatory particle. The regulatory particle functions as an ATPase motor, engaging substrates through ubiquitin receptor subunits Rpn1, Rpn10, and Rpn13, unfolding

them via ATP hydrolysis, and translocating them into the core particle—a barrel-shaped complex that houses the proteolytic degradation chamber. This process is a central component of the ubiquitin-proteasome system (UPS), which is responsible for the rapid degradation of ubiquitin-tagged proteins, enabling timely responses to changes in the dynamic cellular environment, such as during cell cycle progression, genotoxic stress or immune response.

Another important role of ubiquitin in proteolysis is the regulation of lysosomal degradation pathways, such as autophagy [38], [39]. Ubiquitin marks certain proteins — including protein aggregates or invading bacteria — as cargo for autophagy [40]. These marked proteins are then recruited to autophagosomes by selective autophagy receptors such as p62/SQSTM1 and NBR1 [38], [39], [41]. Additionally ubiquitin ligase Parkin is involve in regulation of mitophagy (Autophagic Degradation of Damaged Mitochondria) [42]. It ubiquitinates multiple proteins on mitochondrial outer membrane allowing autophagy receptor recruitment.

In addition to 26S proteasome, VCP/p97 another important ATPase ubiquitin reader involved in proteostasis. VCP/p97 is a hexameric AAA+ ATPase that uses ATP hydrolysis energy to structurally remodels substrates either directly or via adaptor proteins containing ubiquitin-binding domains (UBDs), such as UFD1 and NPL4 [43], [44], [45], [46]. VCP is crucial for unfolding proteins and extracting them from the protein complexes, a necessary step for subsequent proteolysisc for a number of substrates. This function is particularly important in processes such as endoplasmic reticulum-associated degradation (ERAD) and the regulation of stress granule dynamics [43], [47], [48]. By adding a regulatory pre-processing step, VCP serves as a key mediator in maintaining cellular protein homeostasis.

Beyond proteolysis, ubiquitylation also plays key roles in signaling processes. For example, 53BP1 and RNF168 are involved in recognizing ubiquitylated histones at sites of DNA double-strand breaks [49], [50], [51]. In addition, ubiquitin can function as a scaffold for assembling signaling complexes, such as those required for activation of the transcription factor NF-κB, which is central to inflammatory and immune responses [52].

In summary, ubiquitylation is one of the central post-translational modifications governing cellular proteostasis. It is regulated by a tightly coordinated network of ubiquitin writers, readers, and erasers. Understanding this regulatory network is a key objective in proteostasis research. However, it is the specific topology of the ubiquitin modification that ultimately determines the fate of the tagged protein, whether it undergoes degradation, experiences altered activity, changes localization, or engages in signaling processes. Grasping the linkage-specific functions of distinct ubiquitin architectures is therefore essential for deciphering how the ubiquitin system orchestrates cellular signaling pathways and drives large-scale remodeling of the proteome. This knowledge forms the foundation for understanding the regulatory logic and physiological consequences of ubiquitin-mediated cellular control.

1.2 Ubiquitin code decryption: from topology to fate

1.2.1 Monoubiquitylation

Monoubiquitylation is the most prevalent form of ubiquitylation in human cells. A 2011 study revealed that approximately 65% of the cellular ubiquitin pool exists in a monomeric form [53]. Notably, this monomeric form remains dominant even after proteasome inhibition. Monoubiquitylation is critical for mediating interaction networks. Monoubiquitin can facilitate binding via ubiquitin-binding domains, as seen in the interaction between polη and PCNA, or by inducing conformational changes in the substrate, as in the case of FANCI and FANCD2 interactions with DNA [54], [55]. However, ubiquitin-induced structural changes may also inhibit complex formation such as in case SMAD4 affecting its ability for R-SMAD (SMAD1/2/3/5)–SMAD4 complex assembly [56].

Monoubiquitylation-controlled interactions are often stimulus-dependent as in the examples mentioned above. Monoubiquitylation of PCNA is essential for the recruitment of polη to the replication fork, enabling translesion DNA synthesis in response to DNA damage, such as UV-induced cyclobutane pyrimidine dimers [54]. Likewise, allosteric changes induced by monoubiquitilation of FANCI-FANCD2 transform complex into a scaffold of the DNA

repair machinery at the site of DNA-crosslinkinks [55]. In case of SMAD4 monoubiquitylation is facilitated upon TGF-β stimulation that prevents both proteins from forming DNA-binding complexes, thus, providing feedback to terminate TGF-β signaling [56].

Monoubiquitylation is particularly abundant on histones and plays a crucial role in regulating the epigenetic landscape. Histone monoubiquitylation is essential for both gene repression and activation. For instance, monoubiquitylation of histone H2A inhibits methylation of histone H3 at lysine 4 (H3K4), a marker of active transcription, through the action of ubiquitin ligases associated with transcriptional repressor complexes, such as BRCA1 (in the BRCA1–BARD1 complex) or RNF2 (in the polycomb repressive complex 1, PRC1) [57], [58]. In contrast, monoubiquitylation of histone H2B by RNF20 and RNF40 in mammals is required for H3K4 methylation, making it a marker of transcriptional activation[59]. Beyond histones, monoubiquitylation also regulates transcriptional activation via the TET family of dioxygenases. Monoubiquitylation of TET proteins enhances their association with chromatin, which is necessary for the demethylation of 5-methylcytosine—an epigenetic mark associated with gene silencing [60].

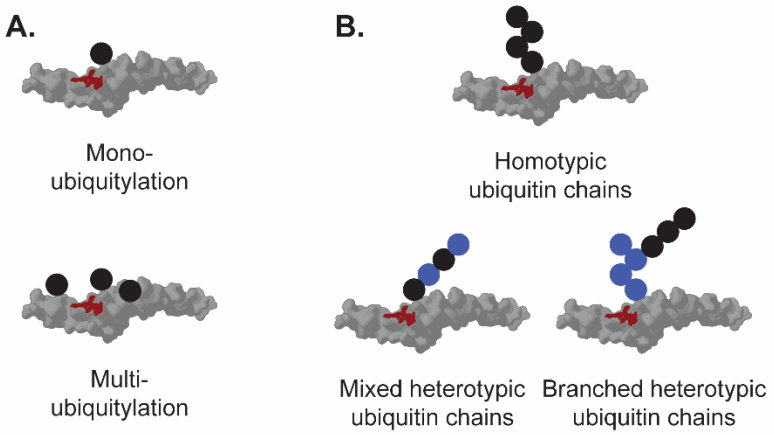

Figure 3. Schematic representation of diverse ubiquitin modifications within 'ubiquitin code'.
A. Mono- and multi-monoubiquitylation**. B.** Polyubiquitylation, with distinct ubiquitin linkages indicated by different colors. Polyubiquitin chains can be homotypic (built through a single linkage type), heterotypic (containing multiple linkage types), or branched (a ubiquitin modified at two or more sites within a heterotypic chain).

1.2.2 Polyubiquitylation

Monoubiquitination and multi-monoubiquitination realize a broad regulatory potential of ubiquitylated substrates. Importantly, they serve as priming events for ubiquitin chain elongation, threreby increasing the complexity of the ubiquitin code. The conformation of ubiquitin chains is determined by their linkage composition, distinguishing homotypic chains, which are linked through the same acceptor ubiquitin site and heterotypic chains, which incorporate multiple linkage types (Fig. 3B).

Among the various chain types, K48-linked and K63-linked chains are the most prevalent, collectively representing approximately 70%–90% of all ubiquitin linkages in cells [61]. Due to their abundance and biological relevance, these chains are the most extensively studied and are commonly referred to as canonical or typical ubiquitin chains. K48-linked ubiquitylation plays a central role in maintaining protein homeostasis by facilitating the rapid recognition and degradation of substrates by the 26S proteasome, a process described in the previous chapter. These chains initiate selective protein turnover across all cellular processes, allowing the proteome to adapt to specific cellular needs. For example, K48-linked ubiquitylation regulates protein abundance to ensure timely progression through the cell cycle. Another key instance is the K48-linked ubiquitylation of the tumor suppressor p53, whose levels are tightly linked to cell fate decisions both under steady-state conditions and in response to genotoxic stress [62]. Overall, K48 serves as a central signal in protein quality control, continuously remodeling the proteome to maintain cellular homeostasis. In contrast, K63-linked ubiquitylation goes beyond proteolytic functions by assembling molecular scaffolds on its substrates that regulate key cellular processes such as selective autophagy and NF-κB-mediated inflammation . For example, K63 chains a mark of damaged mitochondria, that is being recognized by autophagy adapters such as p62/SQSTM1 or NDP52 that trigger autophagosome formation. K63 linkages also orchestrate non-degradative steps of the NF-κB pathway via multiple substrates at distinct stages of activation such as RIP1/2, TRAF6 or NEMO [63], [64], [65]. Understanding of K48- and K63-linked ubiquitin chains has advanced considerably, yet many aspects of their functions remain the focus of ongoing research. In

recent years, it has been revealed that K48 and K63 ubiquitin chains often serve as base chains for the formation of heterotypic, particularly branched, ubiquitin chains. This branching can amplify signaling to ubiquitin readers or even alter the cellular fate of the modified protein.

Less prevalent chain types (K6, K27, K33 and linear M1) are referred as non-canonical or atypical chains. Their low abundance combined with limitations of available experimental approaches make it challenging to study these chains. Nonetheless, some roles of atypical chains have already been uncovered revealing their unique roles in maintaining cellular homeostasis.

K6-linked chains have an implied role in mitophagy via PARKIN-mediated ubiquitination of mitochondrial membrane proteins, a key step in mitochondrial quality control [42], [66]. K6-linkage serves as a tag that marks damaged mitochondria for clearance and help facilitate the recruitment of autophagy receptors and other components of mitophagy machinery. Additionally recent study suggests that K6-linked ubiquitin chains play a direct role in protein quality control during genotoxic stress responses, such as those caused by formaldehyde-induced RNA–protein crosslinks [67]. Stalled translation complexes tagged with K6-linked ubiquitin engage the VCP/p97 ATPase and proteasome machinery, which extracts and degrades the damaged complexes to restore translation homeostasis [68].

K11-linked chains produced by UbcH10/Ube2S and anaphase-promoting complex (APC/C) function as proteasome degradation signals particularly during exit from mitosis for cell cycle drivers such as AURKA, CCNB1 and PLK1 [69], [70]. In fact, in 2010 study it has been proposed that APC/C is involved into synthesis of the most K11-linked chains in cells, making K11 an essential regulation signal of mitotic degradation [70].

K27-linked ubiquitin chains are another ubiquitin chain type that have been implicated in cell cycle progression [71]. Following JNK-mediated phosphorylation, the HECT-type E3 ligase ITCH catalyzes K27-linked ubiquitylation of BRAF, a pivotal component of the MEK/ERK oncogenic signaling cascade [72]. This modification supports sustained BRAF activity and promotes the proliferation and invasive capacity of melanoma cells. In addition to

this function, K27 linkages contribute to the activation of the DNA damage response [73]. Specifically, RNF168-mediated K27-linked ubiquitylation of histone H2A facilitates the recruitment of DNA repair factors such as 53BP1, Rap80, and BRCA1 to sites of chromatin damage. More recently, K27-linked ubiquitin chains have been characterized as predominantly nuclear chains. Same study suggests a functional role for K27 linkages in p97/VCP-dependent substrate processing within the nuclear compartment [71].

K29-linked ubiquitin chains are the third most abundant chain type within cells. Despite this prevalence, their cellular functions remained poorly understood until recently. In yeast K29-linked ubiquitin chains regulate of ribosome biogenesis through degradation of maturing ribosomes, disrupting their assembly and activating a specific ribosome assembly stress response [74]. A growing number of studies highlight the functional significance of K29 linkages, particularly in the context of branched ubiquitin chains, a topic that will be adressed in the following section.

K33-linked ubiquitin chains are generally resistant to proteasomal degradation and act predominantly in non-proteolytic cellular functions, such as protein trafficking and immune response regulation. For example, K33-linked ubiquitylation of Coronin-7 (Crn7) by the Cul3-KLHL20 E3 ligase facilitates Crn7's interaction with Eps15, which is essential for actin polymerization—a key step supporting post-Golgi trafficking [75]. In the immune system, K33-linked ubiquitylation of the T cell receptor ζ (TCR-ζ) chain inhibits its phosphorylation, thereby suppressing T cell activation and helping to prevent spontaneous autoimmune responses [76]. Additionally, a 2018 study by Nibe and et al. demonstrates that the autophagy receptor SQSTM1/p62 colocalizes with K33-linked polyubiquitin in cells [77]. This interaction suggests a role for K33-linked chains in selective autophagy.

Linear ubiquitin chains are primarily associated with canonical NF-κB signaling in inflammatory and immune responses. These chains are uniquely synthesized by the linear ubiquitin chain assembly complex (LUBAC), which promotes NF-κB activation through linear ubiquitylation of of several immune receptors including NEMO, a subunit of the IκB kinase complex [78], [79]. While NEMO is modified by K63-linked chains which is important for

JNK activation, its linear ubiquitylation plays a distinct role by stabilizing the TNF-R1 signaling complex [80]. While linear ubiquitin chains are best known for sustaining canonical NF-κB signaling and inflammatory gene expression, their role in cell death regulation is supported but not as thoroughly understood as their immune functions [81].

1.2.3 Branched ubiquitin chains code

Theoretically, combinations of ubiquitin linkages can result in 28 distinct branched chain types. However, only a few of these particularly K11/K48-, K48/K63-, M1/K63 and K29/K48-linked chains have been functionally characterized in vivo [82], [83], [84], [85], [86]. Advances in biochemical and proteomic assays have suggested the existence of additional linkages, such as K6/K48-, K6/K11-, K27/K29- and K29/K33-linked chains [87]. However, their presence in vivo and the functional consequences for the modified substrates remain largely unexplored. What is known is cellular interpretation of ubiquitin code depends on the context particular chain types are combined which results in increased complexity. While some physiological enzymes capable of assembling branched chains have been identified, understanding how branched architectures emerge and function in cells continues to be an evolving focus in the ubiquitin field. Perhaps UBR4, UBR5 and HUWE1 are the most studied ligases in the context of K48 branch elongation on pre-existing ubiquitin chains [82], [83], [85], [86], [88]. These enzymes demonstrate to collaborate with multiple E3s to form distinct types of branched linkages, including and will appear a lot across this section.

We begin our discussion with the collaboration between the two most abundant ubiquitin chains in the context of branched ubiquitylation: K48- and K63-linked chains. To date, several studies have aimed to identify the enzymes involved in the assembly and recognition of these branched chains, as well as their substrates. Quantitative proteomics experiments have revealed that K48/K63-branched linkages are abundant in mammalian cells, with up to 20% of K63 linkages being part of such branched structures [89]. In some cases, the non-degradative ubiquitin code conveyed by K63 chains can be converted into a degradation signal through branching with K48 linkages. This is consistent with the accumulation of both

K63- and K48-linked chains observed upon proteasome inhibition with MG132 treatment. A notable example of such proteasome-targeting regulation involves the co-regulation of the pro-apoptotic regulator TXNIP by the E3 ligases ITCH and UBR5 [90]. Given the non-proteolytic role of K63 linkages in mediating protein–protein interactions, branched chains have been proposed to temporally and spatially separate the consequences of ubiquitin modifications. Additionally, branched ubiquitylation may protect pre-existing chains from recognition by deubiquitinating enzymes (DUBs), as observed in the cooperation between HUWE1 and TRAF6 [89]. K48/K63-branched chains on TAB2—an adaptor protein that requires K63 linkages for recognition by downstream components of the NF-κB signaling pathway—illustrate another functional consequence of branching. The K48 branch restricts the activity of CYLD, a K63-specific DUB, thereby promoting signal amplification in the NF-κB pathway. A recent study by Lange et al. demonstrated that K48/K63-branched chains are recognized by multiple VCP/p97-associated proteins and accumulate upon VCP/p97 inhibition, suggesting a potential role for p97 in the processing or debranching of branched ubiquitin substrates [91].

It remains unclear whether K63/M1-linked ubiquitin chains are branched or mixed, but their structural diversity is biologically significant. Like some other hybrid chains (e.g., K29/K48), K63/M1 chains are more resistant to deubiquitination and help coordinate signaling complexes [86]. Specifically, NEMO binds M1-linked chains to recruit the IKK complex, while TAB2/TAB3 bind K63-linked chains to recruit TAK1. This scaffolding ensures efficient TAK1-mediated activation of IKK, which is essential for NF-κB signaling and innate immune responses.

As mentioned in the previous section, K11-linked ubiquitin chains elongated by UBE2S on APC/C substrates are crucial for efficient proteasome degradation during cellular exit from mitosis [83], [84]. The APC/C relies on UBE2C and UBE2D to initiate ubiquitin chain formation, with UBE2S extending these chains via K11 linkages. APC/C generates ubiquitin chains of mixed or branched topology, especially K11/K48-linked chains, which are central for the rapid degradation of mitotic substrates [83]. Beyond the APC/C, E3 ligases such as UBR4 and UBR5 have been identified putative contributors to K11/K48-branched chain

assembly, particularly during proteotoxic stress, although it remains unresolved which E3 ligases are involved in ubiquitin chain initiation [84], [92]. K11/K48-branched chains are especially abundant during proteotoxic stress, where they target nascent or misfolded proteins for degradation and play a critical role in translation-coupled quality control. Both in mitosis and under proteotoxic stress, these branched chains facilitate proteasomal recognition and substrate degradation more efficiently than homotypic chains, as the 26S proteasome has a higher affinity for branched K11/K48 ubiquitin chains. This specialized recognition underpins highly effective substrate turnover in both cell cycle regulation and protein quality control contexts.

Recent studies have established that K29/K48-branched polyubiquitin chains are predominantly formed by the E3 ligase TRIP12 in humans and its yeast homolog Ufd4, mainly by adding K29 linkages onto pre-existing K48 chains [93], [94]. Whether these enzymes can initiate chain formation on unmodified substrates (i.e., act as priming ligases) remains unresolved. Structural and biochemical data suggest that these branched chains typically arise through elongation of existing chains rather than de novo assembly. The primary function of K29/K48-branched chains is to promote proteasomal degradation, with the K29 component making them more resistant to deubiquitinases and thus enhancing the degradative signal—a role now widely recognized in both yeast and humans [95], [96]. In human cells, TRIP12 often works cooperatively with the K48-specific E3 ligase UBR5, with both acting as chain elongators [96], [97]. However, the identity of the initial (priming) E3 ligase is still unknown. These branched chains are important not only for regulated protein degradation but also for controlling pathways such as NF-κB signaling, particularly through the targeting of substrates like OTUD5. While the involvement of K29/K48 chains in these processes is supported, the detailed mechanisms are still being elucidated.by which K29/K48-branched chains influence this pathway are still being elucidated.

The ubiquitin code orchestrates a dynamic and finely tuned regulatory landscape, essential for cellular protein homeostasis and signaling. While considerable progress has been made in delineating the functions of distinct ubiquitin chain types, much remains to be

uncovered about how specific chain linkages are generated, interpreted, and regulated. In a lot of cases intricate interplay of ubiquitin ligases (E3s) and deubiquitinating enzymes (DUBs) regulate the linkage function and activity. As research progresses, the collaborative actions and crosstalk among these enzymes have emerged as central themes in the precise control of protein fate and signaling pathways.

1.3 Ubiquitin signaling networks: E3-DUB crosstalk

While discovery of substrate specificity principles of E3 ligases and DUBs remain central to ubiquitin research, a number of studies explore of the regulatory relationships within the ubiquitin machinery itself. Large-scale proteomics study from 2009 showed that nearly half of all DUBs physically associate with at least one E3 ligase, highlighting this as a widespread phenomenon and a fundamental aspect of cellular regulation [98]. While E3 ligases and DUBs are often seen as having antagonistic roles (adding versus removing ubiquitin), emerging evidence demonstrates that DUBs can in fact improve or adjust the activity of specific E3 ligases according to homeostatic requirements (Fig. 4A). In the following section, we will explore the sophisticated regulatory networks formed through E3–DUB interactions and their implications for cellular ubiquitin signaling.

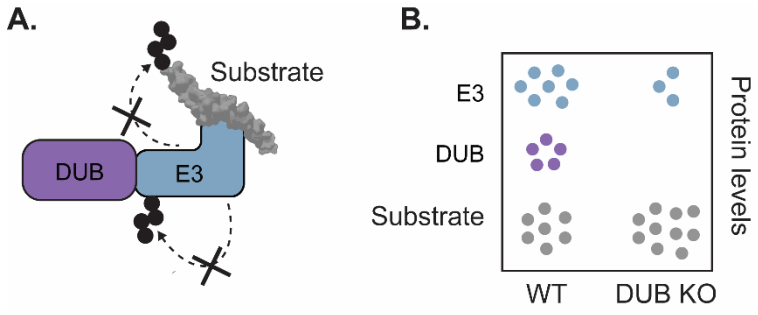

Figure 4 E3–DUB crosstalk.
A. E3–DUB interactions stabilize E3 ligases and/or promote selective substrate processing through antagonizing substrate ubiquitylation. **B.** Schematic representation of changes in E3 and substrate abundance upon knockout (KO) of associated DUBs.

The interplay between E3 ligases and DUBs has been most extensively studied in the context of gene regulation and the control of transcription factor stability. Among these, the MDM2–USP7–p53 regulatory axis serves as the most intensively studied example with profound implications for cell fate decisions and cancer biology. MDM2, a RING-family E3 ligase, targets the tumor suppressor p53 for ubiquitin-mediated degradation and is itself stabilized by USP7 [62], [99], [100]. Although MDM2 can undergo auto-ubiquitination, this process primarily modulates its E3 ligase activity and proteasomal degradation signaling is rather phosplorylation-dependant [101], [102]; thus, the precise mechanism by which USP7 controls MDM2 stability remains incompletely understood. Both USP7 and USP2 play pivotal roles in maintaining MDM2 levels, thereby exerting critical control over p53 stability and cellular stress responses [103]. Beyond p53, the influence of the MDM2–USP7 axis extends to other regulatory proteins such as chromatin-associated methyltransferase SUV39H1, implicating broader roles in gene expression and chromatin modification [104]. The KEAP1-CUL3 complex, another E3 ligase system, is regulated by DUBs like USP25, which deubiquitinates and stabilizes KEAP1, thus restraining NRF2 stability. Loss of USP25 leads to KEAP1 degradation and consequent NRF2 activation, promoting antioxidant responses [105].

Of particular interest is the dual regulation of Fbw7 and its substrates by the deubiquitinase USP28 [106]. Fbw7 serves as the substrate recognition component of the SCF (SKP1–CUL1–F-box) E3 ligase complex and targets multiple proto-oncoproteins for proteasomal degradation. A study published in 2014 demonstrated that USP28 not only stabilizes Fbw7 itself but also plays a key role in maintaining the physiological levels of a number Fbw7 substrates. The authors showed that USP28 forms a complex with Fbw7, antagonizing substrate ubiquitination under normal conditions. Upon activation of the DNA damage response, this complex dissociates, enabling Fbw7 to ubiquitinate and trigger the degradation of its substrates. When USP28 is overexpressed, this regulatory balance is disrupted, leading to enhanced stabilization of Fbw7 substrates. The authors propose that the stabilization of both Fbw7 and its substrates under basal conditions is transient and serves to prevent excessive or prolonged proliferative and survival signaling.

Such regulatory circuits, where E3 ligase levels and activity are coupled to DUB action, enable rapid adaptation of gene expression programs without altering direct transcriptional output. Dysregulation, such as mutations in MDM2 or KEAP1 or USP28 overexpression is a driver in several cancers [107], [108], [109]. While mutations in these axes are frequent in certain tumor types (e.g., KEAP1 in lung adenocarcinoma and MDM2 in multiple cancers via amplification or mutation), they are not uniformly among the most common events in all cancers. Disruption of these E3/DUB modules affects cancer progression and highlights both classes of proteins as attractive therapeutic targets in a tissue-specific manner. However, further studies aimed at decoding the spatiotemporal regulation and substrate specificity within E3–DUB crosstalk are essential to fully harness their therapeutic potential and understand their role in complex cellular signaling.

1.4 Degron recognition: from sequence motifs to structural landscapes

Understanding the specificity of E3 ligases requires defining minimal structural determinants of substrate recognition, known as degrons [110]. Systematic studies mapping extensive E3–substrate networks have identified a diverse set of degrons for approximately 50 distinct E3 ligases. A single E3 can recognize multiple distinct degrons, while similar degrons may be targeted by different E3s. Typically, degrons are as short as a few amino acids. Although first characterized at protein termini, degrons are not restricted to these regions and can also be located internally within the protein sequence. Depending on their localization, structure, and recognition mechanism, degrons can be classified as terminal or internal, intrinsically disordered or structured, and either constitutive or conditional. Understanding the diversity and recognition logic of degrons is essential for elucidating how E3 ligases achieve substrate specificity within the ubiquitin system. In the following section, we discuss recent advances in degron discovery and how they shape UPS selective protein degradation.

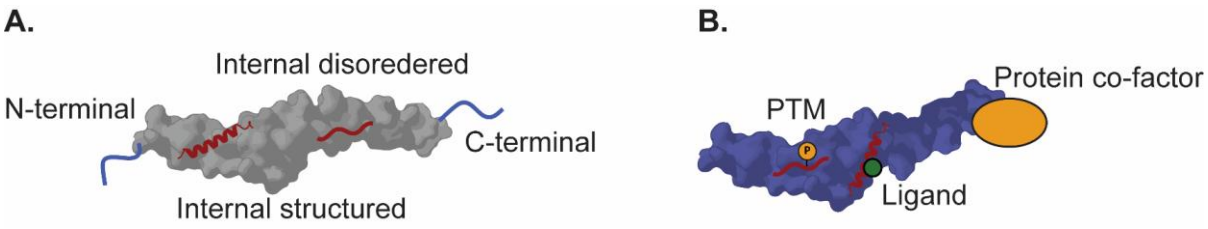

Figure 5. Types of degrons and their regulation.
A. Terminal and internal degrons. Classic N-degrons and C-degrons are disordered and located at protein termini, whereas internal degrons can be both ordered or disordered**. B** Conditional degrons include degradation signals that are only recognized under specific conditions. Exposure of this signals is triggered by post-translational modifications, ligand binding or co-factor interactions.

1.4.1 Degrons at protein termini

Protein termini are particularly enriched in degrons, as these regions are less likely to be buried within the folded protein structure. This accessibility makes terminal degrons easier to identify and characterize. The unique properties of protein termini play a central role in defining the principles of E3 substrate specificity [111]. In particular, E3 ligases enriched in tandem repeat domain families—such as Kelch, armadillo (ARM), and WD40 repeats—are frequently involved in recognizing terminal degrons [112]. The rules governing terminal substrate recognition are therefore shaped by the distinct structural and chemical features of both the N- and C-termini of the substrate.

1.4.1.1 N-degron recognition

N-terminal degron (N-degron) pathways regulate protein stability according to features at exposed N-termini, where residues behave as destabilizing or stabilizing and can be conditionally converted into degradation signals [111], [113]. In the Arg/N-degron branch, primary destabilizing residues such as Arg, Lys, His, Leu, Phe, Tyr, Trp, Ile, or Met (followed by a bulky hydrophobic amino acids) are directly recognized by UBR-family ligases, whereas secondary (Asp/Glu) and tertiary (Asn/Gln/Cys) residues require prior processing. This processing relies on deamidation for Asn/Gln or oxidation for Cys followed by ATE1-dependent arginylation to enable recognition. Beyond proteasomal processing, p62/SQSTM1 can engage Arg/N substrates in selective autophagy, underscoring the pathway's role in

clearing proteolytic fragments or aberrant N-termini [114]. A second branch, the Ac/N-degron pathway, arises from co-translational N-terminal acetylation, which is widespread in human proteins. Generally, acetylated N-termini are inert when buried within folded or assembled states but become degradation signals when exposed, for example during ER or membrane quality control mediated by Doa10/TEB4 [115]. A third branch, the Pro/N-degron pathway is coordinated by the modular CTLH E3 complex (GID in yeast), whose exchangeable receptors confer recognition of substrates bearing N-terminal proline (or Pro at position 2 in yeast) and support stress- or starvation-responsive turnover in mammals exemplified by HMGCS1 [116], [117]. Finally a fourth and broader branch termed GASTC/N-degrons, encompasses small N-termini (Gly, Ala, Ser, Thr, Cys) that are recognized by CUL2 adaptors such as ZYG11B and ZER1 [118]. Substrate binding is carried out through armadillo repeat domains with complementary preferences for Gly versus small polar residues, and by IAP proteins whose BIR domains bind unmodified Ala/Ser [119]. Conceptually, N-degrons in the nucleus are often conditional and emerge when protease cleavage, mislocalization, or complex dissociation reveal previously hidden termini. This network of E3 ligases and substrate receptors forms a comprehensive quality control system that senses and eliminates proteins with these small, exposed N-termini, helping maintain cellular proteostasis and responding to the production of aberrant or damaged proteins.

1.4.1.2 C-degron recognition

C-terminal degrons (C-degrons) constitute sequence- and chemistry-defined signals at protein C-termini that route substrates to the proteasome, most commonly via CRL2 and CRL4 adaptors. Unlike N-degrons, recognition typically depends on multi-residue motifs near the terminus rather than a single residue identity. Within CRL2, Kelch-like adaptors exemplify motif-specific binding: KLHDC2 favors compact di-glycine ends, KLHDC3 recognizes RxxG-like termini, and KLHDC10 binds A/W/P–G motifs and contributes to ribosome-associated quality control by engaging poly-A-extended incomplete chains [110]. Other CRL2 receptors broaden the landscape: APPBP2 recognizes RxxG-type signatures with positional flexibility and tolerance for flanking residues, while FEM1A/B/C preferentially detect C-

terminal arginine, with evidence that FEM1B can also accommodate proline. CRL4 adaptors exhibit distinct chemistries, as CRBN binds cyclic Gln/Asn termini that arise in aged or aberrantly processed proteins, DCAF12 recognizes acidic motifs centered on −2 glutamate consistent with WD40 electrostatics, and TRPC4AP, via ARM-like repeats, engages Arg-biased motifs typically positioned a few residues from the terminus [120]. Outside the CRL family, CHIP links apoptotic processing to degradation by targeting caspase-cleaved proteins that expose C-terminal aspartate [121]. Functionally, C-degrons are enriched in aberrant, truncated, or prematurely terminated proteins and therefore frequently report orphan states created by failed assembly or proteolysis in the nucleus.

1.4.2 Internal degrons

Similarly to terminal degrons, bioinformatic analyses have revealed that internal degron motifs are evolutionarily conserved. However, this class of degrons is more complex than terminal degrons. Internal degradation signals are typically longer, structurally diverse, and exhibit position-independent functionality. Although the first internal degron was identified in the 1990s, characterization of internal degrons remains a challenging task. Despite extensive studies on E3–substrate relationships in the ubiquitin–proteasome system, corresponding degrons have been identified for relatively small amount of E3s. This limitation arises because internal degrons are often buried within the protein core and become accessible only under specific conditions, such as unfolding, misfolding, or dissociation of protein complexes. The regulation of internal degrons is broad and remains insufficiently understood, warranting further investigation.

1.4.2.1 Mechanisms of internal degron recognition

When an internal degron sequence is directly recognized by an E3 ligase, the sequence motif is referred to as a constitutive degron. These “built-in” degrons possess a primary structure sufficient to form a degradation signal without the need for additional activation steps. A classical example is the first discovered internal degron, the RXXLXXXXN motif—known as the destruction box (D box) of cyclin B—which is sufficient for recognition by the

anaphase-promoting complex/cyclosome (APC/C) upon E3 ligase activation during the cell cycle [122]. The APC/C engages substrate degrons through a seven-blade β-propeller WD40 repeat domain located in the C-terminal half of its activator subunit. Notably, APC/C recognizes multiple constitutive degron motifs, including the D box, the ABBA motif [ILVF]x[ILMVP][FHY]x[DE], and the KEN box (KENXXXN) [123]. Many substrates contain multiple degron sequences, enabling cooperative binding to the APC/C co-activator and contributing to a complex regulatory network that determines the ordered degradation of APC/C substrates. While constitutive degrons are well exemplified by APC/C-target motifs, the majority of identified internal degradation signals require conditional activation. Such conditional degrons are activated through post-translational modifications, co-factor binding, or small-molecule interactions, reflecting the increasing complexity of regulated proteolysis.

While a wide range of post-translational modifications regulate internal degron recognition, phosphorylation remains the best-studied example. Proteome-wide bioinformatic analyses have revealed that phosphorylation signals are significantly enriched within and around degron motifs [124]. Substrate proteins undergo phosphorylation in response to upstream cellular signaling, enabling rapid degradation during processes such as cell differentiation, cell cycle progression, and apoptosis. Not all APC/C substrates are directly recognized by the E3 ligase; in some cases, phosphorylation of sites proximal to the D box motif is required. The introduction of a negatively charged phosphoryl group can enhance the resemblance of the motif to the consensus D box, thereby promoting APC/C recognition [125]. Beyond the APC/C complex, the Skp1–Cullin–F-box (SCF) ligases also play a central role in cell cycle–dependent degradation. Several F-box proteins, including BTRC/FBXW1, FBXW11, and FBXW7, rely on substrate phosphorylation for recognition. A classical example of a phosphodegron is Cyclin E, which is targeted by FBXW7 [126]. In this case, recognition requires the convergence of two kinase activities: CDK2 phosphorylates S384, while GSK-3 phosphorylates T380, ensuring efficient Cyclin E turnover. Interestingly, phosphorylation can also inhibit degron function, as exemplified by p53 degradation, which is blocked when threonine adjacent to the MDM2-bound degron motif is phosphorylated [102].

In addition to regulation by post-translational modifications, certain conditional degrons are modulated through the binding of protein cofactors or small molecules. One of the most extensively studied examples originates from auxin signaling in plants, where the binding of auxin facilitates small-molecule-dependent protein degradation. This mechanism has been adapted to develop auxin-inducible degradation systems in heterologous contexts [127]. Small-molecule binding has attracted considerable interest due to its therapeutic potential in enabling the conditional degradation of target proteins. For example, investigations into the clinical efficacy of thalidomide and lenalidomide in multiple myeloma revealed that these compounds function as molecular glue degrader [128]. They achieve this by promoting the direct recruitment of the CRBN–CRL4 ubiquitin ligase complex, thereby inducing the degradation of the transcription factors IKZF1 and IKZF3 . Notably, lenalidomide now serves as a cornerstone therapy for multiple myeloma as well as for certain subsets of myelodysplastic syndrome (5q-MDS). The development of molecular glue degraders represents a growing area of research within the clinical application of the ubiquitin–proteasome system (UPS). Structure-based design and high-throughput screening approaches are increasingly being employed to identify novel compounds with targeted degradation activity.

Understanding the principles of E3 ligase substrate recognition is crucial not only for the characterization of known substrates but also for the prediction of novel ones. However, the presence of a degron motif alone is insufficient for the reliable identification of genuine E3 recognition sites. Part of the false-positive predictions can be reduced through evolutionary conservation analysis. Nevertheless, it is essential to consider the synergistic relationship between E3 recognition, ubiquitylation, and proteasomal degradation processes. In 2016, Guharoy et al. proposed a three-component degron model, which includes: (i) the E3 recognition motif or docking site (primary degron), (ii) the ubiquitylation site (secondary degron), and (iii) the proteasomal degradation initiation site (tertiary degron) [129]. The spatial arrangement between the primary and secondary degrons restricts ubiquitylation to lysine residues located in close proximity to the primary degron. Similarly, the spatial relationship between the secondary and tertiary degrons plays a critical role in the initiation of proteasomal degradation. Importantly, ubiquitylation alone is often insufficient to enable ATP-dependent

unfolding of the substrate protein; the presence of an intrinsically disordered region in close proximity to the degradation initiation site is frequently required.

In summary degron discovery continues to be a one of the key drivers in advancing our understanding of the ubiquitin–proteasome system. Elucidating substrate recognition principles of enables both systematic characterization of known substrates and the identification of novel ones. Degron discovery is also important for the development of next-generation therapeutic strategies based on targeted protein degradation. As research increasingly integrates structural biology, high-throughput screening, and computational prediction, degron characterization is poised to bridge fundamental molecular insights with translational applications in drug discovery.

1.5 E3 ligases as guardians of protein complex integrity

Fundamental biological processes, such as transcription and splicing, depend on the coordinated function of multimeric protein complexes with precise architectures and compositions. Proteomic analyses of the soluble protein fraction reveal that nearly half of the proteome typically participates in complex assembly at any given time [130], [131]. Establishing the correct stoichiometry, abundance, localization, and partner interactions for each protein is therefore critical. However, these assembly processes are inherently error-prone, due to both random fluctuations in subunit synthesis and external or internal disruptions, resulting in the frequent emergence of unpaired subunits and misassembled complexes [130], [132], [133]. Historically, cellular models emphasized a sequential and compartmentalized framework where biosynthetic events were spatially and temporally shielded from quality control mechanisms, protecting nascent chains from premature degradation. Recent studies, however, indicate that protein synthesis, assembly, and quality control are tightly integrated. Unpaired protein clearance is a continuous, essential aspect of proteostasis, not confined to the aftermath of biosynthetic failure. Instead, it is dynamically coordinated alongside complex assembly and network regulation, utilizing the flexible interplay of chaperones, E3 ubiquitin ligases, and ubiquitin signaling. It is increasingly recognized that quality control of complex

assembly, together with the removal of mislocalized proteins, might represent a major source of substrates for the ubiquitin–proteasome system under steady-state conditions [130]. Within this context, E3 ligases act as pivotal guardians, ensuring the integrity and adaptability of cellular protein complexes through targeted degradation.

1.5.1 Protein complexes synthesis and assembly

To understand the quality control of complex assembly, it is first necessary to consider the mechanisms that regulate the assembly process itself. The crowded and dynamic cellular environment poses significant challenges for the efficient formation of multi-subunit complexes, particularly in the cytoplasm. One major strategy employed by eukaryotic cells is co-translational assembly, whereby complex formation is initiated during translation. A 2019 study demonstrated that in yeast, mRNAs encoding subunits of the same protein complex are localized to cytoplasmic condensates [134], [135]. This model, which is particularly relevant for heteromeric complexes, depends on RNA-binding proteins that drive condensate formation and thereby act as matchmakers to bring corresponding subunits into proximity. Co-translational assembly can proceed through different mechanisms. The most studied one relies on a fully synthesized subunit engaging directly with a nascent polypeptide that is still associated with the ribosome [136]. As the elongating chain emerges, newly synthesized domains are sequentially exposed to their binding partners, allowing interactions either with fully folded proteins or even with the N-terminally folded regions of other nascent chains [137]. This ensures efficient complex formation and reduces the risk of misfolding and inappropriate interactions.

However, complex assembly is not restricted to co-translational mechanisms. An alternative strategy relies on dedicated assembly factors, predominantly protein chaperones, which facilitate the establishment of correct interactions in a temporally and spatially regulated manner. The best-characterized example of chaperone-assisted assembly is the biogenesis of the 20S proteasome [138]. Here, a defined set of chaperones orchestrates the sequential formation of the α-rings, followed by the ordered incorporation of β-subunits to generate half-

proteasomes, whose dimerization ultimately yields the mature 20S core particle. The transient association of these chaperones with assembly intermediates is indispensable for proper proteasome maturation.

Importantly, proteasome assembly represents only one paradigm of this broader mechanism. Many other multi-subunit complexes also depend on time-resolved chaperone interactions for correct assembly. In some cases, subcomplexes are partially formed co-translationally and subsequently stabilized or integrated into higher-order structures through chaperone assistance [136], [139]. This interplay between co-translational assembly and chaperone-mediated regulation highlights the diverse strategies that eukaryotic cells employ to ensure fidelity in complex biogenesis. When these mechanisms fail, unpaired subunits or complex intermediates are rapidly recognized and eliminated by the ubiquitin–proteasome system, underscoring the tight coupling between complex assembly and quality control.

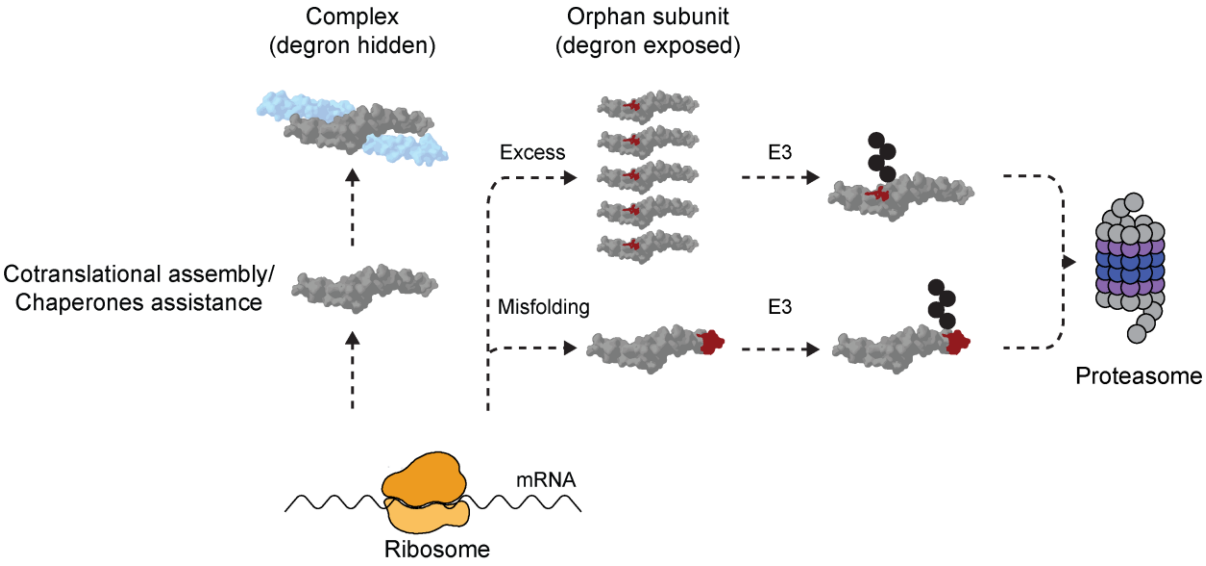

Figure 6. Protein complex assembly quality control.
Nascent subunits engage assembly factors or chaperones at the ribosome, burying degrons within interaction interfaces. Orphaned subunits retain exposed degrons and are recognized by E3s, leading to ubiquitination and proteasomal degradation. Chaperones can transiently shield orphans, but persistent misassembly triggers quality control, maintaining subunit balance and proteostasis.

1.5.2 Quality control of orphaned proteins

As described in previous chapter, a central mechanism of protein quality control is the recognition of degrons by E3 ubiquitin ligases. In fully assembled protein complexes, degrons are typically buried and inaccessible to ubiquitylation machinery. However, when a subunit remains unpaired or a complex fails to incorporate all required components, degrons become exposed, effectively marking so-called “orphan” subunits for degradation.

In eukaryotic cells, protein production often faces stochastic fluctuations in gene expression and translation, producing variable amounts of individual subunits. This “noise” in synthesis frequently generates excess orphan proteins, which can threaten cellular homeostasis if not efficiently cleared. The accumulation of uncleared orphans may lead to toxic aggregates or inclusions that disrupt intracellular processes and increase cellular stress. To maintain protein level balance, cells deploy rapid elimination of orphan proteins immediately after their synthesis. Several E3 ubiquitin ligases have recently been implicated in targeting and degrading these orphan subunits, including HUWE1, UBR4 and many others [140], [141], [142], [143]. These ligases efficiently coordinate the removal of a wide range of structurally diverse substrates either by engaging their multiple protein-binding domains or through the use of adaptor proteins, which bridge recognition of varied degrons and orphan states across the proteome. For example, HUWE1 features a giant ring-like structure incorporating multiple substrate engagement sites (BH3 domain, WWE domain, ubiquitin-binding domain, and negatively charged disordered loop), together with a flexible catalytic domain that facilitates efficient ubiquitylation of many substrate types [144]. In contrast, UBR4 achieves broad substrate specificity by employing adaptor proteins such as KCMF1, which help it recognize and target a diverse array of orphaned proteins for degradation [143]. This multi-tiered system—combining structural versatility and adaptor-mediated recognition—underpins robust protein quality control and ensures the integrity of the cellular proteome.

On the opposite end of the protein synthesis spectrum, lies the problem of incomplete complex assembly, which commonly arises from loss or reduction of specific protein subunits

due to genetic mutations or disrupted gene expression. Such deficits can destabilize multiprotein complexes, with profound consequences for cellular signaling [145], [146]. Systematic experiment has shown that deleting or mutating genes encoding complex subunits (e.g., through knockouts or knockdowns) leads to reduced abundance of the remaining subunits, as their degrons become exposed and unprotected [147]. For proteins serving as subunits in multiple complexes, the loss of one binding partner can lower their overall levels, thereby impacting assembly and function of other complexes that share the same subunit. A well-studied example involves the COPII vesicle trafficking complex: reduction of the subunit SEC31A causes a collateral drop in its partner SEC13, since both form a heterotetramer crucial for COPII coat structure [147]. Importantly, SEC13 also serves as a subunit of the GATOR2 regulatory complex; thus, SEC13 depletion due to COPII disruption can further compromise assembly and stability of GATOR2—a striking illustration of how loss of a shared protein can propagate effects across distinct cellular pathways.

In conclusion, E3 ubiquitin ligases have emerged as central regulators of protein complex assembly and quality control in eukaryotic cells. Their ability to detect and eliminate orphan subunits or misassembled complexes is crucial for preventing protein aggregation, preserving signaling fidelity, and safeguarding against disease. Moreover, emerging therapeutic strategies that modulate E3 ligase activity or shield critical interaction surfaces present new opportunities to influence proteostasis and intervene in disease progression. Understanding and harnessing these mechanisms opens new frontiers for both fundamental biology and targeted clinical applications.

1.6 UBR5: an architect of nuclear protein quality control

Nuclear protein quality control is essential for preserving genomic stability by facilitating the recognition and degradation of aberrant or misfolded proteins within the nucleus. In contrast to the cytoplasmic and endoplasmic reticulum quality control systems, however, the nuclear quality control pathways remain comparatively less characterized. Among the critical regulators of nuclear protein homeostasis is UBR5 (ubiquitin protein ligase

E3 component n-recognin 5), a large HECT-type E3 ubiquitin ligase. UBR5 has been implicated in diverse nuclear processes, including transcriptional regulation, DNA replication, DNA damage response, and cell cycle progression. Like HUWE1, UBR5 can engage a structurally and functionally diverse set of substrates. This versatility is enabled by the presence of multiple substrate-binding and protein–protein interaction domains, which allow UBR5 to act as a signaling hub in nuclear protein maintenance and regulation.

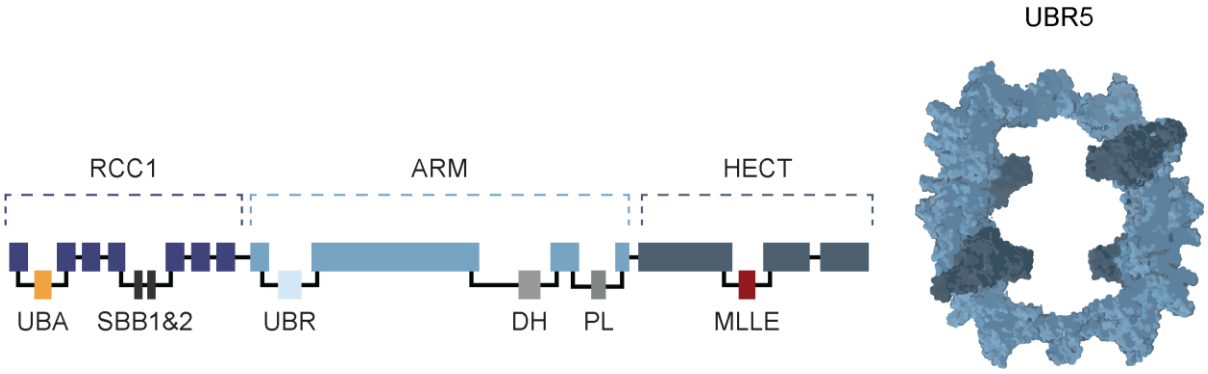

Figure 7. UBR5 structure.
A. Linear domain map of UBR5: N-terminal RCC1 β-propeller (discontinuous) harboring insertions for UBA and two small β-barrels SBB1/2; central ARM helical scaffold spanning residues 876–2209; embedded UBR box degron receptor at residues 1177–1244; dimerization helix within ARM at residues 1912–1931; short "plug loop" from the solenoid that wedges between HECT lobes; C-terminal HECT domain spanning residues 2210–2799 containing catalytic Cys2768; MLLE (PABC) module inserted within the HECT N-lobe via flexible linkers rather than preceding HECT in sequence. Functionally, the UBA binds ubiquitin/E2~Ub to enhance transfer, the UBR box recognizes type-I N-degrons, ARM builds the crescent scaffold and main dimer interface, the DH stabilizes the antiparallel dimer, MLLE binds PAM2 motifs from partners, and the HECT carries out transthiolation and chain elongation, predominantly K48-linked on primed substrates. **B.** Cryo-EM oligomer view of UBR5 tetramer showing two antiparallel dimers arranged face-to-face into a ring-like assembly with a central cavity; all four HECT catalytic domains and UBR boxes orient toward the chamber interior, and tetramerization is mediated by SBB2–SBB2 contacts, while dimers constitute the primary stable species in solution.

1.6.1 Structure of UBR5

Recent advances in structural biology, particularly through cryogenic electron microscopy (cryo-EM), have provided important insights into UBR5 architecture [30], [88], [148]. A central structural element of the UBR5 monomer is an extended α-helical solenoid, which is formed by tandem armadillo (ARM) and HEAT repeats extending from the N- to the C-terminus. This solenoid acts as a scaffold, organizing multiple protein–protein interaction domains along the entire length of the protein and thereby supporting UBR5's role as a

versatile regulator. Recent studies published in 2023 have further demonstrated that UBR5 couples substrate recognition to its catalytic activity through oligomerization. In this context, the antiparallel homodimer represents the minimal functional catalytic unit of the E3 ligase. Subsequently, dimers associate into a tetrameric, ring-shaped assembly in which all catalytic sites are oriented toward the central cavity, potentially enabling coordinated substrate processing. Importantly, dimerization and tetramerization are mediated by distinct interaction surfaces: dimer formation relies on a single helix spanning residues 1912–1931 of each monomer, whereas tetramerization is facilitated by interactions between small β-barrel (SBB) domains that bind two oppositely oriented dimers. While SBB domains primarily facilitate tetramerization, soma studies suggests they may also participate in recognizing RNA-binding domains, implying a possible role in substrate recognition that warrants further investigation [149].

Another notable protein binding scaffold in UBR5 is its N-terminal RCC1-like domain, consisting of seven tandem repeats that adopt a structure similar to the chromatin-binding protein RCC1. SBB domains are inserted between these RCC1 repeats via extended, flexible loops, alongside the ubiquitin-associated (UBA) domain, which interacts with both mono- and polyubiquitin chains and is functionally important for ubiquitin chain elongation. UBR5 also contains a UBR domain capable of recognizing N-degron signals in vitro. However, this domain is structurally distinct from a well-characterized N-dergon pathway regulator UBR1, with a less prominent and more extended hydrophobic binding pocket, potentially influencing degron selection and broadening UBR5's substrate range beyond the canonical N-degron pathway. Finally, the catalytic HECT domain of UBR5 includes an MLLE domain, which is separated from the rest of HECT by flexible linkers and engages substrates through recognition of short linear motifs.

Building on these structural insights, the current mechanistic understanding of UBR5 substrate processing emphasizes its role in ubiquitin chain elongation rather than initiation. UBR5 has been shown to extend pre-existing K11- and K63-linked chains with K48 linkages, thereby marking substrates for proteasomal degradation [82], [84]. Importantly, UBR5 does

not catalyze polyubiquitylation de novo but instead engages acceptor ubiquitin molecules already attached to substrate proteins [30], [148]. Ubiquitylation can occur in *cis*, where the catalytic HECT domain modifies a substrate bound to the same UBR5 molecule, or in *trans*, where the active site of one subunit within a dimer or tetramer acts on a substrate positioned by the other. This arrangement suggests that UBR5 oligomerization may directly facilitate coordinated substrate processing. The ubiquitin-associated (UBA) domain provides strong and direct ubiquitin binding, while additional domains contribute to fine-tuning substrate specificity and enhancing overall binding affinity. Nevertheless, despite significant advances in resolving UBR5's structural architecture, the molecular principles that govern its substrate recognition remain poorly understood and represent a key focus for future studies.

1.6.2 UBR5-dependant nuclear protein quality control

Having outlined the structural and mechanistic basis of UBR5 function, it is equally important to consider how these molecular properties are reflected in cellular physiology. As a large and multifunctional E3 ubiquitin ligase, UBR5 is involved in diverse signaling pathways that control cell fate decisions. In particular, UBR5 has emerged as a critical regulator of processes that require precise timing and coordination, such as transcriptional regulation and cell cycle progression. Disruption of these pathways by UBR5 loss or dysregulation has profound consequences for genome stability, proliferation, and ultimately tumorigenesis.

A considerable body of work has therefore focused on the role of UBR5 in transcriptional regulation and cell cycle control. One of the recently characterized functions of UBR5 is its involvement in the G1/S transition through the degradation of the retinoblastoma protein (Rb) [150]. Although the exact molecular details of the UBR5–Rb interaction remain incompletely understood, UBR5 appears to act as an anti-phosphodegron ligase. In this system, UBR5 preferentially recognizes and ubiquitylates the unphosphorylated form of Rb in early G1, thereby targeting it for proteasomal degradation. Phosphorylation of Rb by Cdk4/6 and Cdk2 induces conformational changes that reduce UBR5 binding affinity, effectively

stabilizing Rb and preventing its degradation. In addition to regulating the G1/S transition, UBR5 also influences S-phase progression. It interacts with translesion synthesis polymerase η, a replication fork component critical for maintaining replication efficiency [151]. Loss of UBR5 leads to S-phase accumulation, slower replication fork progression, and elevated replication stress. Finally, UBR5 plays a crucial role in mitosis by binding to and promoting the polyubiquitylation of the checkpoint proteins BubR1, Bub3, and Cdc20, thereby facilitating the disassembly of the mitotic checkpoint complex (MCC) from the APC/C [152]. This activity is essential for anaphase onset and proper mitotic exit. Consistent with this, immunodepletion studies demonstrate that UBR5 loss delays checkpoint satisfaction and prolongs mitotic arrest, underscoring its importance in ensuring timely chromosome segregation.

UBR5 plays an important nuclear role in transcriptional regulation through orphan quality control, recognizing and eliminating unpaired transcription factors to establish dynamic gene regulatory network interactions that shape cell fate and adaptability. This includes c-Myc – normally part of the c-Myc/MAX transcriptional activation complex – and SPT5 – a subunit of the transcriptional elongation DSIF complex [153], [154]. Both substrates engage UBR5 through similar structural degron motifs located in their basic helix-loop-helix (c-Myc) and DNA-binding region (SPT5), which become accessible only upon complex dissociation. c-Myc contains two distinct degrons – one of which is a hydrophobic motif located in leucine zipper domains – that are both required for efficient UBR5-mediated degradation. Additionally, UBR5 mediates ligand-dependent degradation of RARA as part of the RARA/RXRA complex through competition with nuclear coactivators [155]. UBR5 competes with nuclear coactivators for binding to the conserved hydrophobic cleft in the receptor's ligand-binding domain.

1.6.3 UBR5 in ubiquitin signaling networks: interplay between OTUD5 and TIP12

In addition to its roles in transcription and cell cycle regulation, UBR5 also participates in more complex regulatory networks that integrate multiple ubiquitin-modifying enzymes. A recent study has uncovered a sophisticated interplay between UBR5, OTUD5, and TRIP12 that

establishes a combinatorial ubiquitin code for precise substrate regulation [96]. At the core of this system lies a feedback loop that couples the activities of E3 ligases and a deubiquitinase OTUD5.

OTUD5 acts both as a regulator and as a regulated substrate within this loop. On the one hand, it stabilizes UBR5 by removing K48-linked ubiquitin chains, thereby preventing UBR5 auto-ubiquitination. On the other hand, UBR5 targets OTUD5 for degradation, a process that is facilitated by TRIP12. TRIP12 initiates this pathway by assembling K29-linked ubiquitin chains on OTUD5, which are resistant to OTUD5's own DUB activity. These K29 chains then serve as recognition sites for UBR5, which extends them with K48 linkages to generate K29/K48 branched ubiquitin chains that promote OTUD5 degradation.

This cooperative system creates a regulatory triangle in which UBR5, OTUD5, and TRIP12 mutually control each other's stability and, most likely, the abundance of shared substrates. For instance, SPT16, a subunit of the FACT complex, has been implicated in the OTUD5–UBR5 regulatory axis, linking transcriptional repression with DNA repair [156]. Similarly, both TRIP12 and UBR5 contribute to RNF168 homeostasis, thereby preventing the excessive accumulation of DNA repair factors on chromatin [97]. However, whether SPT16, RNF168, and similar examples are truly shared substrates subject to simultaneous regulation by all three enzymes, or whether they represent separate bilateral interactions within the network, remains unresolved.

The question of which proteins constitute bona fide shared substrates of the UBR5–OTUD5–TRIP12 system is therefore a critical gap in our current understanding . Identifying such substrates would not only clarify the biological scope of this E3–E3–DUB circuit but also provide insight into how branched ubiquitin architectures are integrated into transcriptional control, DNA repair, and potentially oncogenic signaling. Addressing this challenge will require comprehensive proteomic approaches capable of detecting branched chain linkages, as well as functional studies to determine the physiological relevance of putative shared targets.

1.6.4 UBR5 accumulation promotes pan-cancer progression.

Given the broad spectrum of UBR5 function and its association with numerous agents of cell fate desisins such as MYC, it is logical that UBR5 expression affects malignant cell transformation. Multiple pan-cancer and tumor-specific analyses report recurrent UBR5 copy-number amplification and overexpression across diverse cancers, with particularly clear evidence in breast ovarian and colon cancers and supportive signals in others [150], [157], [158]. In METABRIC breast cancer (n=1,894), UBR5 was amplified in most subtypes and was enriched in poor-prognosis groups. Amplification associated with worse distant relapse-free survival, suggesting selection for increased expression to drive proliferation [150]. In ovarian cancer TCGA data, UBR5 was amplified in about 22% of cases and overexpressed, correlating with aggressive behavior and immunosuppressive tumor microenvironments [158]. A pancreatic cancer study citing TCGA found UBR5 amplification as a common alteration across cancers and showed UBR5 mRNA/protein upregulation broadly in tumor datasets [159]. Collectively, these findings support describing UBR5 as clinically relevant and as a potential therapeutic target in pan-cancer treatment.

In conclusion, UBR5 is a central organizer of nuclear protein quality control, leveraging a modular, oligomerization-enabled HECT architecture to edit ubiquitin chains and time the turnover of key nuclear factors involved in transcription, DNA replication/repair, and mitosis. By coupling substrate recognition to K48-biased chain elongation—often in cis/trans across dimers and tetramers—UBR5 enforces orderly G1/S entry, replication dynamics, and checkpoint exit, while orchestrating orphan quality control of transcriptional regulators. Its embedding within E3–DUB circuits (e.g., with OTUD5 and TRIP12) further integrates branched ubiquitin codes into chromatin-associated regulation. Dysregulation of these functions contributes to pan-cancer progression, highlighting UBR5 as both a guardian of nuclear proteostasis and a therapeutically promising, yet mechanistically complex, target. While recent progress has proven UBR5 as a crucial player in nuclear processes regulation, comprehensive, systematic studies are still required to fully define its functions and therapeutic potential.

1.7 Aim of the study

In this study, we comprehensively investigate the phenotypic consequences of UBR5 loss in both non-malignant and colon cancer cell lines, with a particular focus on its function as an E3 ubiquitin ligase in key nuclear processes, including transcriptional regulation, RNA splicing, and chromatin remodeling. We hypothesize that UBR5 represents a central regulator of nuclear proteome integrity and aim to provide evidence for this by systematically assessing alterations in protein stability, ubiquitylation patterns, and downstream functional outcomes across UBR5-dependent proteins. In doing so, we seek to delineate UBR5's contribution beyond transcriptional regulation, distinguish between universal versus disease-specific phenotypes resulting from its loss, and identify direct UBR5 substrates within the splicing machinery.

2. Results

2.1 Phenotypic consequences of UBR5 loss

2.1.1 UBR5 knockout reduces proliferative potential of the cells

For the systematic characterization of UBR5 function, we selected a knockout (KO) model using the CRISPR/Cas9 gene-editing system, as it provides the most definitive approach to assess physiological roles by eliminating protein activity (Fig. 8A). This strategy enables the identification of the full spectrum of biological consequences, such as substrate accumulation or loss of ubiquitylation, by directly comparing UBR5 KO and wild-type (WT) cells. The initial goal of the proteomic screen is to characterize UBR5 function under normal homeostatic conditions.

To achieve this, human retinal pigment epithelium cells immortalized by hTERT (RPE-1 cells) were chosen for the study. RPE-1 cells are widely used as a “normal-like”, non-transformed cell line in cell biology research. They maintain a stable near-diploid karyotype with a modal chromosome number of 46 and lack transformed phenotypes, making them highly amenable to CRISPR-mediated gene knockouts. These characteristics establish RPE-1 cells as an ideal system for comparative proteomic screening in a cellular context that closely resembles native physiological conditions.

Generation of UBR5 knockout (KO) cells (Fig. 8B) was followed by analyses of cell growth and cell-cycle profiles. Compared to wild-type (WT) control cells, UBR5 KO cells exhibited a reduced growth rate, detectable as early as 24 hours after plating (Fig. 8C). This phenotype was consistently observed in three independent CRISPR-derived KO clones (2.4, 3.7, and 3.9), generated using two single guide RNAs (sgRNAs) targeting distinct loci of the UBR5 gene. This growth defect is consistent with data from DepMap, a disease-focused resource that systematically assesses the proliferative potential of cells following CRISPR/Cas9 knockout or RNAi knockdown. Genomic screens from DepMap similarly show that UBR5 depletion reduces proliferative capacity in a wide range of cell lines (Fig. 8D).

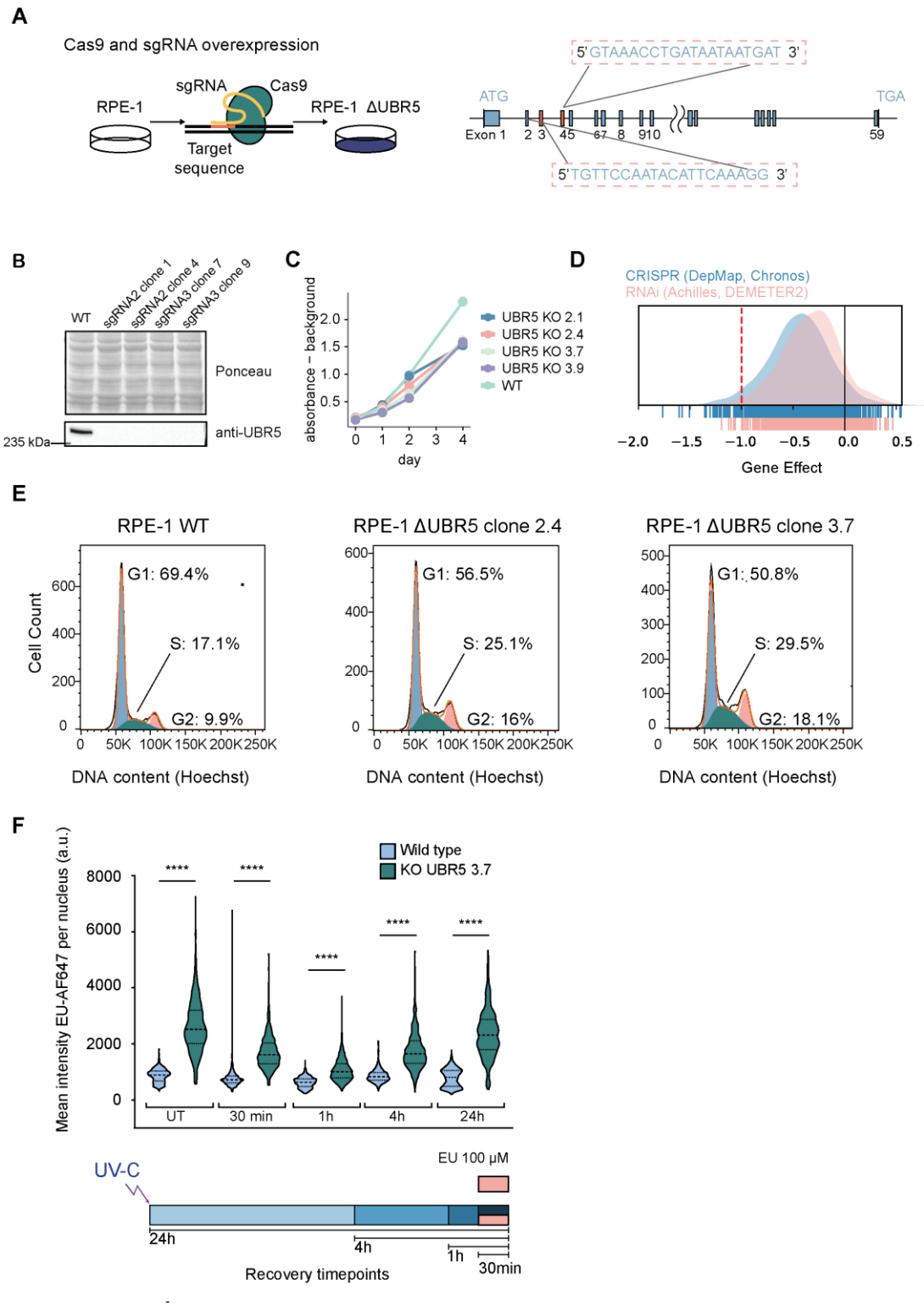
A
Cas9 and sgRNA overexpression
sgRNA
Cas9
RPE-1
RPE-1 ΔUBR5
Target sequence
5' GTAAACCTGATAATAATGAT 3'
ATG
TGA
Exon 1
2 3
45
67
8
910
59
5' TGTTCCAATACATTCAAAGG 3'
B
WT
sgRNA2 clone 1
sgRNA2 clone 4
sgRNA3 clone 7
sgRNA3 clone 9
Ponceau
anti-UBR5
235 kDa
C
absorbance – background
day
UBR5 KO 2.1
UBR5 KO 2.4
UBR5 KO 3.7
UBR5 KO 3.9
WT
D
CRISPR (DepMap, Chronos)
RNAi (Achilles, DEMETER2)
Gene Effect
E
RPE-1 WT
RPE-1 ΔUBR5 clone 2.4
RPE-1 ΔUBR5 clone 3.7
Cell Count
G1: 69.4%
S: 17.1%
G2: 9.9%
G1: 56.5%
S: 25.1%
G2: 16%
G1: 50.8%
S: 29.5%
G2: 18.1%
DNA content (Hoechst)
F
Wild type
KO UBR5 3.7
Mean intensity EU-AF647 per nucleus (a.u.)
UT
30 min
1h
4h
24h
UV-C
EU 100 µM
Recovery timepoints

Figure 8 UBR5 KO cell line generation and phenotypical consequences of UBR5 loss.
A. Schematic representation of the CRISPR/Cas9-based strategy of UBR5 KO cells generation. The schematic on the right shows the position of UBR5 gene targeting, and the targeting sequence. **B.** Western blot analysis showing the efficiency of UBR5 depletion in four different clones of RPE-1 cells, Ponceau: loading control. **C.** Growth curves of RPE-1 WT and RPE-1 UBR5 KO. Data are presented as mean of three independent experiments (N = 3). **D.** Probability of Gene dependency in human cells. A score of 0 is equivalent to a non-essential gene while -1 corresponds to the median of all common essential genes. **E.** Cell-cycle distribution of RPE-1 WT and UBR5 KO clones 2.4 and 3.7. **F**. Nascent RNA signal across recovery in WT and UBR5 KO. Violin plots show the distribution of mean nuclear EU-AF647 intensity per cell under untreated conditions and after UV irradiation with 30 min, 1 h, 4 h, and 24 h recovery (**** represents p-value < 0.0001, t-test).

Cell-cycle profiling of asynchronous cells using flow cytometry revealed a shift toward actively cycling populations in UBR5 KO cells, with an increase in the proportion of cells in the S and G2 phases and a corresponding decrease in the G1 phase (Fig. 8E). These findings are consistent with previous reports that UBR5 depletion disrupts cell-cycle regulation [151], further supporting its role in replication control.

Finally, RNA production dynamics analysis by EU incorporation — which labels nascent RNA — showed that UBR5 is required for proper transcriptional repression immediately following genotoxic stress (UV-induced DNA damage) (Fig. 8F). Loss of UBR5 impairs shutdown of RNA synthesis (higher EU at 1 h) and accelerates transcription recovery (elevated EU at 4 h and 24 h). The exaggerated and prolonged EU incorporation in UBR5 KO cells indicates that UBR5 normally enforces both damage-induced transcriptional silencing and controlled resumption of RNA synthesis during recovery.

2.1.2 UBR5 loss reshapes nuclear proteome

To investigate the impact of UBR5 loss on cellular processes, we first assessed changes in the global proteome by comparing total protein expression levels between the WT RPE-1 cell line and four independent UBR5 KO RPE-1 clones. Comparative analysis of the proteomic profiles across these clones revealed a correlation with their growth dynamics in culture. Heatmap visualization of the proteome changes demonstrated that clone 2.1 exhibited the fewest alterations, consistent with its fastest growth rate (Fig. 1C, Fig. 9A). In contrast, clones 2.4 and 3.7, generated with different sgRNAs targeting distinct genomic loci, showed a similar median magnitude of proteome changes and moderately slower growth rates, while

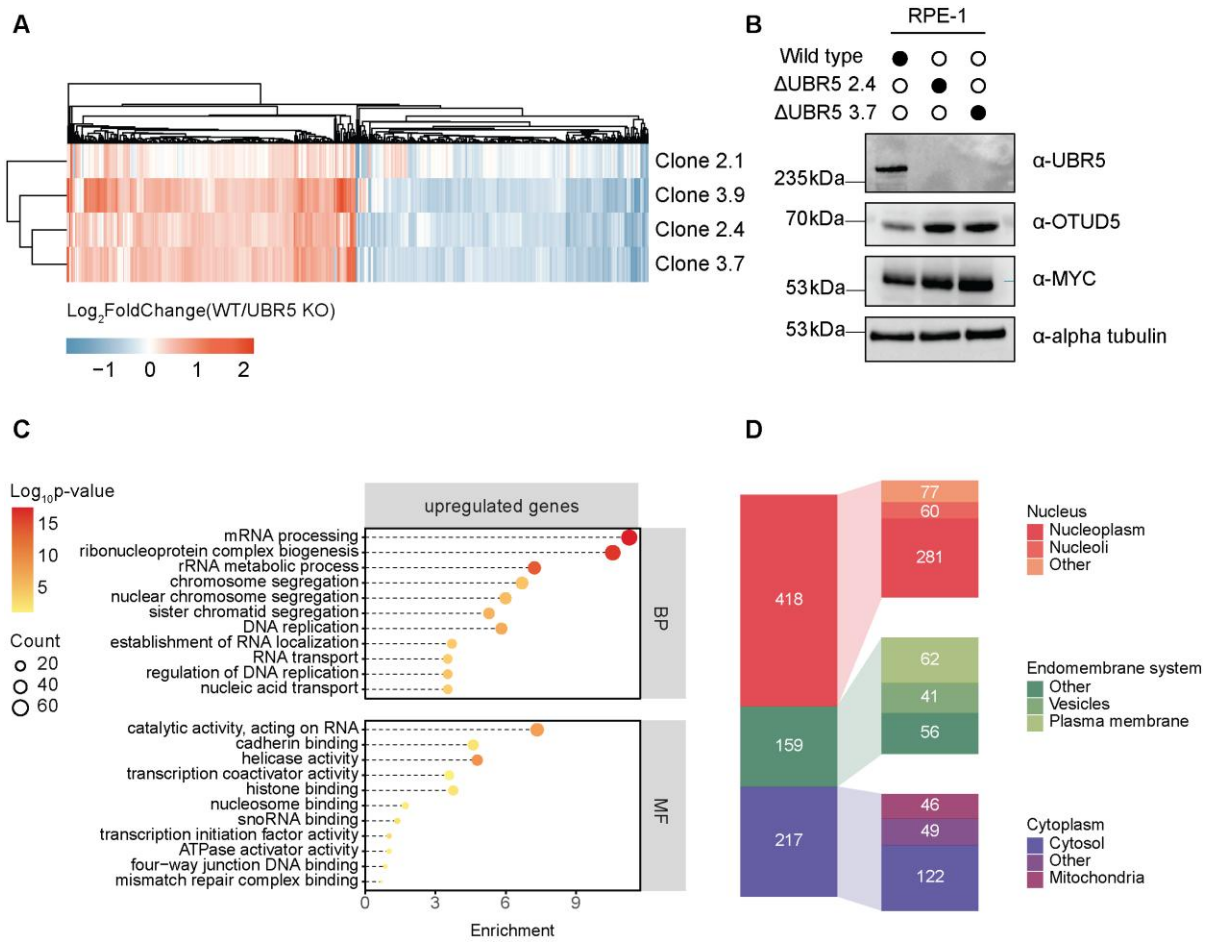

Figure 9. Proteomic consequences of UBR5 loss. A. Hierarchical clustering of log2-transformed fold changes of protein abundance in the RPE-1UBR5 KO clones compared to the RPE-1 WT cells. Columns represent genes that show statistically significant increase or decrease in at least two different clones (q-value < 0.05, limma moderated t-test.). **B.** Western blot analysis showing increased levels of of known UBR5 substrates OTUD5 and MYC in UBR5 KO clones 2.4 and 3.7 compared to the WT. Alpha-tubulin: loading control. **C.** Functional enrichment analysis performed with ClusterProfiler R package showing top ten significantly enriched GO terms associated with biological process (BP) and molecular function (MF) (q-value ≤ 0.05) across proteins upregulated in at least two UBR5 KO clones compared to WT. **D.** Primary cellular location of proteins significantly upregulated in at least two UBR5 KO clones compared to WT according to Human Protein Atlas (HPA) database.

clone 3.9 displayed the most pronounced proteomic alterations, potentially reflecting off-target effects, and corresponded to the slowest growth rate. Given our objective to characterize the cellular consequences of UBR5 loss-of-function, we focused subsequent analyses primarily on clones 2.4 and 3.7, as they represent the biologically relevant and reproducible models of UBR5 depletion including consistent gain of MYC and OTUD5 (Fig. 9B). Notably, MYC is a well-characterized substrate of UBR5, while OTUD5 is an emerging functional associate.

Clone 3.9 was included in some analyses to capture the broader phenotypic spectrum but was interpreted with caution due to the possibility of confounding off-target effects.

As mentioned above, since UBR5 is reported to be involved in proteasomal degradation, its depletion is expected to result in an accumulation of target proteins. Therefore, proteins showing significant upregulation upon UBR5 loss in at least two of the three analyzed clones are considered the primary focus of our total protein expression analysis. Functional enrichment analysis using Gene Ontology (GO) terms revealed that the upregulated proteins are predominantly associated with nuclear processes (Fig. 9C), which could be broadly clustered into three interconnected functional groups. The first group includes proteins involved in chromatin remodeling and transcription initiation (e.g., “transcription coactivator activity,” “histone binding,” and “nucleosome binding”) suggesting alterations in the gene expression program that may underlie the observed elevated transcriptional activity. The second group comprises regulators of RNA metabolism and ribonucleoprotein assembly (e.g., “catalytic activity acting on RNA,” “mRNA processing,” “ribonucleoprotein complex biogenesis”), indicating a potentially impaired splicing program. The third group includes proteins involved in DNA replication and genome maintenance (e.g., “regulation of DNA replication” and processes related to “chromosome,” “nuclear,” and “sister chromatid segregation”), reflecting observed alterations in S-phase progression, possibly reflecting disrupted replication fork control, impaired repair of replication-coupled lesions, and improper mitotic apparatus preparation for timely G2 entry. Consistent with these findings, the top enriched GO terms also reflect the subcellular localization of the upregulated proteome (Fig. 9D): more than half of the proteins with increased abundance are localized in the nucleus, with a notable fraction enriched in the nucleoplasm.

2.1.3 UBR5 loss decreases ubiquitylation levels of the nuclear proteins

To identify which nuclear pathways are directly regulated by UBR5, we complemented our global proteome analysis with ubiquitin remnant profiling coupled with quantitative mass spectrometry using stable isotope labeling by amino acids in cell culture (SILAC). This

technique enriches lysine residues carrying a di-glycine (K-ε-GG) remnant produced during tryptic digestion of ubiquitylated proteins, enabling their site-specific quantification (Fig. 10A). By mapping these modified lysines across the proteome, the ubiquitylome provides a high-resolution view of how ubiquitin occupancy changes in response to UBR5 loss. Given UBR5's E3 ligase catalytic activity, we expect that its depletion would reduce ubiquitylation level of direct substrates, reflecting its loss in the cells. However, the method is inherently biased toward detecting changes at primary ubiquitylation sites and doesn't capture ubiquitin chain elongation, branching or non-canonical topologies. This limitation is particularly relevant because UBR5's enzymatic behavior depends on its substrate recognition mechanism. As previously mentioned, the UBA domain of UBR5 favors substrates that are already ubiquitylated, positioning UBR5 primarily as a chain elongator rather than a chain initiator. At the same time, UBR5 oligomers can present multiple catalytic domains to a substrate, enabling "secondary" ubiquitylation of nearby lysines once the substrate is properly engaged. Although diGly-based profiling cannot fully resolve these primary attachment events, it nevertheless provides biologically meaningful and reliable readouts of UBR5-dependent ubiquitylation. Thus, in the context of UBR5 biology, ubiquitylome profiling remains a valid approach to identify the subset of substrates and regulatory pathways directly governed by UBR5 ligase activity.

Two independent double-SILAC experiments were performed in triplicate using UBR5 KO clones 2.4 and 3.7, each compared to wild-type RPE-1 cells. In both clones, we identified a predominance of decreased ubiquitylation sites relative to increased ones, consistent with the ligase activity of UBR5 (Fig. 10B). Specifically, we quantified 312 significantly decreased sites in clone 2.4 and 271 in clone 3.7. Additionally, we pooled the datasets to ensure reproducibility and sufficient coverage of UBR5-dependent ubiquitylation sites. This approach increased the detectable UBR5-dependent ubiquitylation signature, revealing 407 decreased sites and underscoring the power of aggregated analysis to enhance coverage. As expected, the transcription factor MYC was among the hits and displayed multiple ubiquitylation sites that were reduced upon UBR5 loss (Fig. 10C). Importantly, a substantial fraction of proteins that lose ubiquitylation upon UBR5 loss demonstrated multi-site regulation: 26% of affected

proteins harbored more than one decreased ubiquitylation site, and under a more permissive statistical cutoff, this percentage rose to 55% (Fig. 10D).

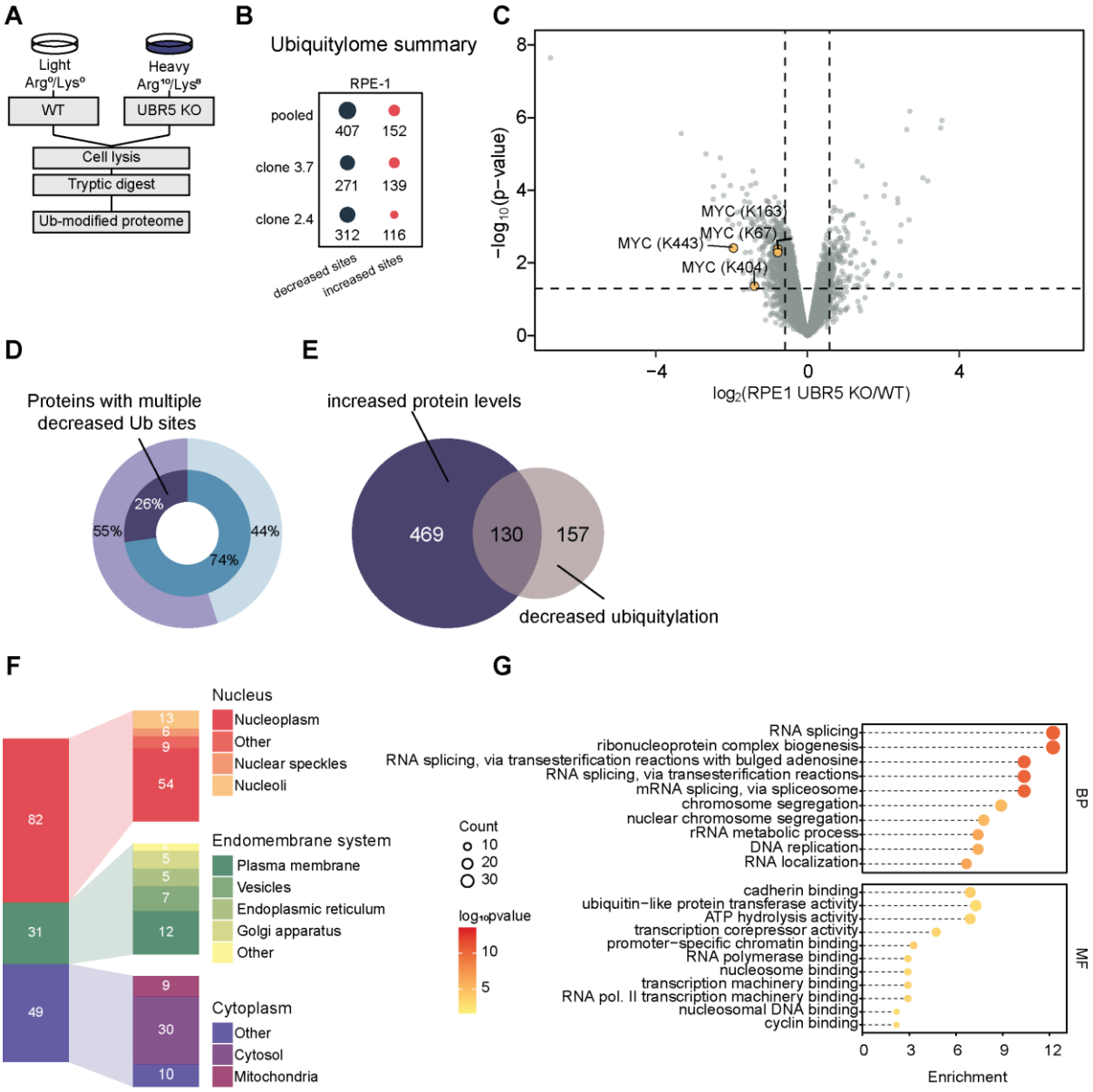

Figure 10 Changes in ubiquitylation profile in RPE-1 cells upon UBR5 loss.
A. Experimental outline of the comparative analysis of ubiquitin profiles between RPE-1 WT and RPE-1 UBR5 KO cells. Each UBR5 KO clone (2.4 and 3.7) was compared separately to WT in a double SILAC-labelling setup. Ubiquitin remnant peptides were enriched using diglycine-lysine–specific antibodies prior to analysis by liquid chromatography–tandem mass spectrometry (LC–MS/MS). For computational analyses, both datasets were pooled to increase data robustness. **B.** Summary of ubiquitylation sites that show statistically significant increases or decreases in ubiquitylation in UBR5 KO cells compared to WT (log2 fold change ≤ -1.5, p-value < 0.05, limma moderated t-test). **C.** Volcano plot of ubiquitylation sites quantified by ubiquitin remnant profiling in pooled analyses of UBR5 KO clones (three biological replicates each). The mean log2-transformed SILAC ratio (UBR5 KO/WT) across replicates is plotted against the −log10-transformed p-value. **D.** Proportion of proteins harboring multiple significantly decreasing ubiquitylation sites compared to single sites in the pooled analysis. Purple hues indicate proteins with multiple decreased sites; blue hues indicate proteins with single decreased site. Dark colors: log2 fold change ≤ −1.5, p-value < 0.05; light colors: log2 fold change ≤ −1.25, p-value < 0.05. **E.** Overlap between proteins showing an increase in protein abundance and a decrease in ubiquitylation site occupancy. **F.** Primary cellular location of proteins containing significantly decreased ubiquitylation sites in the pooled analyses of two UBR5 KO clones (2.4 and 3.7) compared to WT according to Human Protein Atlas (HPA) database. **G.** Functional enrichment analysis performed with ClusterProfiler R package showing top ten significantly enriched GO terms associated with biological process (BP) and molecular function (MF) (q-value ≤ 0.05) across proteins that exhibit decreased ubiquitylation in a pooled analyses of UBR5 clones compared to WT.

Analogous to total proteome profiling, we next assessed the subcellular localization and functional enrichment of proteins harboring UBR5-dependent ubiquitylation sites. Mapping to annotated cellular compartments revealed that approximately 50% of proteins with reduced ubiquitylation localize to the nucleus (Fig. 10F), paralleling changes in protein abundance. Functional enrichment analysis of these proteins are enriched for the same functional GO term categories that were identified in the total proteome dataset (Fig. 10G). The most statistically significant terms were associated with RNA metabolism and ribonucleoprotein assembly, with a particularly prominent enrichment in processes linked to RNA splicing. Additional enriched categories included chromatin-associated processes and DNA replication-related modules, consistent with the nuclear-centric role of UBR5.

Our data backs up more established roles of UBR5 in transcriptional regulation and cell-cycle control alongside with less characterized regulation of RNA splicing machinery. While experiments in B-cells support the role UBR5 in maintaining spliceosome component stability and modulating alternative splicing, the precise molecular mechanism and direct substrates of UBR5 within spliceosome are still under active investigation [160].

2.2 Colon cancer cells exhibit a stronger phenotype upon UBR5 loss

2.2.1 Orphan protein quality control: transcription and beyond

Next, we wanted to test whether the UBR5-dependant signatures observed in “normal-like” cells are biologically relevant in a disease context. Therefore, we extended our study to colon cancer cells. First, we obtained alteration frequencies, co-alteration comparisons, z-scored mRNA expression, and mutation maps via cBioPortal for Cancer Genomics (https://www.cbioportal.org), querying TCGA PanCancer Atlas colorectal studies and associated RNA-seq datasets. Colorectal cancer (CRC) cell lines frequently have UBR5 alterations such as mRNA overexpression or gene amplification (Fig. 11A), and these alterations have been linked to p53 pathway dysfunction in CRC (Fig. 11B). Additionally, many colon cancers also carry APC mutations, however, a direct statistical link between UBR5 and APC alterations in patient data is less established compared to the p53 connection and is significant only on the level of mRNA expression (Fig. 11C). Colorectal adenocarcinoma pseudodiploid human cell line DLD-1, which harbors mutations in both TP53 and APC, was selected as a representative CRC model for further analysis.

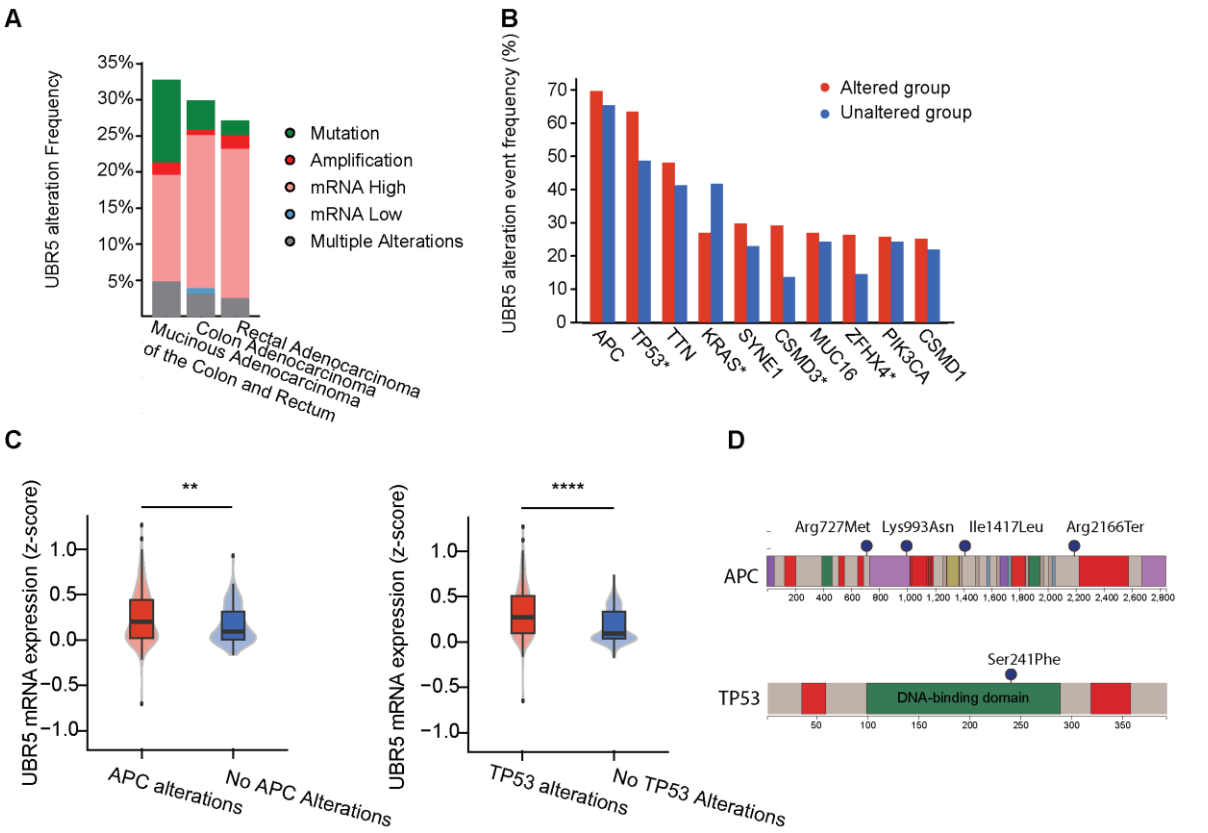

Figure 11 UBR5 alterations in colon cancer.
A. Summary of UBR5 alteration frequencies by study cohort. **B.** Bar graph ranking co-alteration event frequencies of recurrent colorectal cancer genes in samples with UBR5 alterations (Altered group) versus those without UBR5 alterations (Unaltered group); y-axis indicates percentage of patients per group with an alteration in the indicated gene. **C.** Z-scored expression of UBR5 mRNA between tumors with versus without APC alterations (left) and with versus without TP53 alterations (right); p-values from two-sided t-tests are indicated above each comparison. **D.** Positions of APC and TP53 mutations in DLD-1 cell line.

Using the same genome-editing strategy and proteomic workflows applied in RPE-1 cells, we generated UBR5 KO cell lines in DLD-1 and performed proteome abundance comparison between DLD-1 UBR5 KO and DLD-1cells. Although the number of differentially abundant proteins per clone was similar between the non-malignant and cancerous proteomes, DLD-1 showed a higher inter-clone overlap, resulting in a larger set of directionally consistent changes (Fig. 12C). This greater consensus likely reflects some inflation of overlap due to cancer-associated baseline variabilities. Nevertheless, the key functional enrichments observed in RPE-1, in particular, RNA processing, chromatin remodeling, transcriptional regulation, and

DNA replication/cell cycle processes were preserved in DLD-1, indicating that the UBR5-dependent signature is robust across cellular contexts (Fig. 12B).

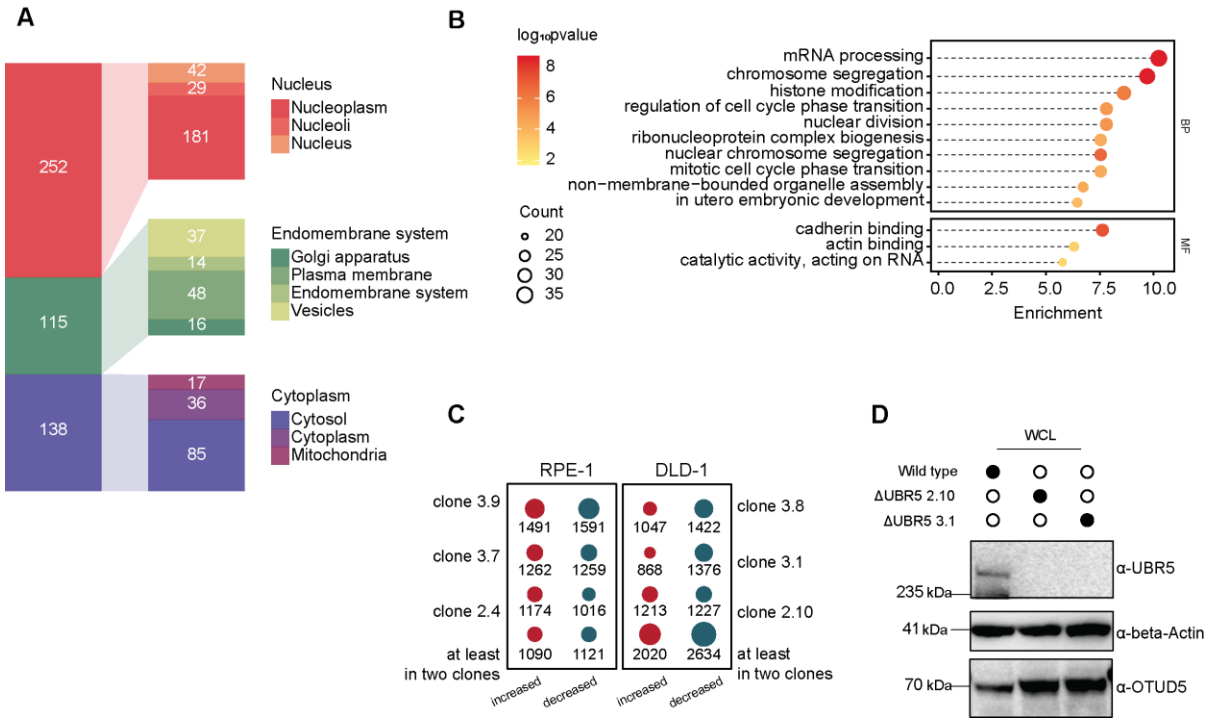

Figure 12 Proteomic consequences of UBR5 loss in cancer context.
A. Primary cellular location of proteins significantly upregulated in at least two UBR5 KO clones compared to WT according to Human Protein Atlas (HPA) database. **B.** Functional enrichment analysis performed with ClusterProfiler R package showing top ten significantly enriched GO terms associated with biological process (BP) and molecular function (MF) (q-value ≤ 0.05) across proteins upregulated in at least two UBR5 KO clones compared to WT. **C.** Summary of proteins that show statistically significant increases or decreases in abundance in UBR5 KO cells compared to WT in normal-like RPE-1 cells and in colon cancer DLD-1 cells (q-value < 0.05, limma moderated t-test). **D.** Western blot analysis showing increased levels of known UBR5 substrates OTUD5 and in DLD-1 UBR5 KO clones 2.10 and 3.1 compared to the DLD-1 WT. Beta-actin: loading control.

UBR5 has been implicated in the regulation of nuclear processes through the targeted ubiquitination of orphan proteins, suggesting that its loss may disrupt not only the levels of individual proteins but also the stoichiometry and functional integrity of critical nuclear complexes. Such disruption can affect the turnover of direct UBR5 substrates as well as their binding partners, thereby altering broader regulatory networks. To systematically assess this, proteome profiling was integrated with curated complex annotations retrieved from the EMBL Complex Portal.

Our analysis shows that indeed, many proteins associated with the functional groups of UBR5-dependant proteins were found to be components of defined protein complexes, and a number of complexes exhibited a coordinated increase in the abundance of multiple subunits (Fig. 13A). Notably, changes in protein levels associated with these protein complexes are often less pronounced in non-malignant RPE-1 cells compared to colon cancer DLD-1 cells. In several complexes, we observe a greater number of subunits being significantly affected (Intron binding complex, U2 small nuclear ribonucleoprotein complex, U4/U6.U5 small nuclear ribonucleoprotein complex, PAF1 complex, Integrator complex), and in some cases, additional complexes within the same functional network also exhibiting coordinated changes in protein levels (SIN3B histone deacetylase complex, ATAC complex, anaphase-promoting core complex).

Consistent with previous studies on known UBR5 substrates, we observed a coordinated increase in SUPT4H1 and SUPT5H, which together form the heterodimeric DRB Sensitivity-Inducing Factor (DSIF) transcription elongation factor complex, as well as in the mitotic checkpoint complex subunits BUB1B, BUB3, and CDC20. Additionally, a subunit of the PAF1 complex (CDC73) has previously been reported to depend on UBR5 enzymatic activity, and our proteomic data expand this observation by demonstrating that the abundance of other PAF1 subunits is also UBR5-dependent. Beyond these, several other transcriptional regulators, such as components of the Integrator complex and the BRE1 E3 ubiquitin ligase complex, displayed a coordinated upregulation upon UBR5 loss. Proteins involved in chromatin remodeling and epigenetic regulation also formed a tightly interconnected protein network, notably centered around HDAC2/HDAC1. This pattern reflects a phenomenon wherein the dysregulation of a single subunit destabilizes the stoichiometric balance across associated protein complexes.

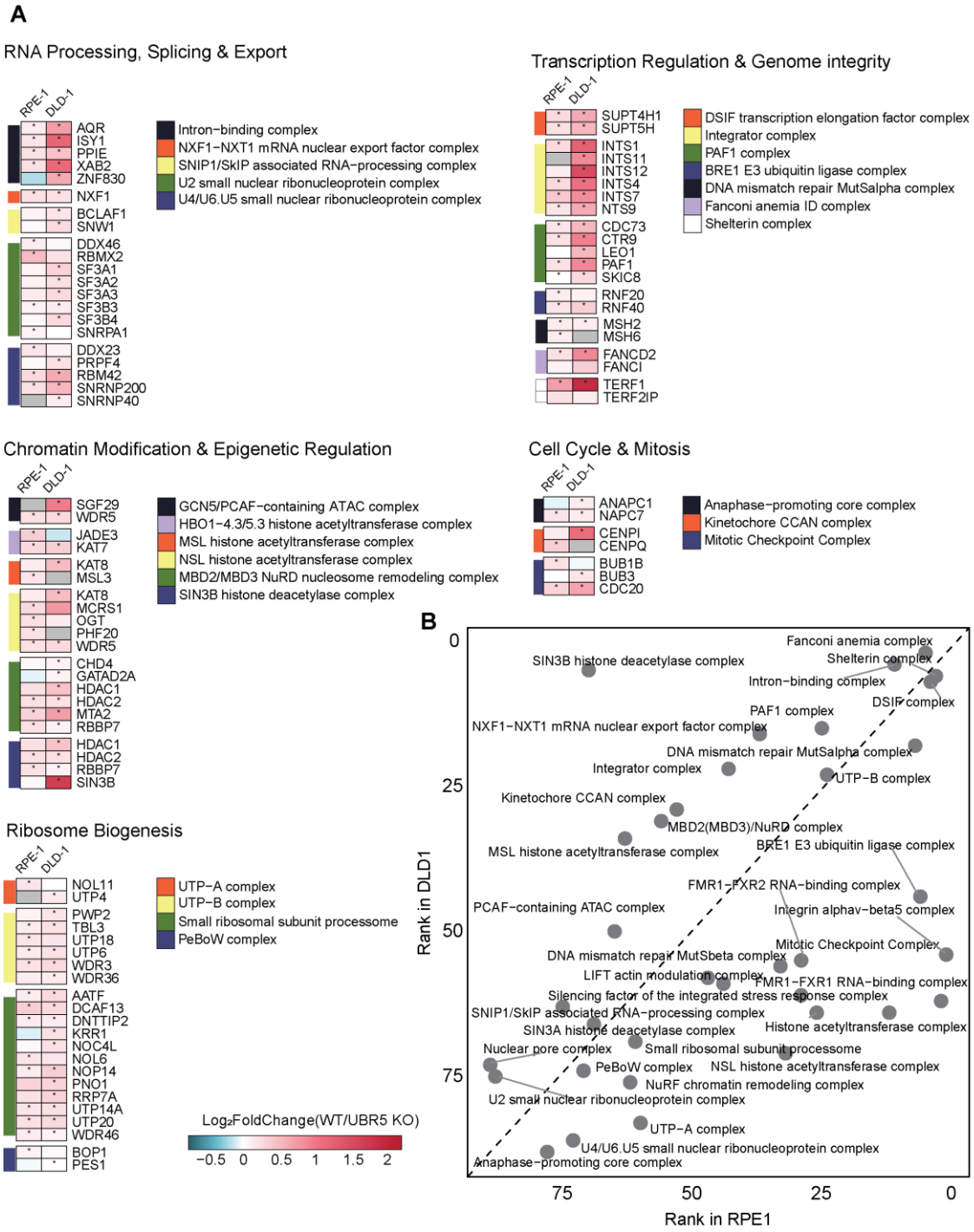
A
RNA Processing, Splicing & Export
RPE-1
DLD-1
AQR
ISY1
PPIE
XAB2
ZNF830
NXF1
BCLAF1
SNW1
DDX46
RBMX2
SF3A1
SF3A2
SF3A3
SF3B3
SF3B4
SNRPA1
DDX23
PRPF4
RBM42
SNRNP200
SNRNP40
Intron−binding complex
NXF1−NXT1 mRNA nuclear export factor complex
SNIP1/SkIP associated RNA−processing complex
U2 small nuclear ribonucleoprotein complex
U4/U6.U5 small nuclear ribonucleoprotein complex
Transcription Regulation & Genome integrity
SUPT4H1
SUPT5H
INTS1
INTS11
INTS12
INTS4
INTS7
INTS9
CDC73
CTR9
LEO1
PAF1
SKIC8
RNF20
RNF40
MSH2
MSH6
FANCD2
FANCI
TERF1
TERF2IP
DSIF transcription elongation factor complex
Integrator complex
PAF1 complex
BRE1 E3 ubiquitin ligase complex
DNA mismatch repair MutSalpha complex
Fanconi anemia ID complex
Shelterin complex
Chromatin Modification & Epigenetic Regulation
SGF29
WDR5
JADE3
KAT7
KAT8
MSL3
KAT8
MCRS1
OGT
PHF20
WDR5
CHD4
GATAD2A
HDAC1
HDAC2
MTA2
RBBP7
HDAC1
HDAC2
RBBP7
SIN3B
GCN5/PCAF−containing ATAC complex
HBO1−4.3/5.3 histone acetyltransferase complex
MSL histone acetyltransferase complex
NSL histone acetyltransferase complex
MBD2/MBD3 NuRD nucleosome remodeling complex
SIN3B histone deacetylase complex
Cell Cycle & Mitosis
ANAPC1
NAPC7
CENPI
CENPQ
BUB1B
BUB3
CDC20
Anaphase−promoting core complex
Kinetochore CCAN complex
Mitotic Checkpoint Complex
Ribosome Biogenesis
NOL11
UTP4
PWP2
TBL3
UTP18
UTP6
WDR3
WDR36
AATF
DCAF13
DNTTIP2
KRR1
NOC4L
NOL6
NOP14
PNO1
RRP7A
UTP14A
UTP20
WDR46
BOP1
PES1
UTP−A complex
UTP−B complex
Small ribosomal subunit processome
PeBoW complex
Log2FoldChange(WT/UBR5 KO)
−0.5 0 0.5 1 1.5 2
B
Rank in DLD1
Rank in RPE1
0
25
50
75
Fanconi anemia complex
SIN3B histone deacetylase complex
Shelterin complex
Intron−binding complex
DSIF complex
PAF1 complex
NXF1−NXT1 mRNA nuclear export factor complex
DNA mismatch repair MutSalpha complex
Integrator complex
UTP−B complex
Kinetochore CCAN complex
MBD2(MBD3)/NuRD complex
MSL histone acetyltransferase complex
BRE1 E3 ubiquitin ligase complex
FMR1−FXR2 RNA−binding complex
PCAF−containing ATAC complex
Integrin alphav−beta5 complex
Mitotic Checkpoint Complex
DNA mismatch repair MutSbeta complex
LIFT actin modulation complex
FMR1−FXR1 RNA−binding complex
Silencing factor of the integrated stress response complex
SNIP1/SkIP associated RNA−processing complex
Histone acetyltransferase complex
SIN3A histone deacetylase complex
Nuclear pore complex
Small ribosomal subunit processome
PeBoW complex
NSL histone acetyltransferase complex
NuRF chromatin remodeling complex
U2 small nuclear ribonucleoprotein complex
UTP−A complex
U4/U6.U5 small nuclear ribonucleoprotein complex
Anaphase−promoting core complex

Figure 13. UBR5 loss causes directed accumulation of nuclear complexes subunits.
A. Heatmap of average log2-transformed fold changes in protein abundance in RPE-1 UBR5 KO clones compared to RPE-1 WT cells, and in DLD-1 UBR5 KO clones compared to DLD-1 WT cells. Asterisk (*) indicates statistical significance in at least two out of three clones ($q < 0.05$, limma moderated t-test). Proteins are grouped according to complex annotations and biological processes associated with the complexes. **B.** A rank-rank plot of complexes enriched in UBR5 KO compared to WT cells in DLD-1 and RPE-1 cells. Rank is calculated baes on z-scored values of complex coverage (upregulated proteins in complex/detected proteins in complex) and on z-scores of average log2-transfored fold change of complex subunits. Rank–rank plot of complexes enriched in UBR5 KO compared to WT cells in DLD-1 and RPE-1. Ranks were calculated based on z-scored values of complex coverage (upregulated proteins in complex / detected proteins in complex) and z-scores of the average log2-transformed fold change of complex subunits.

Interestingly, the broadest response to UBR5 depletion was observed among regulators of RNA metabolism and ribonucleoprotein assembly, highlighting a potentially critical role of UBR5 in maintaining the integrity of RNA-processing machinery. Both early nucleolar stages of ribosome biogenesis (UTP-B complex and the small ribosomal subunit processome) and early stages of spliceosome assembly on pre-mRNA (intron-binding complex, U2 snRNP, and the U4/U6·U5 tri-snRNP of the pre-catalytic B complex) are affected by UBR5 loss. Together, these central signatures, along with the broader complex-level effects, represent the characteristic proteomic response to UBR5 depletion.

A comparison of the proteome datasets revealed that a number of the same multiprotein complexes displayed coordinated changes upon UBR5 loss. In addition to alterations in the steady-state abundance of complex subunits, we also observed corresponding shifts in ubiquitylation levels within these assemblies. Although direct UBR5 substrates are not always unambiguously detected—owing to the site-specific and initiation-dependent bias of di-glycine profiling—these concordant patterns strongly suggest that UBR5 governs the functional integrity of several nuclear complexes through both direct and indirect mechanisms.

2.2.2 Universal and contextual outcomes of UBR5 loss

Next, we compared complex-level effects resulting from UBR5 loss in both cell lines. To do this, we ranked protein complexes by integrating subunit coverage and quantitative regulation within each cell line (Fig. 13B). For each annotated protein complex, a rank was assigned based on (i) the proportion of subunits showing significant differential regulation relative to the total number of detected subunits, and (ii) the magnitude of change, calculated

as the average log2-transformed fold change of UBR5-dependent subunits. Then these ranks were compared between the non-malignant and colon cancer cell lines. A higher similarity in complex ranks between the two cell lines indicates stronger evidence of a conserved complex-level phenotype attributable to UBR5 loss. This approach enables systematic identification of both the most conserved effects of UBR5 loss and cell line–specific, potentially cancer-specific, responses. To further reduce background noise in the analysis, we applied an additional filter, retaining only those complexes that also showed corresponding changes in the ubiquitylome dataset in at least one knockout cell line. We identify DSIF complex, Fanconi anemia complex, Shelterin complex, UTP-B and Intron binding complex as complexes that have consistently coordinated response across both cell lines. While top-ranking splicing-associated complexes display consistent, cross-context behavior, chromatin-associated complexes show mixed rank–rank concordance, indicating context-dependent regulation. In particular, the SIN3B histone deacetylase complex and the MBD2/MBD3-containing NuRD complex exemplify this pattern (Fig. 14B, D): despite using distinct recruitment modules and targets on chromatin, they share HDAC1/2 as the enzymatic core, which could account for their coordinated regulation in the colorectal cancer background. Notably, SIN3B's binding partner p53 is upregulated in DLD-1 but not in RPE-1 (Fig. 14A) [161]; although SIN3B can be recruited to p53-repressed promoters under stress, such recruitment typically requires promoter engagement by functional, DNA-binding-competent p53. Consequently, how altered p53 abundance, particularly in the setting of DNA-binding mutant p53—modulates SIN3B-dependent repression remains unresolved.

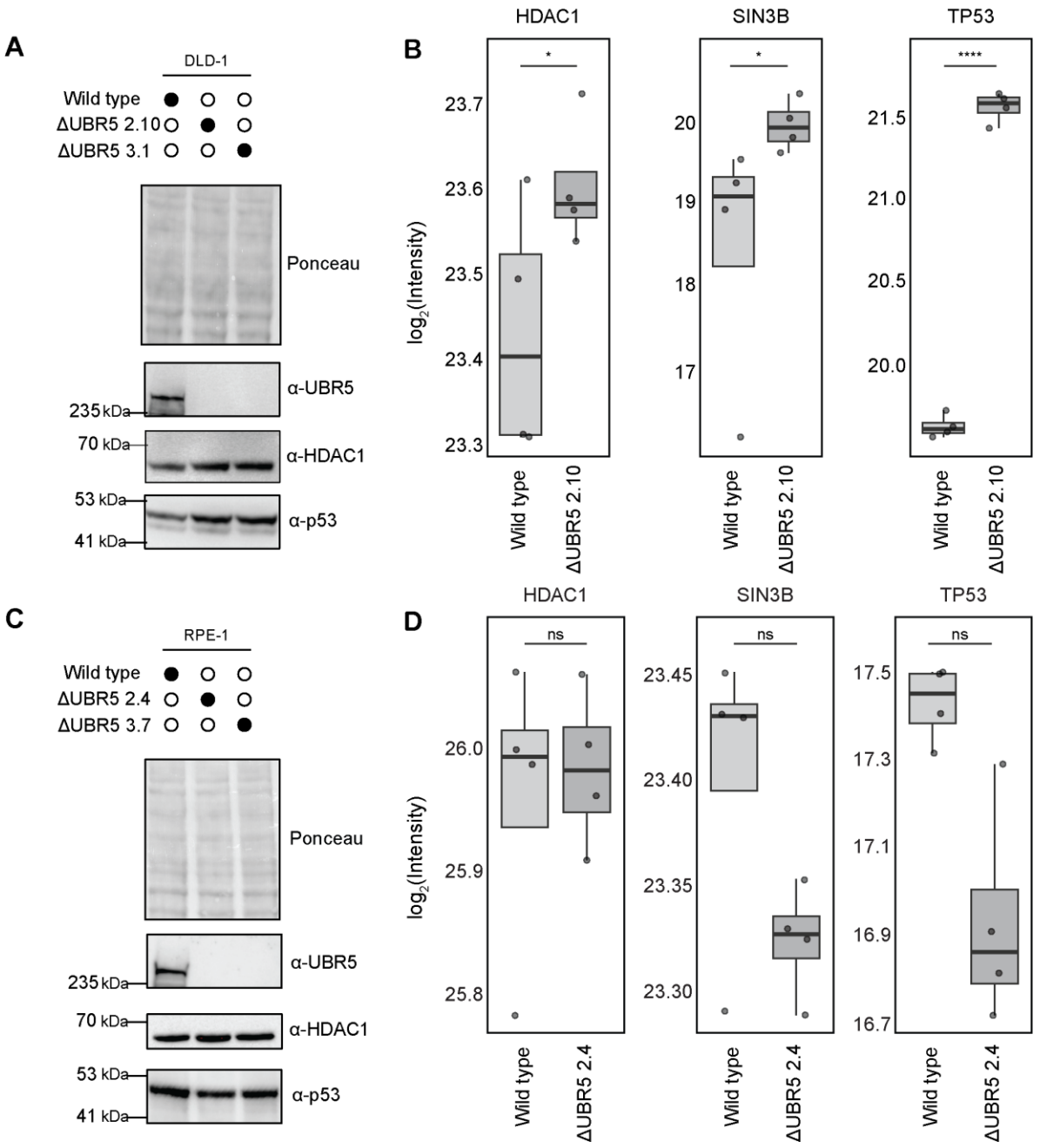

Figure 14. UBR5 loss reshapes epigenetic modulator abundance in disease-specific context. A., C, Western blot analysis showing p53 and HDAC1 accumulation upon UBR5 depletion in colon cancer DLD-1 cells (**A**), but not in normal-like RPE-1 cells (**C**). Ponceau: loading control. **B.** Peptide intensity of HDAC1, SIN3B and TP53 in WT and UBR5 KO in DLD-1 (**B**) and RPE-1 cells (**D**). Proteins were digested with trypsin, and peptides were analyzed by LC-MS/MS. The error bars represent the standard deviation from four biological replicates (ns – non-significant, *q < 0.05, **q < 0.01, ***q < 0.0001, ****q < 0.00001 limma moderated t-test).

2.2.3 Loss of UBR5 affects the stoichiometry of multiple interconnected splicing-associated complexes.

As discussed in the previous section, we identified splicing-associated factors among context-independent substrates of UBR5. This finding aligns with the modular and hierarchical assembly of the human spliceosome, whose core sub-complexes exhibit conserved compositions across cell types. Such conservation provides a stable framework for detecting and correcting perturbations in complex stoichiometry. When the balance of protein abundance is disrupted, coordinated changes in gene expression are often triggered to maintain the integrity of splicing-associated complexes.

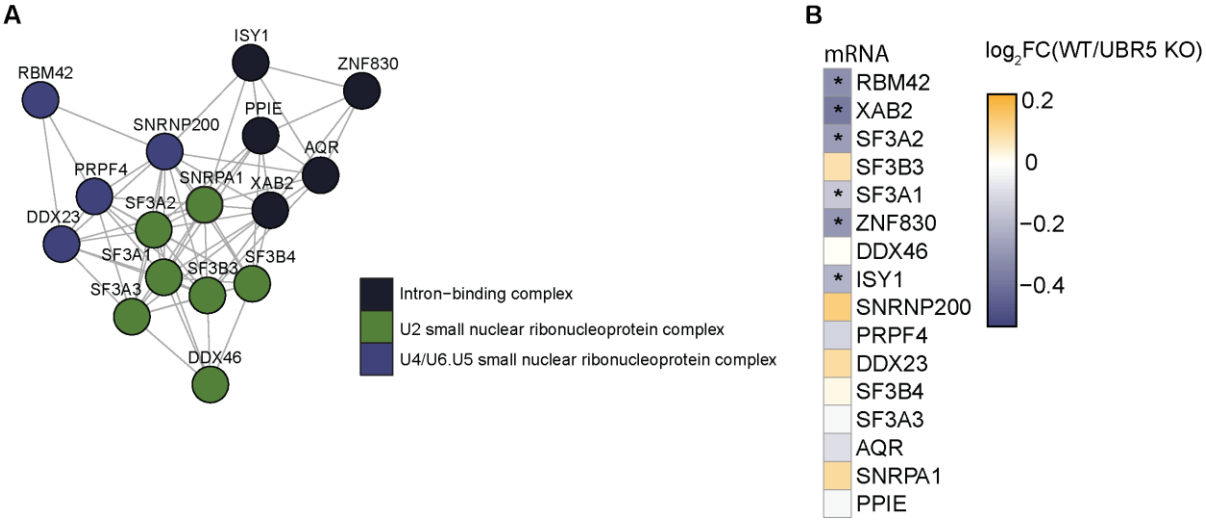

Figure 15 UBR5 loss causes splicing factors accumulation.
A. Predicted functional association network of splicing regulatory factors identified in our screen. The network is based on experimental evidence, text mining, and database parameters provided by STRING (https://string-db.org/), with a minimum required interaction score cutoff of 0.9.**B.** Heatmap of average log2-transformed changes in mRNA expression in RPE-1 UBR5 KO clones 2.4 and 3.7 compared to RPE-1 WT. Asterisk (*) indicates statistical significance in both clones ($q < 0.05$, t-test).

Building on this principle, we constructed a high-confidence functional network using STRING, focusing on proteins that exhibited significant upregulation in the total proteome or reductions in site-specific ubiquitin occupancy within the ubiquitylome of either model cell line (Fig. 15A). This approach allowed us to enrich the network for candidates potentially under direct or proximal control of UBR5 ligase activity. Notably, these proteins showed

consistent changes at both the proteomic and ubiquitylomic levels following UBR5 loss, while their transcript-level responses remained largely uncoordinated — consistent with post-transcriptional regulation of protein stability and complex homeostasis (Fig. 15B). Among these candidates, subunits of the intron-binding complex that emerged as prominent hits in rank–rank complex enrichment comparisons (Fig. 13B). Based on this observation we follow up intron-binding complex to reveal if it is a direct target of UBR5-mediated quality control.

2.3 Dissecting UBR5 substrate specificity within the intron-binding complex

2.3.1 UBR5 as a selective regulator of intron-binding complex subunit AQR

Previous studies in our laboratory conducted by Francesca Conte focused on the functional characterization of intro-binding complexes. To investigate its role, we performed low- and high-throughput proteomics experiments following siRNA-mediated knockdown (KD) of individual subunits—AQR, XAB2, or ISY1 (Fig. 16A). Interestingly, both high- and low-throughput proteomic approaches consistently demonstrated changes in the abundance levels of all three subunits upon depletion of any single subunit in different model cell lines (Fig. 16A, 16B). One possible explanation is changes in complex stoichiometry upon loss of one subunit expose degradation signals in the remaining subunits, leading to their destabilization in cell.

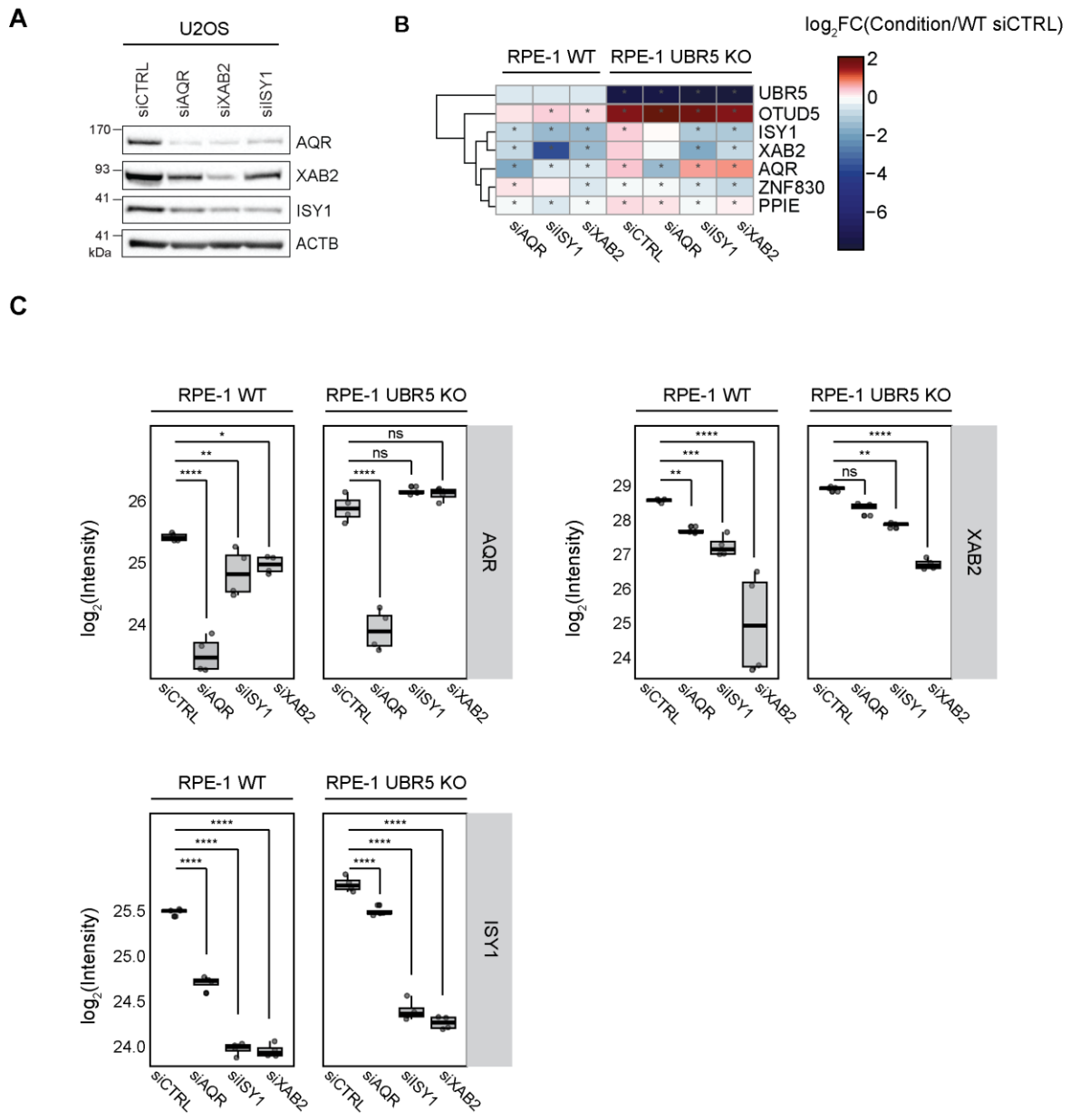

Figure 16. UBR5 KO rescues collateral loss of intron-binding complex subunit AQR.
A. Western blot analysis showing collateral loss of intron binding complex subunits AQR, XAB2 and ISY levels upon knockdown of each subunit (siAQR, siISY1, siXAB2). Beta-actin: loading control. **B.** Heatmap of log2-transformed fold changes in protein abundance in RPE-1 UBR5 KO clones compared to RPE-1 WT cells in either unchallenged conditions or upon knockdown of each subunit (siCTRL, siAQR, siISY1, siXAB2). Asterisk (*) indicates statistical significance in at least two out of three clones ($q < 0.05$, limma moderated t-test). **C.** Peptide intensity of AQR, XAB2 and ISY1 in RPE-1 WT and RPE-1 UBR5 KO in either unchallenged conditions or upon knockdown of each subunit (siCTRL, siAQR, siISY1, siXAB2). Proteins were digested with trypsin, and peptides were analyzed by LC-MS/MS. The error bars represent the standard deviation from four biological replicates (ns – non-significant, *$q < 0.05$, **$q < 0.01$, ***$q < 0.0001$, ****$q < 0.00001$ limma moderated t-test).

Given these observations, we hypothesized that one or more subunits of the intron-binding complex could be direct substrates of the ubiquitin ligase UBR5. To test this hypothesis, we repeated the siRNA KD experiments in RPE-1 UBR5 knockout (KO) cells. We reasoned that if a subunit is a direct substrate of UBR5, its proteomic response upon knockdown would be altered in the absence of the ligase. Indeed, our experiments revealed that, upon UBR5 loss, AQR abundance no longer followed the collateral changes observed in the other subunits of the complex, while XAB2 and ISY1 still showed the co-depletion to some extent (Fig. 16C). These findings strongly suggest that AQR is a direct substrate of UBR5, whereas XAB2 and ISY1 are indirectly affected through complex destabilization.

2.3.1 Dual E3 ligase control of AQR stability

UBR5 is a chain-elongating E3 ligase that promotes protein degradation by extending branched ubiquitin chains with K48 linkages on its substrates. To investigate whether UBR5, together with other E3 ligases, functions as a direct mediator of AQR stability**,** we employed an APEX-based proximity proteomics approach. This method relies on the biotinylation of proteins in close proximity to the tagged protein, providing insights into the interaction environment of AQR and revealing potentially multifaceted mechanisms of AQR quality control. To minimize artifacts associated with overexpression, AQR was endogenously tagged in U2OS cells (AQR-APEX2-3×FLAG), ensuring expression at physiological levels. In our experimental design, cells were treated with biotin-phenol and subsequently either exposed to hydrogen peroxide (H_2O_2) to induce proximity-dependent biotinylation or left untreated as a negative control (Fig. 17A).

As expected, functional enrichment analysis of enriched proteins showed a strong association with biological processes linked to RNA splicing and ribonucleoprotein complex biogenesis (Fig. 17B). In line with these findings, we also detected subunits of the intron-binding complex among the enriched proteins (Fig. 17D). Collectively, these results

underscore both the specificity and robustness of the APEX-based labeling and enrichment approach.

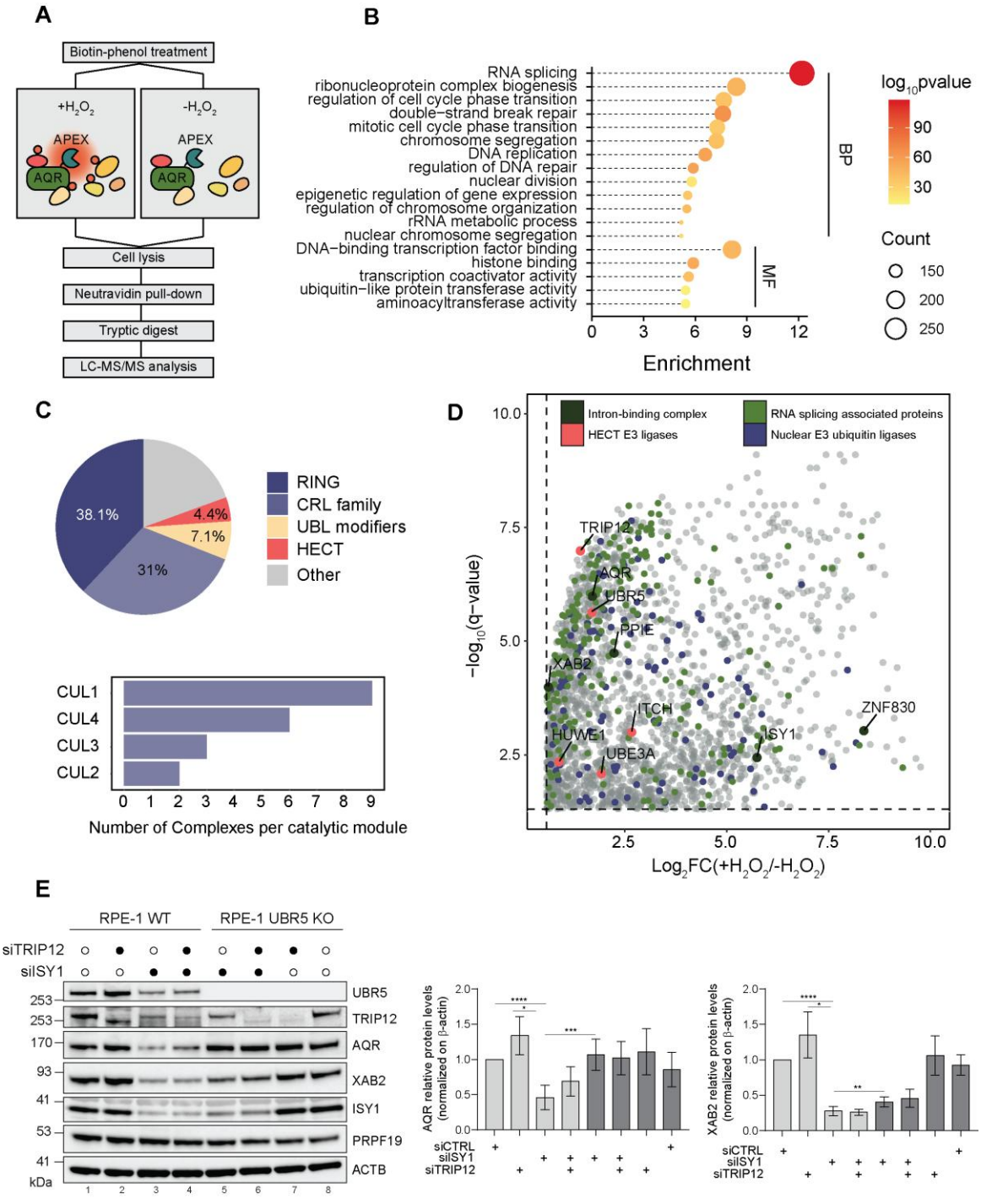

Figure 17. UBR5 and TRIP12 directly control AQR stability.
A. Experimental setup for AQR-APEX2-3×FLAG cell line proximity proteomics. **B.** Functional enrichment analysis performed with ClusterProfiler R package showing top ten significantly enriched GO terms associated with biological process (BP) and molecular function (MF) (q-value ≤ 0.05) across proteins enriched in AQR-APEX2-3×FLAG cell line treated with biotin-phenol with or H_2O_2 exposure. **C.** Upper panel: Enriched E3 ligase annotations according to the Human Proteostasis Consortium. Lower panel: Number of unique CRL complexes identified per catalytic subunit (CRL1, CRL2, CRL3, or CRL4) among the enriched E3 ligases. **D.** Volcano plot Volcano plot of the enriched proteins in AQR proximal proteome. Dashed lines indicate cut-offs for statistical significance (fold-change ≥ 1.5; q-value < 0.05). **E.** Western blot analyses and quantification of intron-binding complex subunits levels in upon single or co-depletion of ISY1 and TRIP12 in RPE-1 WT and RPE-1 UBR5 KO cells. Quantification of AQR, XAB2 and ISY1 levels from the respective Western blot experiments (n=3) is shown on the right. Protein levels were normalized on endogenous β-Actin levels and represented as log2 fold-change over siCTRL (*p<0.05, **p<0.01, ***p<0.001, ****p<0.0001, t-test).

Interestingly, we also detected a significant enrichment of proteins with ubiquitin-like protein transferase activity (Fig 17B). To further contextualize these findings, we integrated our dataset with annotated proteostasis network genes from the Proteostasis Consortium. This comparative analysis revealed that APEX-proximal E3 ligases include multiple functional classes, including RING, CRL family, and HECT ligases (Fig. 17C). Among the HECT-type ligases associated with AQR, we identified both UBR5 and TRIP12 (Fig. 17D). Notably, these enzymes have previously been implicated in the regulation of overlapping substrate degradation pathways, raising the possibility that AQR may represent an additional shared substrate. However, since both UBR5 and TRIP12 primarily function as ubiquitin chain elongators rather than initiators, it is possible that another E3 ligase serves as the initiating factor in the regulation of RNF stability. Although we identified a significant number of RING and CRL family members among the potential AQR interactors, the question of which E3 ligase serves as a priming ubiquitylation enzyme for AQR remains open.

We confirmed that TRIP12 influences AQR protein stability using western blot analysis. Experiments were performed in RPE-1 WT and RPE-1 UBR5 KO cells upon TRIP12 siRNA-induced depletion to determine whether TRIP12 is essential for AQR efficient degradation under steady-state conditions and whether its loss has any additive effect in the absence of UBR5. Similarly to UBR5, TRIP12 depletion alone in WT cells impaired AQR degradation (Fig, 17E). Notably, TRIP12 knockdown could also partially rescue collateral loss of AQR upon ISY1 knockdown. This confirms that ubiquitin chains generated by TRIP12 are necessary for AQR turnover. At the same time, TRIP12 loss in UBR5-depleted cells did not significantly

alter AQR stability, nor was stability further affected by additional knockdown of ISY1. These results suggest that UBR5-mediated ubiquitin chains act as a scaffold for TRIP12, which in turn ensures efficient degradation signal for AQR.

2.3.2 UBR5 loss facilitates changes in architecture of heterotypic ubiquitin chains

Finally, we focused on directly assessing ubiquitylation changes of AQR caused by UBR5 ligase loss. To this end, we performed pull-down of ubiquitylated proteins using OtUBD—a high-affinity ubiquitin-binding domain (UBD) derived from the Orientia tsutsugamushi deubiquitylase (DUB) (Fig. 18A, B). Compared to ubiquitin remnant profiling, this approach enables detection of total ubiquitylation levels of a protein of interest instead of specific ubiquitylation sites. Moreover, this approach detects lower- and higher–molecular-weight ubiquitylated species, which reflect differences in ubiquitin chain length. This distinction is particularly important for UBR5, which has been characterized as a ubiquitin chain elongator. For lower–molecular-weight substrates of the E3 ligase, such as OTUD5, ubiquitin chain remodeling is particularly evident (Fig.18C). We see that upon UBR5 loss its substrates exhibit lower–molecular-weight species ubiquitylated accumulation compared to the WT cells. This suggests that, in the absence of UBR5, its substrate accumulates as ubiquitylated species with non-degrative chains, highlighting the role of the ligase in controlling K48-linked chain elongation. Overall, these findings suggest that UBR5 ligase loss does not simply reduce ubiquitylation, but fundamentally alters the ubiquitin landscape of its substrates, causing increase in their stability.

Similar changes are more difficult to detect for AQR when comparing simple UBR5 KO cells to WT cells (Fig. 18D, E). This may be due to the limited availability of free intron-binding complex subunits, as their abundance is tightly coordinated to maintain stoichiometry. To overcome this limitation, we ‘force’ the system by knocking down individual complex subunits, XAB2 or ISY1. This depletion exposes previously masked binding surfaces, allowing AQR to engage with the priming E3 ubiquitin ligase and thereby reveal direct ubiquitylation

events that are otherwise difficult to observe in the intact complex. Notably, knockdowns of either XAB2 or ISY1 produced similar changes in AQR ubiquitylation upon E3 KO.

Upon intron-binding complex disruption in WT cells, the ubiquitylated population of AQR exhibits a diverse "laddering" pattern, reflecting the presence of multiple ubiquitin chain lengths (Fig. 18D, E). In contrast, UBR5 KO cells show an accumulation of lower–molecular-weight ubiquitylated AQR species, indicating impaired chain elongation. Interestingly, knockdown of TRIP12 in WT cells generates a distinct laddering pattern, which is disrupted in UBR5 KO cells, where the UBR5-specific pattern is maintained. These observations suggest that the UBR5 engages with AQR first, establishing ubiquitin modifications, which are then elongated or remodeled by TRIP12. Overall, this highlights a sequential and cooperative mechanism in which UBR5-induced chains create a scaffold for downstream chain elongation by TRIP12.

Figure 18. Validation of OtUBD pulldown of ubiquitylated proteins
A. Schematic illustrating the ubiquitin-binding domain (OtUBD) capturing ubiquitylated proteins**. B.** Western blot analysis of bulk ubiquitylated proteins in RPE-1 WT and RPE-1 UBR5 KO cell lines (clones 2.4 and 3.7), showing efficient OtUBD pulldown of ubiquitylated proteins. **C.** Western blot analysis of ubiquitylated OTUD5 and HDAC2 in RPE-1 WT and RPE-1 UBR5 KO cell lines (clones 2.4 and 3.7) enriched in the OtUBD pulldown. **D. – E.** Western blot analysis of ubiquitylated AQR in RPE-1 WT and RPE-1 UBR5 KO cells (clone 2.4) upon knockdown of the intron-binding complex subunit XAB2 (**D**.) or ISY1 (**E.**), and/or TRIP12 knockdown, with or without E1-activating enzyme inhibition.

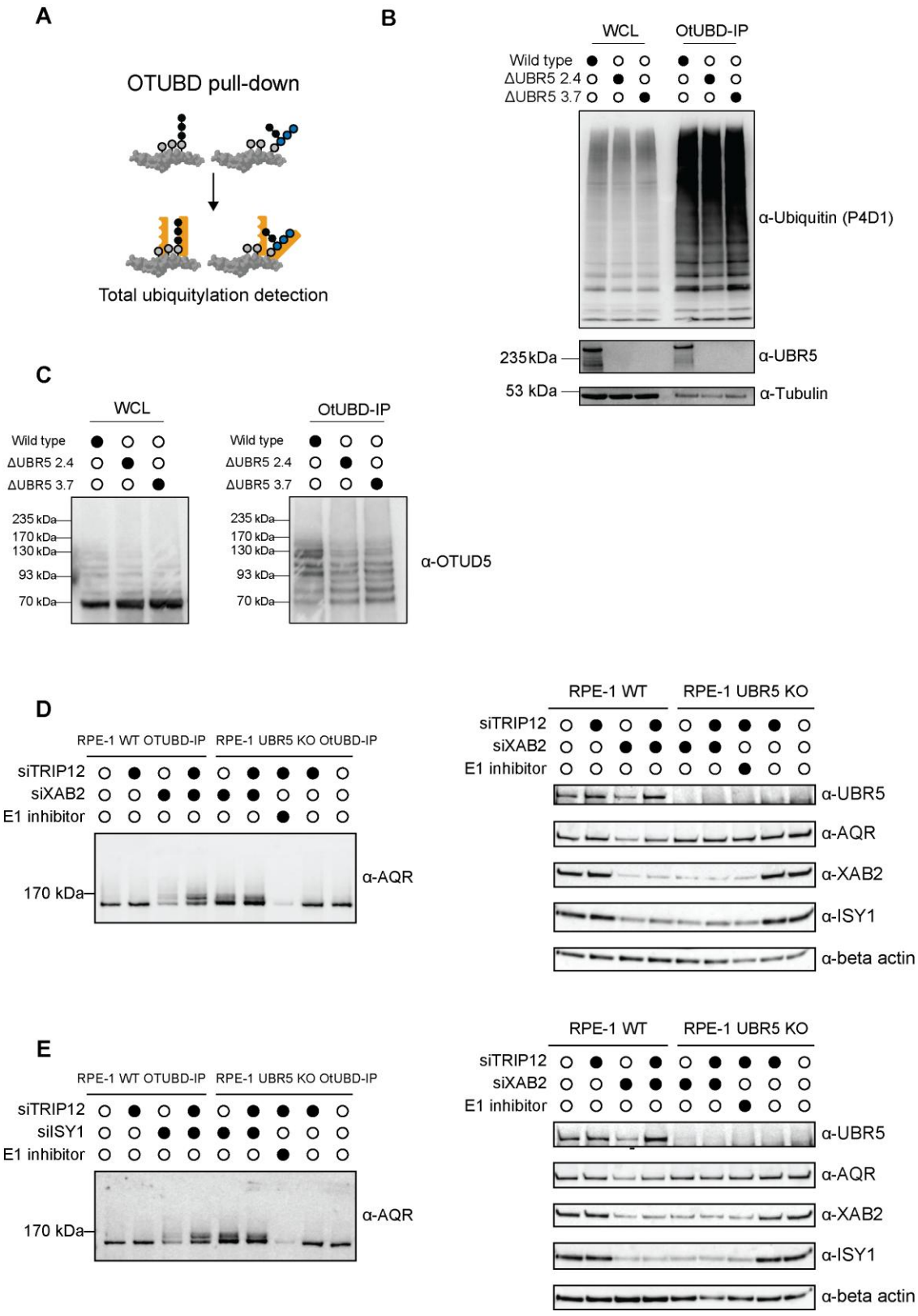
A
OTUBD pull-down
Total ubiquitylation detection
B
WCL
OtUBD-IP
Wild type
ΔUBR5 2.4
ΔUBR5 3.7
α-Ubiquitin (P4D1)
235kDa
α-UBR5
53 kDa
α-Tubulin
C
WCL
OtUBD-IP
Wild type
ΔUBR5 2.4
ΔUBR5 3.7
235 kDa
170 kDa
130 kDa
93 kDa
70 kDa
α-OTUD5
D
RPE-1 WT OTUBD-IP
RPE-1 UBR5 KO OtUBD-IP
siTRIP12
siXAB2
E1 inhibitor
170 kDa
α-AQR
RPE-1 WT
RPE-1 UBR5 KO
α-UBR5
α-AQR
α-XAB2
α-ISY1
α-beta actin
E
RPE-1 WT OTUBD-IP
RPE-1 UBR5 KO OtUBD-IP
siTRIP12
siISY1
E1 inhibitor
170 kDa
α-AQR
RPE-1 WT
RPE-1 UBR5 KO
α-UBR5
α-AQR
α-XAB2
α-ISY1
α-beta actin

3. Discussion

3.1 UBR5 is a master regulator of nuclear protein homeostasis

In this study, we systematically profiled the cellular consequences of UBR5 loss in both malignant (DLD-1) and non-malignant (RPE-1) setups to distinguish shared and context-specific UBR5-dependant programs. Building on prior work showing UBR5-sensitive orphan regulation within selective subunit pairs (e.g., transcription factor MYC/MAX complex or subunits SPT5/SPT4 within DSIF transcription elongation complex), our global proteomic and ubiquitylomic analyses extend this principle to the network level. We find that UBR5 governs multiple interconnected nuclear processes, including chromatin remodeling and transcriptional control, cell-cycle progression, and RNA metabolism. Although UBR5 directly acts on individual subunits, the dominant consequence of its loss manifests at the complex level, with coordinated, higher-order protein levels shifts observed across numerous nuclear multiprotein assemblies. This highlights the central function of UBR5 in enforcing stoichiometric balance and safeguarding nuclear protein homeostasis across diverse cellular states. Importantly, we also identify direct AQR among direct UBR5 substrates, positioning its direct role pre-mRNA splicing machinery quality control.

3.2 Transcription elongation and pause-release are disrupted upon UBR5 loss

Prior observations established that UBR5 governs the turnover of DSIF subunits, a core complex required for regulating transcriptional pausing and elongation [153]. Consistent with these findings, our data extends this principle by showing that UBR5 loss leads to the accumulation of multiple transcription-associated factors (Integrator complex, PAF1 complex, BRE1 E3 ubiquitin ligase complex), thereby disrupting the stoichiometric balance of transcriptional complexes.

Beyond DSIF, UBR5 also regulates the PAF1 complex, another key player in transcription elongation [162]. In UBR5 knockout (KO) cells, PAF1 accumulates at the complex level, which is likely to impair the dynamic control of pause–release within the transcription machinery. A related study by Aoi et al. 2021 demonstrated that excess SPT5 stabilizes RNA polymerase II in yeast and human cells, allowing polymerases to enter gene bodies more efficiently but with reduced processivity [163]. This is consistent with our observation of increased nascent RNA synthesis and accelerated transcription recovery following UV-induced DNA damage.

Together, these findings suggest that PUBR5 shapes transcription elongation dynamics through the coordinated turnover of both DSIF and PAF1 complexes, thereby influencing transcriptional output under basal and stress conditions. To rigorously test this model, future work should evaluate whether DSIF–PAF1 co-accumulation represents enhanced pause release and stabilized elongation complexes. Critical readouts include elongation-associated phosphorylation patterns such as Pol II CTD Ser2/Ser5, SPT5 phosphorylation, and recruitment/activity of CDK9/BRD4 and CDK12/13. Clarifying these signaling responses will determine whether UBR5 primarily controls elongation stability, pause release, or both.

3.3 UBR5 loss induces context-specific chromatin remodeling

As outlined above, UBR5 loss drives the accumulation of multiple transcription-associated factors, disrupting the stoichiometric balance of transcriptional complexes. This imbalance extends into the chromatin regulatory layer in a context-dependent manner. In colon cancer cells, UBR5 deficiency is associated with more pronounced remodeling of chromatin assemblies, consistent with the highly dynamic and tissue specific nature of epigenetic regulation across tissue types.

Within this axis, MBD2/MBD3 NuRD nucleosome remodeling complex and SIN3B histone deacetylase complex are notably altered, interconnected via histone acetyltransferases HDAC1 and HDAC2 (HATs) acting as catalytic subunits whose specificity is dictated by binding partners. In UBR5 knockout cells, HATs exhibit coordinated shifts across abundance,

ubiquitylation, and ubiquitin-chain remodeling, accompanied by upregulation of their binding partners including SIN3B. SIN3B particularly stands out among colon-cancer-specific hits in the dataset and is a documented interactor of p53, providing a mechanistic bridge between UBR5-dependent epigenetic remodeling and tumor suppressor pathways.

Despite UBR5 is reported to interact with p53 it is not classified as a substrate, aligning with the observed p53 accumulation across all UBR5 knockout clones as an indirect stabilization phenomenon [164]. In DLD-1, p53 protein carries a missense mutation (S241F) in the DNA-binding domain, consistent with loss of canonical tumor-suppressor activity but potential mutant-p53 functions [165]. Because the p53–SIN3B interaction maps to the N-terminal proline-rich region rather than the DNA-binding domain [161], S241F is unlikely to abolish SIN3B binding directly, though mutant p53 may still reprogram SIN3B-dependant gene repression leading to alterations of gene expression program.

This framework motivates targeted assays (e.g., ChIP-seq for SIN3B/p53 occupancy and histone-acetylation mapping) to connect Proteome/Ubiquitylome shifts to regulatory chromatin outcomes. Such analyses can resolve the functional crosstalk between UBR5, SIN3B, and p53, and determine whether p53-mutation–dependent reinforcement of SIN3B activity represents an additional pro-oncogenic consequence of UBR5 overexpression in colon cancer.

3.4 UBR5 loss affects global quality control of splicing machinery

Our findings reveal that the UBR5-mediated response regulates an interconnected network of splicing factors in a context-independent manner. The pre-mRNA processing intron-binding complex emerges as the most affected multiprotein assembly in both malignant and normal-like cells, with coordinated changes extending to U2 snRNP and U4/U6 snRNP—modules essential for building the pre-catalytic B spliceosomal complex. Across datasets, we consistently observe matched shifts in protein stability within these core assemblies, indicating common post-transcriptional regulatory influences rather than isolated subunit effects.

To test whether this organization reflects conserved control, we integrated cross-tissue protein co-abundance with DepMap mRNA co-variation [166]. Protein co-abundance is a robust indicator of shared regulation among functionally linked factors. Consistent with our UBR5 perturbation data, subunits of U2 snRNP and U4/U6 snRNP rank among the top co-abundant partners of the intron-binding complex. In contrast, mRNA-level co-abundance is comparatively weaker, supporting a model in which network behavior is driven primarily at the protein level by quality-control mechanisms rather than by transcriptional co-regulation.

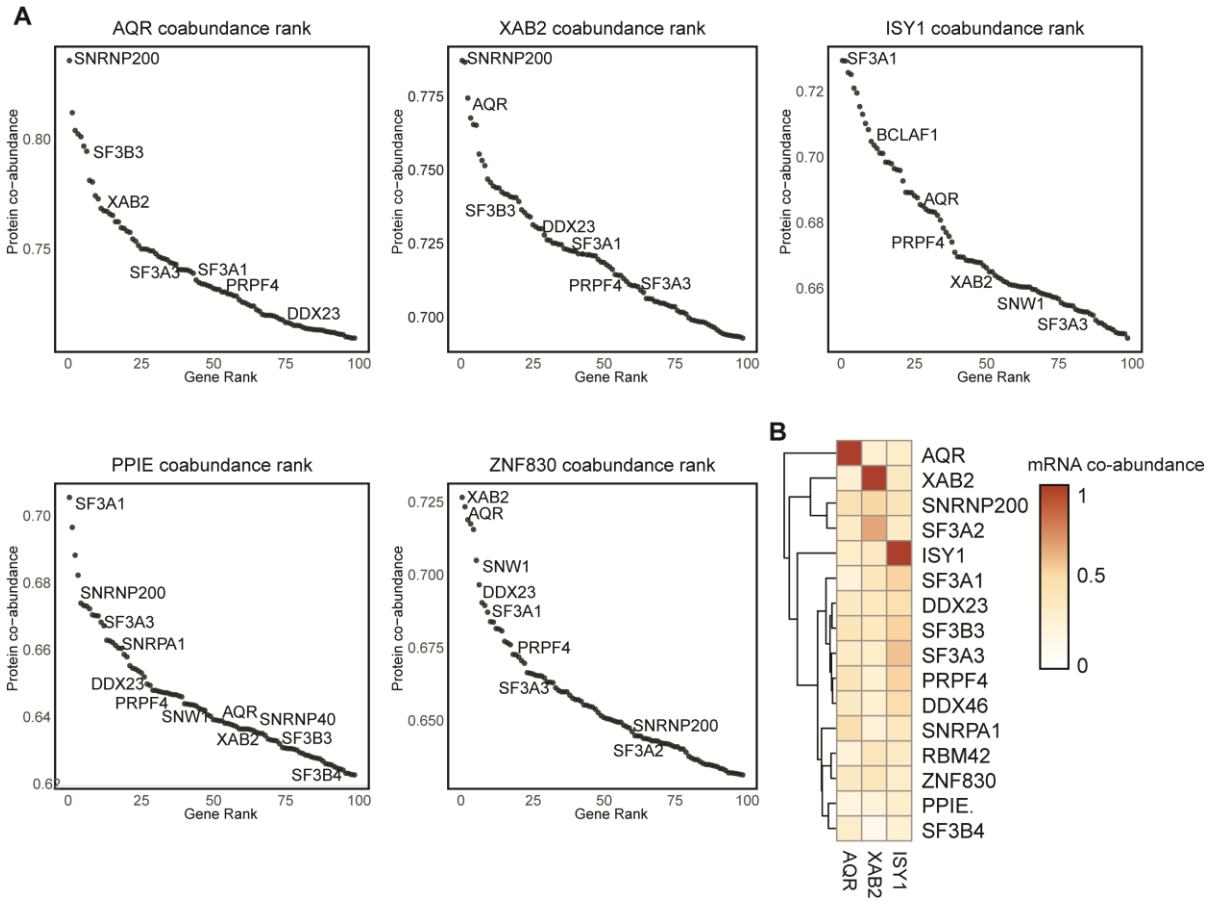

Figure 19. Protein and mRNA co-abundance of UBR5-dependant splicing factors with intron-binding complex subunits.
A. Rank plot of top hundred co-abundant proteins for each subunit of intron-binding complex. **B.** Heatmap representing mRNA co-abundance between AQR, ISY1 and XAB2 and UBR5-dependant splicing factors.

UBR5 has been reported to interact with multiple splicing-associated factors (e.g., ETUD2, SNRNP200, PRPF8, SF3B1, SF3B3, AQR, and XAB2) [160], overlapping with the assemblies implicated here, suggesting the capacity for direct, targeted modulation of factor abundance. At the same time, multiprotein machines are governed by coupled multiple ligases activities, so perturbation of one subunit can propagate through assembly quality control networks to shift composition across modules.

3.5 UBR5 directly regulates targeted protein degradation of pre-mRNA binding protein AQR

As mentioned in a previous section, intron-binding complex subunits AQR, and XAB2 were identified among endogenous UBR5 interactors. However, the role of UBR5 in driving ubiquitylation of splicing-associated factors remained unexplored. We identify a subunit of the intron-binding complex, AQR, as a novel substrate of UBR5. Moreover, we provide new insights into AQR turnover by showing that this subunit is recycled either within impaired intron-binding complex assembly or in its free form, consistent with previous studies implicating UBR5 in orphan protein quality control.

We introduced the orphan form of AQR by depleting other subunits of the intron-binding complex. Knockdown of either XAB2 or ISY1 subunit triggers AQR degradation, which can be reversed by UBR5 loss, indicating that a UBR5-dependent degradation signal is exposed.

In addition to the proteomic consequences of UBR5 loss, our findings provide mechanistic insights into the regulation of UBR5-dependent AQR ubiquitylation. We show that UBR5 loss specifically alters the ubiquitylation pattern of orphaned AQR, whereas under unchallenged conditions these changes remain undetectable. Moreover, AQR ubiquitylation profile in UBR5 knockout cells indicates a shift in ubiquitylation rather than a complete loss, suggesting that UBR5 drives ubiquitylation of a pre-ubiquitylated form of AQR.

Proteomic profiling of the AQR proximity interactome identified a subset of potentially priming E3 ubiquitin ligases, including CRL1-, CRL2-, CRL3-, and CRL4-associated

adaptors. Further analysis revealed that the majority of these adaptors are linked to CRL1. As part of the same collaborative project, Lukas Graf, a PhD student, is pursuing a complementary line of investigation. He has observed that AQR loses its ubiquitylation upon Nedd8 inhibition — a modification required for CRL activation (unpublished). Together, these findings set the stage for future studies aimed at determining which specific CRL catalytic unit is responsible for this priming activity.

While UBR5-driven ubiquitylation is crucial for the efficient degradation of AQR, our data provides evidence that TRIP12 ultimately secures the degradative signal. A 2025 study describes a feedback loop in which UBR5 and TRIP12 cooperate with the deubiquitinase OTUD5 [96]. OTUD5 removes K48-linked signals, thereby stabilizing UBR5 substrates, unless TRIP12 introduces K29 linkages to form K48/K29-branched chains. We hypothesize that a similar mechanism is at play in the case of AQR. In a parallel study, Caio Oliveira, a PhD student investigating the substrate specificity principles of OTUD5, has identified the intron-binding complex among the top hits affected by deubiquitinase loss.

The concept of orphan protein quality control posits that degradation signals are typically buried within protein–protein interaction surfaces and become exposed only upon complex disruption. A 2015 study identified AQR as a central scaffold for intron-binding complex formation, with its ARM-repeat domain being essential for maintaining structural integrity [167]. Cross-linking mass spectrometry further revealed that AQR interacts with other subunits through residues located in domains or insertions unique to AQR, including the ARM, pointer, and thumb domains, as well as large insertions within the β-barrel structure. These regions therefore represent plausible sites where degradation signals could be hidden and subsequently exposed.

To date, only one study has investigated how UBR5 recognizes its substrates, reporting two putative internal degron sequences that influence the stability of the transcription factors MYC and SPT5 [153]. Whether these motifs reflect a general principle of UBR5 substrate recognition or represent protein-specific determinants remains unresolved. Moreover,

ubiquitin itself may contribute as part of the degron signal, raising the possibility that recognition depends not only on linear sequence motifs but also on the ubiquitylation state of the substrate.

Our analysis shows that the degron-like sequences described in MYC and SPT5 correspond to regions of AQR that interact with XAB2 and ISY1 (Fig.20). This observation supports a model in which UBR5 engages AQR through one or both motifs, with priming ubiquitylation events occurring at interaction surfaces that are normally shielded within the intact complex. Future studies will be required to define precisely how UBR5 recognizes AQR and to determine where priming ubiquitylation events initiate UBR5's enzymatic function.

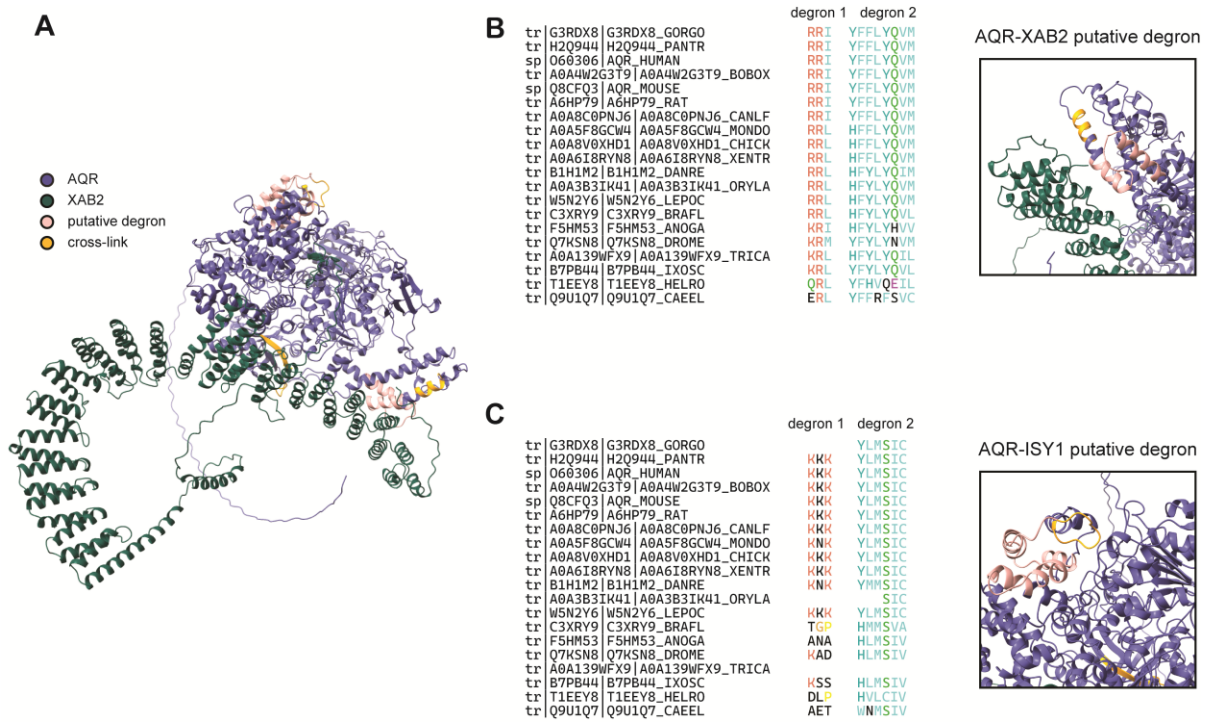

Figure 20. Putative UBR5 degron sequences within AQR.
A. AlphaFold prediction of AQR-XAB2 interaction. **B. – C.** Putative degron sequences within AQR-XAB2 binding interface (**B.**) or AQR-ISY1 binding interface (**C.**) located next to peptides identified in crosslink mass spectrometry of intron-binding complex. Putative degron sequences are based on MYC degron sequences and are identified by *KR*{2,4} rule for degron sequence 1 and *FILMVWY*{3,5})(C|S)?*STDE*{0,3} for degron sequence 2.

3.6 Concluding remarks

In this work, we establish UBR5 as a central regulator of nuclear protein homeostasis by linking orphan protein quality control to the stoichiometric maintenance of transcription, chromatin-remodeling, and RNA-processing assemblies. Proteomic and ubiquitylomic profiling across malignant (DLD-1) and non-malignant (RPE-1) contexts reveals that the consequences of UBR5 loss manifest predominantly at the complex level, outweighing changes in individual subunits. These findings position UBR5 as a systems-level regulator that preserves the composition and turnover of multiprotein machines under both basal and stress conditions. Within this regulatory framework, we focus on the intron-binding complex as a prominent target directly controlled by UBR5 enzymatic activity.

Our findings also provide a framework for understanding how UBR5 regulates AQR through orphan protein quality control. While the precise molecular features of the degradation signal remain undefined, our data suggest it resides within AQR surfaces normally masked by XAB2 and ISY1. We propose a model in which UBR5 engages these exposed regions via priming ubiquitylation, with TRIP12 securing the degradative signal and OTUD5 fine-tuning substrate stability. Rather than functioning as an all-or-nothing cue, ubiquitylation reflects a dynamic balance of priming, branching, and removal events that ultimately govern AQR fate. This model integrates structural, proteomic, and functional insights, providing a foundation for future studies to pinpoint degron elements and clarify UBR5-mediated orphan protein quality control.

In conclusion, this study delivers a reusable data resource as well as mechanistic insight for UBR5 biology, comprising integrated proteomics, ubiquitylomics, and external sources datasets. Follow-on projects launched from this resource are in progress (e.g., AQR priming E3s, UBR5–SIN3B-p53 chromatin crosstalk), and outcomes will be reported in subsequent research project.

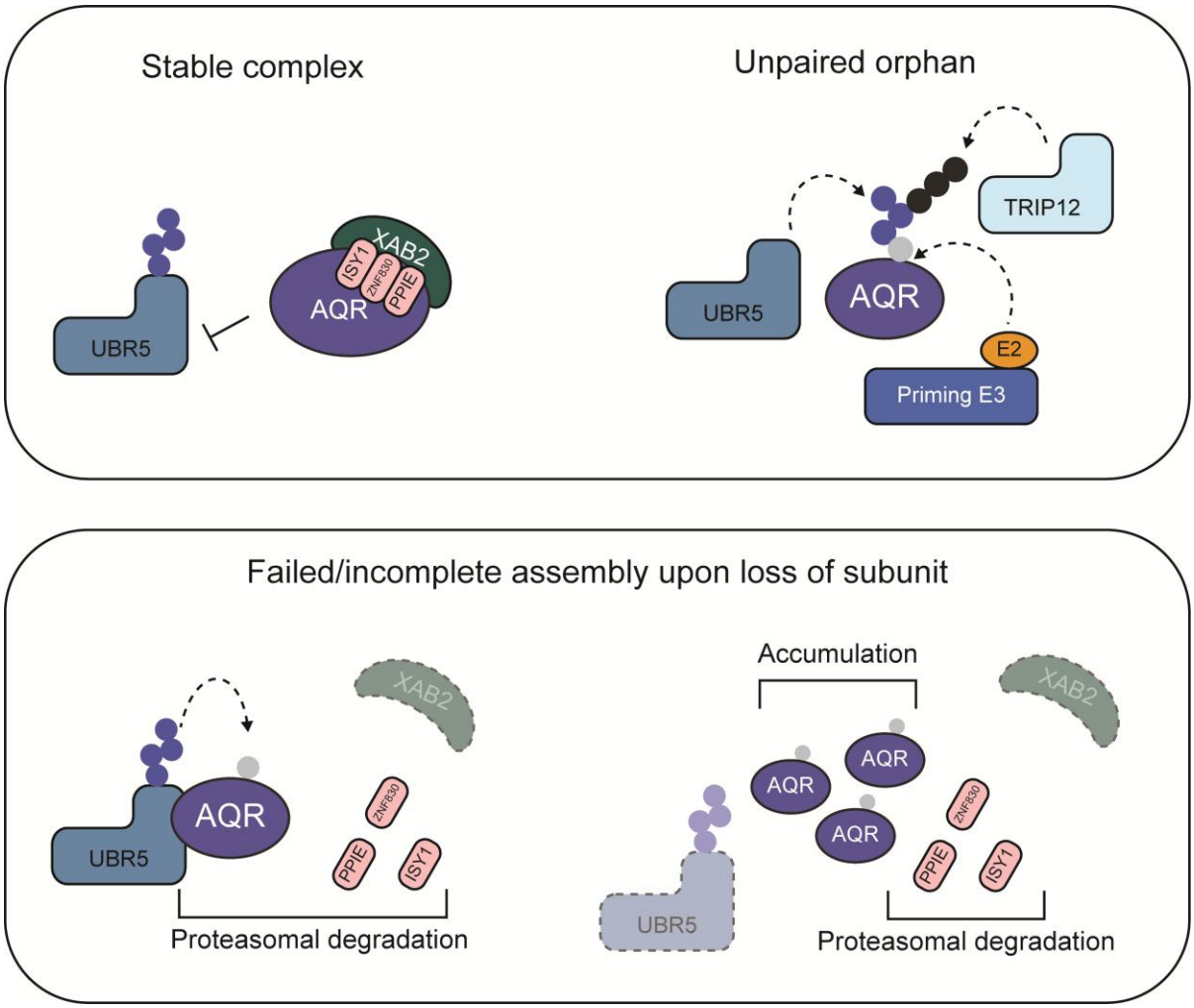

Figure 21. Model for AQR turnover regulation by UBR5.
As part of the intron-binding complex, the degron signal recognized by UBR5 is buried within the interaction interface, preventing AQR recognition and ubiquitylation. When unpaired, AQR is ubiquitylated through the cooperation of three different E3 ligases. UBR5 recognizes AQR following priming ubiquitylation by another ligase, and TRIP12 subsequently secures the degradation signal, completing the orphan quality control of AQR. Upon UBR5 loss, the AQR ubiquitylation signal is compromised, leading to the accumulation of free AQR subunits within incomplete intron-binding complexes.

4. Materials and Methods

4.1 Reagents

4.1.1 Chemicals, solutions, peptides, and recombinant proteins

Table 1. List of chemicals and kits used in this study

Name	Supplier
(+)-Sodium L-ascorbate	Sigma-Aldrich
(±)-6-Hydroxy-2,5,7,8-tetramethylchromane-2-carboxylic acid (Trolox)	Sigma-Aldrich
2-Chloroacetamide	Sigma-Aldrich
500ML SUPERSIGNAL WEST PICO PLUS	Thermo Fisher
5-Ethynyl-uridine (5-EU)	Lumiprobe
Acetone	Carl Roth
Acetonitrile hypergrade for LC-MS LiChrosolv®	Sigma-Aldrich
Biotin Tyramide (=Biotin phenol)	Iris Biotech
bisBenzimide H 33342 trihydrochloride = Hoechst 33342	Sigma-Aldrich
Bovine Serum Albumin	Sigma-Aldrich
C18 Empore 47 mm extraction disks	CDS
Cation Exchange disk	CDS
Copper(II) sulfate pentahydrate	Sigma-Aldrich
Crystal Violet	Sigma-Aldrich
Cys-OtUBD	Protein Production CF
Cysteine HCl	Thermo Scientific

Dimethyl sulfoxide	AppliChem
DL-Dithiothreitol	Sigma-Aldrich
D-MEM for SILAC without lysine and arginine	Thermo Scientific
DMEM, high glucose, pyruvate, no glutamine	Thermo Scientific
Dulbecco's Balanced Salt Solution (DPBS)	Thermo Scientific
EDTA (0,5 M), pH 8,0, RNase-frei	Thermo Scientific
Ethanol absolute	Carl Roth
FastAP Thermosensitive Alkaline Phosphatase (300 units)	Thermo Scientific
FastDigest BpiI (IIs class)	Thermo Scientific
FBS dialyzed	Sigma-Aldrich
FBS Value	Thermo Scientific
Fluorescence Mounting Medium	Dako
FuGENE® HD Transfection Reagent	Promega
Glycerol 87%	AppliChem
HEPES	Sigma-Aldrich
Hydrogen peroxide solution	Sigma-Aldrich
Hydroxylamine solution	Sigma-Aldrich
Immobilon® ECL Ultra Western HRP Substrate	Sigma-Aldrich
L-Arginine -HCl ($^{13}C_6$, 99%) = Arginine 6	Cambridge Isotope Laboratories
L-Arginine monohydrochloride	Sigma-Aldrich
L-Arginine·HCl ($^{13}C_6$, 99%; $^{15}N_4$, 99%)	Cambridge Isotope Laboratories
LB media	Media Lab
L-Glutamine (200 mM)	Thermo Scientific
Lipofectamine™ RNAiMAX Transfektionsreagenz	Thermo Fisher

L-Lysine monohydrochloride	Sigma-Aldrich
L-LYSINE:2HCL (13C6, 99%; 15N2, 99%) = Lysine 8	Cambridge Isotope Laboratories
L-LYSINE:2HCL (4,4,5,5-D4, 96-98%) = Lysine 4	Cambridge Isotope Laboratories
Magnesium chloride hexahydrate	Sigma-Aldrich
Methanol HiPerSolv	VWR
MLN7243 (=TAK-243)	MedChemExpress
MOPS	Sigma-Aldrich
N-Ethylmaleimide	Sigma-Aldrich
Nitrocellulose blotting membranes	Sigma
Nonidet P40 Substitute	Sigma-Aldrich
NuPAGE MOPS SDS Running Buffer (20X)	Thermo Scientific
NuPAGE™ LDS Sample Buffer (4X)	Thermo Scientific
Opti-MEM™	Thermo Scientific
PARAFORMALDEHYDE 16% Aqueous SOL. EM GRADE	Electron microscopy science
PBS, 5x	Media Lab
Penicillin-Streptomycin (10,000 U/mL)	Thermo Scientific
Phosphatase Inhibitor Cocktail (2 Tubes,100X)	Biotool LLC.
Pierce High Capacity NeutrAvidin	Thermo Fisher Scientific GmbH
Ponceau S	AppliChem
Protease Inhibitor cocktail	Sigma-Aldrich
PTMScan® Ubiquitin Remnant Motif (K--GG) Kit	Cell Signaling Technology
Quick Ligation Kit, 30 rx	NEB
Quick Start™ Bradford 1x Dye Reagent	BioRad

RPMI 1640 Medium, no glutamine	Thermo Fisher
Sep-Pak tC18 3 cc Vac Cartridge	Waters GmbH
Sm nuclease	Protein production CF
Sodium azide	Sigma-Aldrich
Sodium chloride	Media Lab
Sodium deoxycholate	AppliChem
Sodium dodecyl sulfate	Sigma-Aldrich
Sodium fluoride	Sigma-Aldrich
Sodium orthovanadate	Sigma-Aldrich
SulfoLink™ Coupling Resin	Thermo Scientific
SYBR™ Safe DNA-Gel-Färbemittel	Thermo Scientific
TAE	Media lab
TCEP solution (BondBreaker® TCEP; Reducing Reagent)	Thermo Scientific
Thiourea	Sigma-Aldrich
TMTpro 16plex Label Reagent	Thermo Fisher Scientific GmbH
Trifluoroacetic acid	Fisher Chemicals
Tris-HCl (ph 6.8)	Abcam
Triton X-100	Sigma-Aldrich
Triton X-100	Sigma-Aldrich
Trypsin from porcine pancreas, proteomics grade	Sigma-Aldrich
Trypsin-EDTA (0,05%), phenol-red	Thermo Scientific
Tween 20	Sigma-Aldrich
Urea	Sigma-Aldrich
Water UP	Media Lab
β-Glycerophosphate disodium salt hydrate	Sigma-Aldrich

4.1.2. Primary and Secondary Antibodies

Table 2. List of primary antibodies used in this study

Name	Species	Supplier	Dilution
alpha tubulin	Rabbit	Cell Signaling	1:5000
IBP160 (AQR)	Rabbit	Bethyl Laboratories	1:1000
beta actin	Mouse	Sigma-Aldrich	1:5000
HDAC1	Mouse	Cell Signaling	1:1000
HDAC2	Mouse	Cell Signaling	1:1000
ISY1	Rabbit	Sigma (Atlas Antibodies)	1:1000
MYC	Rabbit	Cell Signaling	1:1000
OTUD5	Rabbit	Cell Signaling	1:1000
P4D1	Mouse	Cell Signaling	1:1000
PRPF19	Mouse	Santa Cruz Biotechnology	1:500
TP53	Mouse	Santa Cruz Biotechnology	1:1000
TRIP12	Rabbit	Bethyl Laboratories	1:1000
UBR5	Rabbit	Cell Signaling	1:1000
HCNP (XAB2)	Mouse	Santa Cruz Biotechnology	1:1000

Table 3. List of secondary antibodies used in this study

Name	Species	Supplier	Dilution
Mouse HRP	Goat	Agilent	1:10000
Rabbit HRP	Goat	Agilent	1:10000

4.1.3 Oligonucleotides

Table 4 List of DNA and RNA oligonucleotides used in this study.

Name	Sequence 5'-3'
gRNA2 UBR5 frw	CACCGTGTTCCAATACATTCAAAGG
gRNA2 UBR5 rev	AAACCCTTTGAATGTATTGGAACAC
gRNA3 UBR5 frw	CACCGGTAAACCTGATAATAATGAT
gRNA3 UBR5 rev	AAACATCATTATTATCAGGTTTACC
siAQR	CUGAAUAUGGCGGUGUAGU-TT
siCTRL pool	D-001820-10 – Horizon Discovery
siISY1	GAGCCGAGUUAGUGGAAAA-TT
siTRIP12	s17810 - ThermoFisher
siXAB2	ACGCAGCACUCUCGAAUUU-TT

4.2 Reagents preparation

4.2.1 Covalent conjugation of Cys-OtUBD to SulfoLink beads

Cys-OtUBD protein (~1 mg per sample) was covalently coupled to SulfoLink™ Coupling Resin (Thermo Scientific) as describes in [168]. All reagents and beads were equilibrated to room temperature prior to use. The SulfoLink bead slurry was resuspended and washed four times with coupling buffer (50 mM Tris-HCl, 5 mM EDTA, pH 8.5) to remove storage preservatives. Cys-OtUBD protein was diluted in coupling buffer containing 20 mM TCEP and incubated at room temperature with rotation for 30 min to reduce disulfides. The protein solution was then added to the prepared beads and incubated at room temperature for 60 min with rotation or overnight at 4 °C to allow covalent coupling. Beads were washed three times with coupling buffer to remove unbound protein. Nonspecific binding sites on the beads were blocked by incubating with two bead-bed volumes of 50 mM cysteine for 30 min at room

temperature. Finally, beads were washed four times with 1 M NaCl and twice with column buffer (50 mM Tris-HCl, 150 mM NaCl, 1 mM EDTA, 0.5% Triton X-100, 10% glycerol, pH 7.5), resuspended in column buffer containing 0.05% NaN_3, and stored at 4 °C until use.

4.3 Cell culture

4.3.1 Cell cultivation

Human hTERT-immortalized retinal pigment epithelial cells (RPE-1) and human osteosarcoma cells (U2OS) were obtained from the ATCC and cultured in DMEM supplemented with 10% fetal bovine serum, L-glutamine, penicillin and streptomycin. Human colorectal adenocarcinoma cells (DLD-1) were obtained from the ATCC and cultured in RPMI supplemented with 10% fetal bovine serum, L-glutamine, penicillin and streptomycin. The AQR-APEX2-3×FLAG U2OS cell line was generated and characterized by a former Master student previously. Cells were routinely tested for mycoplasma infection using a PCR-based method. For SILAC labeling, cells were cultured in media containing either L-arginine and L-lysine, (13C6) L-arginine and (2H4) L-lysine, or (13C6,15N4) L-arginine and (13C6,15N2) L-lysine (Cambridge Isotope Laboratories). All cells were cultured at 37°C in an incubator containing a humidified 5% CO2 atmosphere.

4.3.2 Generation of CRISPR/Cas9 genome-edited cell lines

All cell lines generated in this study were derived from RPE-1 cells or DLD-1 cells. Guide RNA sequences (gRNAs) were designed using the Broad Institute CRISPick tool (https://portals.broadinstitute.org/gppx/crispick/public). For knockout of the UBR5 locus, RNA guides were used to remove part of the third or fourth exons of the UBR5 locus in RPE-1 cells and DLD-1 cells. Oligonucleotides corresponding to each gRNA and their complementary strands (listed in *Table 4*) were ordered from Sigma. Complementary oligos were phosphorylated, annealed and cloned into the PX458 vector (gifted by Vassilis Roukos lab) following the Zhang lab cloning protocol:
(https://media.addgene.org/cms/filer_public/6d/d8/6dd83407-3b07-47db-8adb-

4fada30bde8a/zhang-lab-general-cloning-protocol-target-sequencing_1.pdf).
Briefly, PX458 was digested with BbsI, annealed oligonucleotides were ligated into the digested backbone, the ligation product was transformed into chemically competent E. coli, and individual clones were sequence-verified by Sanger sequencing (StarSEQ, Germany) prior to plasmid purification.

RPE-1 and DLD-1 cells were transfected with the PX458-gRNA constructs (one guide per construct) using transfection methods described below. Forty-eight hours after transfection, GFP-positive cells were isolated by fluorescence-activated cell sorting (FACS). Single GFP-expressing cells were sorted into 96-well plates and expanded to generate clonal lines. Loss of UBR5 protein expression was confirmed by mass spectrometry–based proteomics (see section 4.4 for details) and by Western blotting using an anti-UBR5 antibody (table 2).

4.3.3 Transfection and treatments

For CRISPR/Cas9 gene editing, cells were transfected with PX458-gRNA constructs using FuGENE® 4K Transfection Reagent (Promega) according to the manufacturer's instructions. For siRNA-mediated knockdown experiments, cells were transfected with siRNAs using Lipofectamine RNAiMAX (Life Technologies) following the manufacturer's protocol. For ubiquitin-activation enzyme inhibition, cells were treated with 5μM/ml TAK-243 for 2h. For UV-C irradiation cells were irradiated with 20 J/cm2 and fixed for follow-up high-throughput confocal microscopy (section) at the for the indicated time-points post irradiation.

4.4 Cell-based methods

4.4.1 Crystal violet proliferation assay

RPE-1 cells ($3x10^5$) were ere seeded per well in six-well plates in triplicate. At the indicated time points, cells were fixed in ice-cold 100% methanol (−20°C) and stained with 0.1% crystal violet for 10–30 min. Plates were washed thoroughly to remove unbound dye and air-dried completely. Bound dye was eluted with 30–33% acetic acid (or ethanol) and absorbance was measured at 590–595 nm using Tecan Infinite M200 Pro.

4.4.2 Cell cycle analysis by flow cytometry

The cells were collected with trypsin, washed with PBS and fixed overnight with 70% EtOH at 4°C. Pelleting post-fixation was performed at 3500xg. Cells were washed once in the wash/permeabilization solution (0.05% Triton-X-100 in PBS), and once in PBS with 2% BSA. They were resuspended in PBS containing 5 µg/ml Hoechst 33342 (Sigma-Aldrich). Acquisition was performed on a BD LSRFortessa flow cytometer, and 40 000 cells were recorded. The 355 nm laser and 450/50 band pass filter were used for analyzing Hoechst fluorescence. Further analysis was done using FloJo. After gating for singlets (FSC/SSC, then Hoechst –H (height) / Hoechst –A (area)) cell cycle profile was determined based on Hoechst staining.

4.4.3 Cell lysis

Cells were washed twice with PBS and lysed in RIPA buffer containing 50 mM Tris HCl (pH 7.5), 150 mM NaCl, 1 mM EDTA, 1% NP40, 0.1% Na-deoxycholate, 0.1% SDS supplemented with phosphatase inhibitors, protease inhibitor cocktail, 100 U/mL Sm Nuclease and 2 mM $MgCl_2$ at 4°C for 30 min on a rotation wheel. Alternatively, lysates were supplemented NaCl up to 1M followed by sonication with Bioruptor from Diagenode (30s ON/30s OFF, 10 cycles, intensity high). Lysates were clarified by centrifugation 16 000 × g for 15 min at 4 degrees and protein concentration was measured using QuickStart Bradford Protein assay (BioRad), followed by addition of NuPAGE LDS Sample Buffer (Life Technologies) supplemented with 1 mM DTT and boiling.. Next, samples

were supplemented with sodium chloride at 450 mM and incubated for 15 min. Protein concentrations were measured using the Bradford assay and adjusted and the supernatant proteins were mixed with 4x LDS Sample Buffer supplemented with 1 mM DTT and boiled for 10 min at 95°C.

4.4.4 SDS-PAGE and Western Blotting

20-40 µg of total protein lysate was resolved on 4-12% gradients SDS-PAGE gels (NuPAGE Bis-Tris Precast Gels, Life Technologies) and transferred onto nitrocellulose membranes. Following the transfer, membranes were stained with Ponceau S and blocked for 30 min in a 3 % BSA solution in PBS supplemented with 0.1% Tween-20 (PBS-T). Membranes were incubated with primary antibodies overnight at 4°C. Following 3× 5 min washes with PBS-T, secondary antibodies coupled to horseradish peroxidase (Agilent) were applied for 1 h at room temperature. Membranes were then washed 3× 10 min with PBS-T and developed with Immobilon ECL Ultra Western HRP Substrate and SuperSignal West Pico detection reagent. Chemiluminescence signal was recorded on ChemiDoc (Bio-Rad).

4.4.5 OtUBD pull-down under denaturing conditions.

Cells were lysed in OtUBD lysis buffer (50 mM Tris-HCl, 300 mM NaCl, 1 mM EDTA, 0.5% Triton X-100, protease and phosphatase inhibitors) on ice and rotated for 30 min at 4 °C, followed by sonication using a Bioruptor (10 cycles, 30s on/30s off, 4 °C) to shear chromatin. Lysates were clarified by high-speed centrifugation (16,000 × g, 15 min, 4 °C), and protein concentration was measured using the Bradford Protein Assay (Bio-Rad). SulfoLink-conjugated OtUBD beads were thoroughly mixed and aliquoted at 25 µL bed volume per 1 mg of protein. Beads were pelleted (1,000 × g, 2 min), washed with 20 bead-bed volumes of column buffer, and supernatant removed. Lysates were then added to the equilibrated beads and incubated with rotation for 2.5 h at 4 °C or overnight to allow binding. Beads were subsequently pelleted, and the supernatant collected, followed by sequential washes with three times 15 bead-bed volumes of column buffer containing 4 M urea followed by a final rinse with MilliQ water to remove residual salts and detergents. For downstream applications,

proteins were eluted from the beads with 50 µL SDS buffer (50 mM Tris-HCl, 2% SDS, 5% glycerol, 100 mM DTT, bromophenol blue) or 2× LDS buffer, incubated for 30 min at 65 °C (or 5 min at 95 °C for LDS buffer), and loaded directly onto polyacrylamide gels for SDS-PAGE or Western blot analysis.

4.3.6 Fluorescent microscopy using Opera Phenix

Glass coverslips were first cleaned with 100% ethanol and placed into 6-well plates. RPE-1 cells were seeded on the coverslips at the following densities per 6-cm plate: RPE-1 WT, 5×10^5 cells; RPE-1 dUBR5 2.4, 6.5×10^5 cells; and RPE-1 dUBR5 3.7, 6.5×10^5 cells. For EU incorporation, cells were incubated with 100 µM EU in complete medium for 30 min at 37 °C. Cells were subsequently washed twice with PBS (or PBS-T if pre-extraction was performed) and fixed with 4% paraformaldehyde (100 µL per well) for 20–30 min at room temperature, followed by two washes with PBS. Cells were permeabilized and blocked in 0.1% Triton X-100 and 0.2% BSA in PBS for 1 h at room temperature and washed twice with PBS. Primary antibodies were diluted in 1% BSA in PBS-T and applied to the coverslips (50 µL per well) overnight at room temperature, followed by two washes with PBS-T. For EU detection, a click reaction was performed in the dark using freshly prepared click mix containing 2 mM $CuSO_4$, 5 µM Alexa Fluor 647-azide, and 10 mM ascorbic acid in PBS (pH ~8.5) for 45 min at room temperature. Coverslips were then washed twice with PBS-T, incubated with secondary antibodies and Hoechst 33342 (1:2500) in the dark at room temperature, and washed three times with PBS-T. Finally, coverslips were mounted with 4 µL of mounting solution, left to dry overnight in the dark, and sealed with nail polish. Sample imaging was performed with the Opera Phenix (Revvity) and analysis for AF647 intensity performed with the Harmony software.

4.4 Proteomics methods

4.4.1 Proteomics sample preparation

4.4.1.1 Total proteome analysis

RPE-1/DLD-1 cells were seeded in one 6-cm dish per sample. All steps up to acetone precipitation were performed at 4 °C. Cells were washed twice with ice-cold PBS and lysed in RIPA buffer (50 mM Tris HCl (pH 7.5), 150 mM NaCl, 1 mM EDTA, 1% NP40, 0.1% Na-deoxycholate, 0.1% SDS) supplemented with inhibitors (complete protease inhibitor cocktail, 1 mM sodium orthovanadate, 5 mM β-glycerophosphate, 5 mM sodium fluoride, 10 mM N-ethylmaleimide). Lysates were incubated for 15 min and chromatin-bound proteins were extracted with NaCl (final concentration 500 mM) followed by sample sonication using Bioruptor Plus (8 cycles, 30s on/30s off, high intensity). Lysates were clarified by centrifugation (16,000 × g, 15 min, 4 °C), and protein concentration was measured using the Bradford Protein Assay (Bio-Rad).

4.4.1.2 Ubiquitin-modified proteome analysis

For ubiquitin remnant profiling, RPE-1 cells were seeded in four 150-mm dishes per sample. Cells were lysed in modified RIPA buffer (50 mM Tris, pH 7.5, 150 mM NaCl, 1 mM EDTA, 1% NP-40, 0.1% sodium deoxycholate) supplemented with inhibitors (complete protease inhibitor cocktail, 1 mM sodium orthovanadate, 5 mM β-glycerophosphate, 5 mM sodium fluoride, 10 mM N-ethylmaleimide). Lysates were incubated for 15 min and chromatin-bound proteins were extracted with NaCl (final concentration 500 mM) followed by sample sonication using a Branson Sonifier (3 × 30s, output setting 1, on ice). Lysates were clarified (16,000 × g, 15 min, 4 °C), and protein concentration was determined by Bradford assay. SILAC-labeled extracts were combined in a 1:1 ratio prior to downstream processing.

4.4.1.3 AQR proximal proteome analysis

For endogenous AQR proximal proteome profiling, U2OS cells were incubated with 10 mM biotin-phenol (in DMEM) for 2 h at 37 °C and treated with 1 mM H_2O_2 for 2 min at room temperature. Labeling was quenched by three rapid washes with quenching solution (10 mM sodium azide, 10 mM sodium ascorbate, 5 mM Trolox in PBS), followed by three washes with ice-cold PBS. Cells were scraped into PBS containing inhibitors (complete protease inhibitor cocktail, 1 mM sodium orthovanadate, 5 mM β-glycerophosphate, 5 mM sodium fluoride, 10 mM N-ethylmaleimide) and lysed in RIPA buffer supplemented with inhibitors. NaCl concentration was adjusted to 1 M, and lysates were sonicated and treated with Sm nuclease and 2 mM $MgCl_2$ for 20 min at 4 °C on a rotating wheel. Lysates were clarified (16,000 × g, 15 min, 4 °C) and diluted 1:4 with no-salt modified RIPA (final NaCl 200 mM). Protein concentration was determined by Bradford assay, and equal amounts of lysates per sample (3 mg) were incubated with pre-equilibrated NeutrAvidin agarose beads for 2 h at 4 °C with rotation. Beads were washed once with modified RIPA and three times with 2 M urea. Bound proteins were eluted in NuPAGE LDS sample buffer containing 1 mM DTT and 10 mM biotin by boiling at 95 °C for 15 min.

4.4.2 Protein precipitation, in-solution digestion, and peptide cleanup (total and ubiquitin-modified proteomes)

Protein lysates were precipitated with a fourfold excess of ice-cold acetone overnight and pelleted (1,000 × g, 5 min). Pellets were air-dried and resuspended in 6 M urea/2 M thiourea buffered with 10 mM HEPES (pH 8.0). Proteins were reduced by 1 mM DTT for 45 min and alkylated with 5.5 mM chloroacetamide for 30 min at room temperature. Digestion was performed overnight at room temperature with trypsin (1:50 enzyme:protein ratio for total proteome, 1:100 for ubiquitin-modified proteome). Reactions were quenched with 0.5% TFA. Peptides were clarified by centrifugation (4,000 × g, 10 min, 4 °C), desalted using Sep-Pak C18 cartridges (Waters), eluted with 50% acetonitrile, and dried by SpeedVac prior to LC-MS/MS analysis in case of DlD-1 total proteome or otherwise prior to downstream processing.

4.4.3 In-gel Digestion (AQR proximal Proteom)

Eluted proteins were alkylated with 5.5 mM chloroacetamide (30 min, dark), separated by SDS-PAGE (4–12% gradient gels), and visualized using colloidal Coomassie staining. Each lane was diced into ~1 mm cubes, destained, dehydrated with 100% ethanol, and rehydrated with sequencing-grade trypsin (125 ng/µL). Digestion was performed overnight at 37 °C. Peptides were extracted sequentially with extraction buffer, in-gel buffer B, and acetonitrile, pooled, vacuum concentrated to ~100 µL, and desalted using Stage Tips [169].

4.4.4 Peptide labeling, enrichment, and fractionation

4.4.4.1 RPE-1 total proteome

Dried peptides were labeled with TMTpro reagents (0.1 µg per sample, dissolved in acetonitrile) for 1 h and quenched with 5% hydroxylamine for 15 min [170]. A 5% aliquot was taken for ratio-check and sample inputs were normalized accordingly. Pooled TMT samples were diluted with 0.1% TFA to reduce organic content (<3% ACN), purified on Sep-Pak cartridges and eluted with 50% ACN (acidified with 6% TFA). Peptides were fractionated by micro-SCX (strong cation exchange)**.**

4.4.4.2 RPE-1/DLD-1 ubiquitin-modified proteome

Desalted peptides were incubated with 80 µL diglycine-lysine (K-ε-GG) antibody resin (Cell Signaling Technology) for 4 h or overnight at 4 °C with rotation [171]. Beads were washed three times with IAP buffer (50 mM MOPS/NaOH pH 7.2, 1000 mM Na_2HPO4, 50 mM NaCl) and three times with water. Enriched peptides were eluted with 0.15% TFA and separated into six fractions by micro-SCX.

4.4.4.3 Micro-tip based strong cation exchange chromatography (Micro-SCX)

SCX tips were assembled using six disks from 47 mm cation exchange extraction disks were cut with a 17-gauge Hamilton syringe and placed into a 200 µL pipette tip. Micro-SCX

tips were equilibrated with 50 µl of methanol, SCX elution buffer pH 4 (diGLY-remnant enrichment) or pH 3 (full proteome), SCX elution buffer pH 11, and 100 µl of SCX wash buffer by centrifugation at 500 x g. Acidified samples (pH < 2) were loaded on micro-SCX tips by centrifugation at 500 x g and fractionated by eluting with 100 µl of SCX elution buffers at 500 x g from lowest to highest pH.

pH of SCX-buffers:
TMT total proteome: 3.0 / 3.6 / 3.9 / 4.25 / 4.8 / 5.5 / 7.0 / 11.0
SILAC DiGly-remnant peptides: 4.0 / 5.0 / 6.0 / 7.0 / 8.5 / 11.0

ACN was removed by vacuum centrifugation for 20 minutes at 45 °C and eluates were subsequently desalted by C18 StageTipping prior to LC-MS/MS analysis.

4.5 LC-MS/MS

Run parameters for the LC-MS/MS runs are listed in the *Table5.*

4.4.5.1 MaxQuant analysis of TMT-labeled total proteome

Raw files from TMT-labeled total proteome samples were analyzed using MaxQuant (version or) with the integrated Andromeda search engine [172], [173]. The human UniProt reference proteome (release 2021) was used as the search database, supplemented with a list of common contaminants provided by MaxQuant. Trypsin/P was specified as the digestion enzyme, allowing up to two missed cleavages. Carbamidomethylation of cysteine was set as a fixed modification, while methionine oxidation and N-terminal acetylation were variable modifications. First peptide search tolerance was set to 20 ppm and main search to 4.5 ppm. Both peptide and protein false discovery rates (FDR) were controlled at 1% using the target-decoy strategy. Protein quantification was performed at the MS2 level with reporter intensity correction applied according to manufacturer-provided TMT lot-specific values. Reporter intensities were normalized within MaxQuant using the internal “Reporter ion normalization” algorithm.

4.4.5.2 MaxQuant analysis of SILAC ubiquitylome

Raw files from SILAC-labeled ubiquitin remnant-enriched samples were analyzed using MaxQuant with multiplicity set to 2 (Lys0/Arg0 and Lys8/Arg10). The human UniProt reference proteome was used as the search database. Trypsin/P was specified as the enzyme, allowing up to two missed cleavages. Carbamidomethylation of cysteine was set as a fixed modification, while methionine oxidation, N-terminal acetylation, and GlyGly-lysine (K-ε-GG) were included as variable modifications. Peptide tolerance was 20 ppm for the first search and 4.5 ppm for the main search. Both peptide and protein FDR were controlled at 1%. SILAC quantification was performed using MaxQuant's built-in normalization, and heavy/light ratios were calculated at the peptide level and collapsed to protein groups.

4.4.5.3 MSFragger analysis of label-free proteome

Raw DDA files from label-free total proteome experiments were analyzed using MSFragger (version 2.2.6) via the FragPipe pipeline (version v23.0) [174]**.** Searches were performed against the human UniProt reference proteome with the contaminant database appended. Trypsin specificity was required, allowing up to two missed cleavages. Carbamidomethylation of cysteine was set as a fixed modification, while methionine oxidation and N-terminal acetylation were variable modifications. Precursor mass tolerance was set to ±20 ppm and fragment mass tolerance to 20 ppm. Results were filtered to 1% peptide and protein FDR using the Philosopher toolkit. Label-free quantification was performed using IonQuant with match-between-runs enabled, minimum 1 peptide per protein, and intensity-based absolute quantification (iBAQ) calculated for protein-level comparison.

4.4.5.4 DIA-NN analysis of APEX label-free DIA data

Raw DIA files from APEX proximal proteome experiments were processed using DIA-NN (version v2.0.2) in library-free mode [175]. The human UniProt reference proteome (release 2024) was used as the search database. Precursor and fragment mass tolerances were automatically optimized by DIA-NN. Trypsin was specified as protease, allowing up to one

missed cleavage. Carbamidomethylation of cysteine was set as a fixed modification, and methionine oxidation and N-terminal acetylation as variable modifications. DIA-NN was run with “match between runs” enabled, using retention time alignment across all files. Protein intensities were reported as MaxLFQ-normalized values, and only proteins passing 1% FDR at both precursor and protein levels were included in downstream analysis.

Table 5 Instrument settings used for MS-based proteomics.

Settings		Total proteome LFQ	Total proteome TMT	Ubiquitylome SILAC	Ubiquitylome SILAC	APEX proximity proteome LFQ
LC	Device name	Neo Vanquish	EASY-nLC 1200	EASY-nLC 1200	Neo Vanquish	Neo Vanquish
	Column	45 cm length, 75 mm inner diameter	55 cm length, 75 mm inner diameter	55 cm length, 75 mm inner diameter	55 cm length, 75 mm inner diameter	45 cm length, 75 mm inner diameter
	Gradient	1.6 to 32% ACN, 100 min	2.4 to 36% ACN, 120 min	2.4 to 32% ACN, 90 min	1.6 to 32% ACN, 70 min	1.6 to 32% ACN, 40 min
MS	Device name	Orbitrap Astral	Orbitrap Exploris 480	Orbitrap Exploris 480	Orbitrap Astral	Orbitrap Astral
MS- full scan	m/z range	325-1300	300-1650	300-1650	325-1300	350-1050
	Resolution	120000	60000	60000	60000	120000
	Target value (%)	300	300	300	300	500
	Max injection time (ms)	20	40	40	25	300
ddMS2 scan/ DIA scan	DDA Dependent scans/DIA	50	20	15	50	DIA
	Normalized collision energy (%)	26	33	30	26	26
	Resolution	-	15000	15000	-	-
	Target value (%)	100	100	100	100	500
	Max injection time (ms)	10	40	40	40	10
	Isolation window (m/z)	1.4	0.8	1.4	1.4	4
	TurboTMT	-	TMTPro	-	-	-

4.5 Genomics methods

4.5.1 mRNA sequencing

RNA was extracted using the RNeasy Plus Mini Kit (Qiagen). In brief, cells were lysed, and genomic DNA was depleted. Samples were treated with DNase to remove residual DNA. After purification using spin columns, RNA was eluted in RNase-free water and stored at −80 °C until library preparation. NGS library prep was performed with Illumina's Stranded mRNA Prep Ligation Kit following Stranded mRNA Prep Ligation ReferenceGuide (June 2020) (Document # 1000000124518 v00). Libraries were prepared with a starting amount of 1000 ng and amplified in 9 PCR cycles. Two post PCR purification steps were performed to exclude residual primer and adapter dimers. Libraries were profiled in a DNA 1000 chip on a 2100 Bioanalyzer (Agilent technologies) and quantified using the Qubit dsDNA HS Assay Kit, in a Qubit 2.0 Fluorometer (Life technologies). All 12 samples were pooled in equimolar ratio and sequenced on 1 NextSeq500 Highoutput FC, SR for 1x 79 cycles plus 10 cycles for the index read and 2 dark cycles upfront Read 1.

4.6 Bioinformatics analysis

4.6.1 Bioinformatics analysis of proteomics data

Processed data were analyzed in R (4.4.2). The identified protein groups were filtered for potential contaminants, reverse-identified peptides, identification only by site, and unique peptides (>1). The p-values were calculated by a moderated t-test using the limma package [176]. The resulting p-values were corrected for multiple hypothesis testing using the Benjamini–Hochberg FDR method. For downstream analysis, only regulated protein groups with FDR <0.05 were considered significant. Similarly, the identified diglycine-lysine peptides were filtered for potential contaminants, reverse-identified peptides, and localization probability (>75%). The p-values were calculated by a moderated t-test using the limma package. For downstream analysis, only regulated ubiquitylation sites with p-value <0.05 were considered significant.

GO functional enrichment analysis across significantly regulated genes was done using the clusterProfiler package in R [177]. The p-values were evaluated using clusterProfiler and corrected using the Benjamini–Hochberg FDR method.

4.6.2 Bioinformatics analysis of mRNA-sequencing data

The mRNA with a read length of 84 bp was sequenced in paired end mode. Demultiplexed was carried out using bcl2fastq v1.19. The samples were mapped against hg38 (Gencode primary release (v26) using STAR (v2.7.10). Reads per gene were quantified using featureCounts (v. 2.0.0). For the mRNA analysis exons were used as a reference to quantify the amount of reads per gene. The differential expression analysis was performed using Bioconductor (v3.14) / DESeq2 (v1.34). Genes were deemed sign. diff. regulated with an FDR below 1%. In the mRNA-Seq splicing event analysis was conducted using rMATS (v4.1.2). Splicing events with an FDR smaller than 5% were considered significant.

4.6.3 AlphaFold3 Prediction of AQR-XAB2 interaction

AlphaFold3 predictions were generated using the monomer or multimer model with 5 recycles and all 5 model parameter sets; models were ranked by the internal confidence metrics (pLDDT and pTM/ipTM) and the top-ranked models were analyzed [178]. MSAs were constructed by the pipeline's default database searches, and structural templates were disabled unless stated. Confidence was assessed by per-residue pLDDT and global pTM/ipTM; segments with pLDDT <50 were not used for mechanistic inference [179], [180]. Protein complexes were modeled with AlphaFold-Multimer and ranked by ipTM+pTM, with interface confidence used to prioritize models; alternative stoichiometries were explored by varying seeds [181]. Precomputed structures from the AlphaFold Protein Structure Database were used for entries AQR, XAB2 (O60306, Q9HCS7). Predictions were treated as testable hypotheses and interpreted in the context of experimental constraints.

5. List of abbreviations

Abbreviation	Full term
20S	20S proteasome core particle
26S	26S proteasome (20S+19S)
5-EU / EU	5-Ethynyl uridine
ACN	Acetonitrile
AF647	Alexa Fluor 647
APEX / APEX2	Ascorbate peroxidase proximity labeling enzyme
APC/C	Anaphase-Promoting Complex/Cyclosome
APPBP2	Amyloid beta precursor protein binding protein 2
ARM	Armadillo repeat
BbsI/BpiI	Type IIS restriction endonuclease
BH	Benjamini–Hochberg
BIR	Baculovirus IAP Repeat
BRCA1	Breast cancer type 1 susceptibility protein
BSA	Bovine Serum Albumin
BTRC/FBXW1	Beta-TrCP1 F-box protein
Bub3	Budding uninhibited by benzimidazole 3
BubR1	Bub1-related kinase
CDK2	Cyclin-dependent kinase 2
Cdk4/6	Cyclin-dependent kinases 4 and 6
CHIP (STUB1)	C-terminus of Hsc70-interacting protein
CRBN	Cereblon
CRISPR	Clustered regularly interspaced short palindromic repeats
CRL	Cullin-RING ligase (family)
CRL2	Cullin-2-based RING ligase
CRL4	Cullin-4-based RING ligase
Cul3-KLHL20	CUL3 with KLHL20 receptor

CUL	Cullin scaffold proteins
CUL2	Cullin-2
CUL3	Cullin-3
CYLD	Cylindromatosis deubiquitylase
DDA	Data-Dependent Acquisition
DCAF12	DDB1- and CUL4-associated factor 12
DIA	Data-Independent Acquisition
DLD-1	Human colorectal adenocarcinoma cell line
DNase	Deoxyribonuclease
DPBS	Dulbecco's Phosphate-Buffered Saline
DSIF	DRB Sensitivity-Inducing Factor
DUBs	Deubiquitylating enzymes
DTT	Dithiothreitol
E1	Ubiquitin/UBL-activating enzyme
E2	Ubiquitin/UBL-conjugating enzyme
E3	Ubiquitin ligase
ECL	Enhanced chemiluminescence
EDTA	Ethylenediaminetetraacetic acid
Eps15	Epidermal growth factor receptor substrate 15
ERAD	Endoplasmic Reticulum-Associated Degradation
FACT	Facilitates Chromatin Transcription
FANCD2	Fanconi anemia D2 protein
FANCI	Fanconi anemia I protein
FACS	Fluorescence-Activated Cell Sorting
FBS	Fetal Bovine Serum
FBXW11	Beta-TrCP2 F-box protein
FBXW7 (Fbw7)	F-box/WD repeat protein 7
GID	Glucose-Induced Degradation complex
GO	Gene Ontology

GFP	Green Fluorescent Protein
GSK3	Glycogen synthase kinase 3
H2A	Histone H2A
H3K4	Histone H3 lysine 4
HDAC1/2	Histone deacetylases 1/2
HEAT repeats	HEAT (Huntingtin, Elongation factor 3, PR65/A, TOR)
HECT	Homologous to E6-AP C-terminus
HEPES	4-(2-Hydroxyethyl)-1-piperazineethanesulfonic acid
HGNC symbols	Gene/protein symbols (e.g., UBR5, AQR)
hTERT	Human Telomerase Reverse Transcriptase
HRP	Horseradish peroxidase
IAP	Inhibitor of Apoptosis Protein
IBR	In-Between RING
IKK	IκB kinase complex
iBAQ	Intensity-Based Absolute Quantification
IκB	Inhibitor of κB
IonQuant	Label-free quant tool
ISG15	Interferon-Stimulated Gene 15
ISY1	Pre-mRNA splicing factor ISY1
JAMM/MPN+	JAB1/MPN domain metallo-DUBs
JNK	c-Jun N-terminal kinase
K-ε-GG	Diglycine remnant on lysine
K6, K11, K27, K33, K48, K63	Lysine N-linked Ub chain
KEAP1	Kelch-like ECH-associated protein 1
KEN box	Lys-Glu-Asn degron
KLHDC2/3/10	Kelch-like domain containing 2/3/10
LB	Lysogeny broth
LC-MS/MS	Liquid chromatography–tandem MS
LDS	Lithium dodecyl sulfate

LUBAC	Linear Ubiquitin Chain Assembly Complex
M1	Met1-linked (linear) Ub chain
MAX	MYC-associated factor X
MaxLFQ	MaxQuant LFQ algorithm
MCC	Mitotic Checkpoint Complex
MDC1	Mediator of DNA Damage Checkpoint 1
MEK/ERK	MAP2K/ERK kinases
MG132	Proteasome inhibitor
MINDY	Motif-Interacting with Ub-containing DUB
MOPS	3-(N-morpholino)propane sulfonic acid
MYC	MYC oncoprotein
NDP52	CALCOCO2
NEDD8	Neural precursor cell expressed, developmentally downregulated 8
NEMO	NF-κB essential modulator
NF-κB	Nuclear factor kappa-B
NPL4	Nuclear protein localization 4
NP-40	Nonidet P-40
NRF2	Nuclear factor erythroid 2-related factor 2
OTU/OTUs	Ovarian Tumor domain proteases
OtUBD	OTU ubiquitin-binding domain
PABC/MLLE	Poly(A) binding C-term/MLLE domain
PAM2	PABP-interacting motif 2
PARP1	Poly(ADP-ribose) polymerase 1
PCNA	Proliferating Cell Nuclear Antigen
Pen/Strep	Penicillin–Streptomycin
PRC1	Polycomb Repressive Complex 1
PRPF19	PRP19 complex subunit
p97/VCP	Valosin-Containing Protein

Rap80	Receptor-associated protein 80 (UIM-containing)
RBX	RING-box protein (RBX1/2)
RCC1 (RLD)	Regulator of Chromosome Condensation 1-like domain
RING	Really Interesting New Gene
RNF168	RING finger protein 168
RNF20/RNF40	RING E3s for H2B K120Ub
RPE-1	Retinal Pigment Epithelial-1
RPMI	Roswell Park Memorial Institute medium
RPN1	Regulatory particle non-ATPase 1 (Rpn1)
RPN10	Regulatory particle non-ATPase 10
RPN13	Regulatory particle non-ATPase 13
R-SMAD	Receptor-regulated SMAD
SCF	Skp1-Cullin1-F-box complex
SCX	Strong Cation Exchange
SDS	Sodium Dodecyl Sulfate
SDS-PAGE	SDS polyacrylamide gel electrophoresis
Sanger sequencing	Dideoxy chain-termination sequencing
SILAC	Stable Isotope Labeling by Amino acids in Cell culture
SQSTM1/p62	Sequestosome-1
SR (seq)	Single-Read
SR (CRL)	Substrate receptor
STAR	Spliced Transcripts Alignment to a Reference
SUMO	Small Ubiquitin-Like Modifier
SUV39H1	Suppressor of variegation 3-9 homolog 1
TAB2	TAK1-binding protein 2
TAK1	MAP3K7 (TAK1)
TAK-243 (MLN7243)	Ubiquitin-activating enzyme E1 inhibitor
TCEP	Tris(2-carboxyethyl)phosphine
TCR-ζ	T-cell receptor zeta chain

TET	Ten-eleven translocation dioxygenase
TFA	Trifluoroacetic acid
TGF-β	Transforming Growth Factor-β
TMTpro (16plex)	Tandem Mass Tag isobaric labels
TNF-R1	Tumor Necrosis Factor Receptor 1
TP53	Tumor protein p53
TRIP12	Thyroid hormone receptor interactor 12
Tris-HCl	Tris(hydroxymethyl)aminomethane-HCl
Trolox	6-Hydroxy-2,5,7,8-tetramethylchromane-2-carboxylic acid
TXNIP	Thioredoxin-interacting protein
U2OS	Human osteosarcoma cell line
UBA	Ubiquitin-Associated domain
UBDs	Ubiquitin-Binding Domains
UBE2C	E2 enzyme (UbcH10)
UBE2D	E2 enzyme family (UbcH5)
UBE2S	E2 enzyme
UBR5	UBR5 E3 ubiquitin ligase
Ub	Ubiquitin
UFM1 (mentioned via ZUFSP name)	Ubiquitin-fold modifier 1
UIM	Ubiquitin-interacting motif
UPS	Ubiquitin–Proteasome System
VCP/p97	Valosin-Containing Protein
WT	Wild type
WW	WW domain
XAB2	XPA-binding protein 2
ZER1	Zer1 homolog
ZUFSP (ZUP1)	Zinc finger with UFM1-Specific Peptidase
ZYG11B	Zyg-11 family member B

6. Appendix

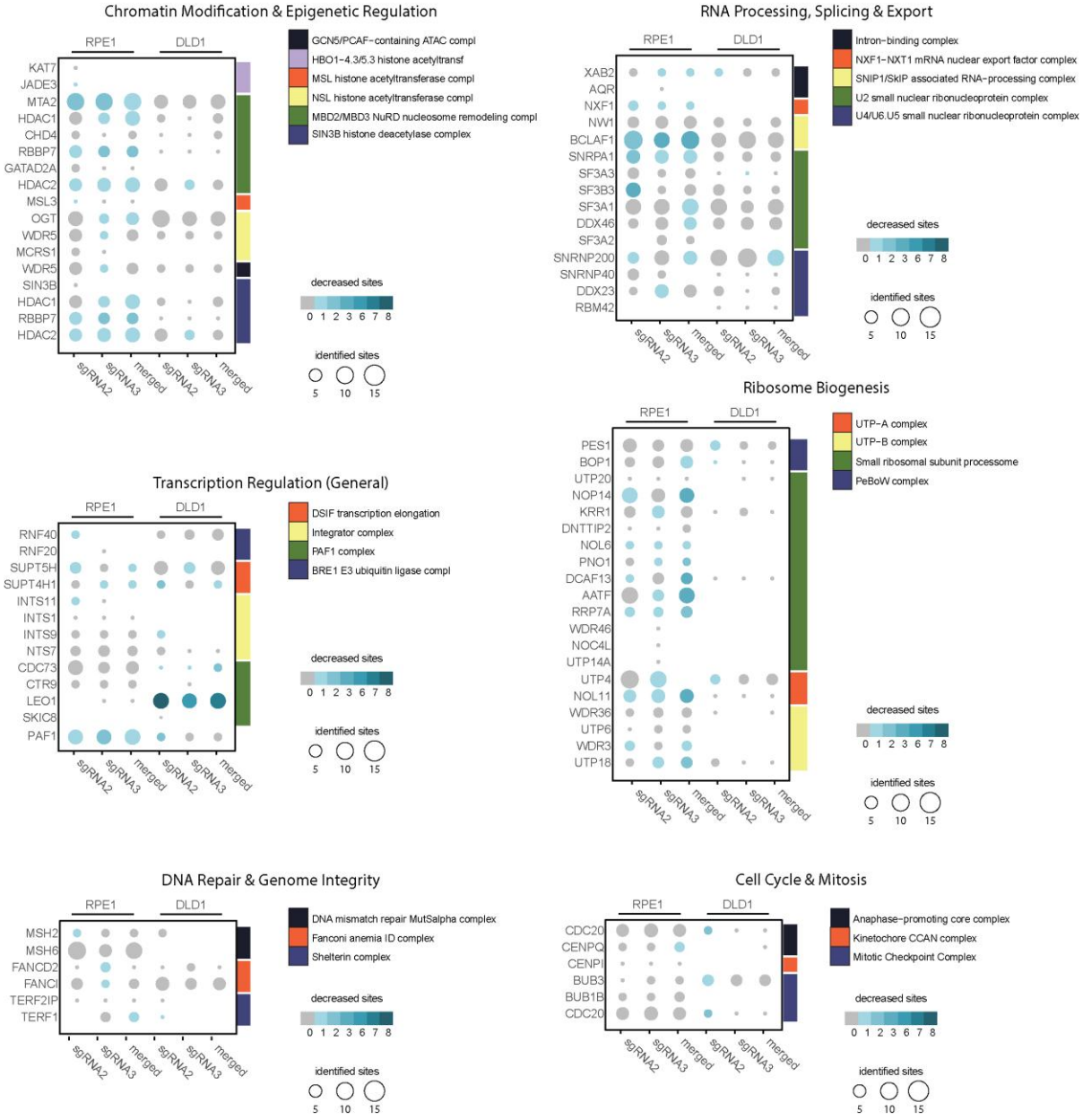

Figure 22. UBR5-dependant ubiquitylation sited within multisubunit protein complexes.

7. References

[1] J. Callis, “The Ubiquitination Machinery of the Ubiquitin System,” *Arab. Book*, vol. 12, p. e0174, Jan. 2014, doi: 10.1199/tab.0174.

[2] J. D. Etlinger and A. L. Goldberg, “A soluble ATP-dependent proteolytic system responsible for the degradation of abnormal proteins in reticulocytes.,” *Proc. Natl. Acad. Sci.*, vol. 74, no. 1, pp. 54–58, Jan. 1977, doi: 10.1073/pnas.74.1.54.

[3] Y. Shimizu, Y. Okuda-Shimizu, and L. M. Hendershot, “Ubiquitylation of an ERAD Substrate Occurs on Multiple Types of Amino Acids,” *Mol. Cell*, vol. 40, no. 6, pp. 917–926, Dec. 2010, doi: 10.1016/j.molcel.2010.11.033.

[4] K.-C. Pao *et al.*, “Activity-based E3 ligase profiling uncovers an E3 ligase with esterification activity,” *Nature*, vol. 556, no. 7701, pp. 381–385, Apr. 2018, doi: 10.1038/s41586-018-0026-1.

[5] I. R. Kelsall, J. Zhang, A. Knebel, J. S. C. Arthur, and P. Cohen, “The E3 ligase HOIL-1 catalyses ester bond formation between ubiquitin and components of the Myddosome in mammalian cells,” *Proc. Natl. Acad. Sci.*, vol. 116, no. 27, pp. 13293–13298, July 2019, doi: 10.1073/pnas.1905873116.

[6] A. Hershko, “OCCURRENCE OF A POLYUBIQUITIN STRUCTURE IN UBIQUITIN-PROTEIN CONJUCATES,” *Biochem. Biophys. Res. Commun.*, vol. 128, no. 3, pp. 1079–1086, May 1985.

[7] V. Chau *et al.*, “A Multiubiquitin Chain Is Confined to Specific Lysine in a Targeted Short-Lived Protein,” *Science*, vol. 243, no. 4898, pp. 1576–1583, Mar. 1989, doi: 10.1126/science.2538923.

[8] M. Hrdinka and M. Gyrd-Hansen, “The Met1-Linked Ubiquitin Machinery: Emerging Themes of (De)regulation,” *Mol. Cell*, vol. 68, no. 2, pp. 265–280, Oct. 2017, doi: 10.1016/j.molcel.2017.09.001.

[9] R. G. Yau *et al.*, “Assembly and Function of Heterotypic Ubiquitin Chains in Cell-Cycle and Protein Quality Control,” *Cell*, vol. 171, no. 4, pp. 918-933.e20, Nov. 2017, doi: 10.1016/j.cell.2017.09.040.

[10] L. Cappadocia and C. D. Lima, “Ubiquitin-like Protein Conjugation: Structures, Chemistry, and Mechanism,” *Chem. Rev.*, vol. 118, no. 3, pp. 889–918, Feb. 2018, doi: 10.1021/acs.chemrev.6b00737.

[11] T. Kamitani, K. Kito, H. P. Nguyen, and E. T. H. Yeh, “Characterization of NEDD8, a Developmentally Down-regulated Ubiquitin-like Protein,” *J. Biol. Chem.*, vol. 272, no. 45, pp. 28557–28562, Nov. 1997, doi: 10.1074/jbc.272.45.28557.

[12] A. L. Haas, P. Ahrens, P. M. Bright, and H. Ankel, “Interferon induces a 15-kilodalton protein exhibiting marked homology to ubiquitin.,” *J. Biol. Chem.*, vol. 262, no. 23, pp. 11315–11323, Aug. 1987, doi: 10.1016/S0021-9258(18)60961-5.

[13] K. Howe, J. Williamson, N. Boddy, D. Sheer, P. Freemont, and E. Solomon, “The Ubiquitin-Homology GenePIC1:Characterization of Mouse (Pic1) and Human (UBL1) Genes and Pseudogenes,” *Genomics*, vol. 47, no. 1, pp. 92–100, Jan. 1998, doi: 10.1006/geno.1997.5091.

[14] J. Prudden *et al.*, “SUMO-targeted ubiquitin ligases in genome stability,” *EMBO J.*, vol. 26, no. 18, pp. 4089–4101, Sept. 2007, doi: 10.1038/sj.emboj.7601838.

[15] F. Aillet *et al.*, “Heterologous SUMO-2/3-Ubiquitin Chains Optimize IκBα Degradation and NF-κB Activity,” *PLoS ONE*, vol. 7, no. 12, p. e51672, Dec. 2012, doi: 10.1371/journal.pone.0051672.

[16] B. A. Schulman and J. Wade Harper, “Ubiquitin-like protein activation by E1 enzymes: the apex for downstream signalling pathways,” *Nat. Rev. Mol. Cell Biol.*, vol. 10, no. 5, pp. 319–331, May 2009, doi: 10.1038/nrm2673.

[17] D. Komander and M. Rape, “The Ubiquitin Code,” *Annu. Rev. Biochem.*, vol. 81, no. 1, pp. 203–229, July 2012, doi: 10.1146/annurev-biochem-060310-170328.

[18] A. Upadhyay and V. Joshi, “The Ubiquitin Tale: Current Strategies and Future Challenges,” *ACS Pharmacol. Transl. Sci.*, vol. 7, no. 9, pp. 2573–2587, Sept. 2024, doi: 10.1021/acsptsci.4c00278.

[19] Y. Wang, D. Argiles-Castillo, E. I. Kane, A. Zhou, and D. E. Spratt, “HECT E3 ubiquitin ligases – emerging insights into their biological roles and disease relevance,” *J. Cell Sci.*, vol. 133, no. 7, p. jcs228072, Apr. 2020, doi: 10.1242/jcs.228072.

[20] R. J. Deshaies and C. A. P. Joazeiro, “RING Domain E3 Ubiquitin Ligases,” *Annu. Rev. Biochem.*, vol. 78, no. 1, pp. 399–434, June 2009, doi: 10.1146/annurev.biochem.78.101807.093809.

[21] X. S. Wang *et al.*, “The unifying catalytic mechanism of the RING-between-RING E3 ubiquitin ligase family,” *Nat. Commun.*, vol. 14, no. 1, p. 168, Jan. 2023, doi: 10.1038/s41467-023-35871-z.

[22] H. I. Chen and M. Sudol, “The WW domain of Yes-associated protein binds a proline-rich ligand that differs from the consensus established for Src homology 3-binding modules.,” *Proc. Natl. Acad. Sci.*, vol. 92, no. 17, pp. 7819–7823, Aug. 1995, doi: 10.1073/pnas.92.17.7819.

[23] R. Dunn, D. A. Klos, A. S. Adler, and L. Hicke, “The C2 domain of the Rsp5 ubiquitin ligase binds membrane phosphoinositides and directs ubiquitination of endosomal cargo,” *J. Cell Biol.*, vol. 165, no. 1, pp. 135–144, Apr. 2004, doi: 10.1083/jcb.200309026.

[24] M. Janosev *et al.*, “Structural basis of ubiquitin ligase Nedd4-2 autoinhibition and regulation by calcium and 14-3-3 proteins,” *Nat. Commun.*, vol. 16, no. 1, p. 4875, May 2025, doi: 10.1038/s41467-025-60207-4.

[25] J. Sala-Gaston *et al.*, “HERC Ubiquitin Ligases in Cancer,” *Cancers*, vol. 12, no. 6, p. 1653, June 2020, doi: 10.3390/cancers12061653.

[26] J. J. Y. Wong, Y. F. Pung, N. S.-K. Sze, and K.-C. Chin, “HERC5 is an IFN-induced HECT-type E3 protein ligase that mediates type I IFN-induced ISGylation of protein targets,” *Proc. Natl. Acad. Sci.*, vol. 103, no. 28, pp. 10735–10740, July 2006, doi: 10.1073/pnas.0600397103.

[27] G. A. Versteeg, B. G. Hale, S. Van Boheemen, T. Wolff, D. J. Lenschow, and A. García-Sastre, “Species-Specific Antagonism of Host ISGylation by the Influenza B Virus NS1 Protein,” *J. Virol.*, vol. 84, no. 10, pp. 5423–5430, May 2010, doi: 10.1128/JVI.02395-09.

[28] M. Brunet, C. Vargas, D. Larrieu, J. Torrisani, and M. Dufresne, “E3 Ubiquitin Ligase TRIP12: Regulation, Structure, and Physiopathological Functions,” *Int. J. Mol. Sci.*, vol. 21, no. 22, p. 8515, Nov. 2020, doi: 10.3390/ijms21228515.

[29] M. Gatti, R. Imhof, Q. Huang, M. Baudis, and M. Altmeyer, “The Ubiquitin Ligase TRIP12 Limits PARP1 Trapping and Constrains PARP Inhibitor Efficiency,” *Cell Rep.*, vol. 32, no. 5, p. 107985, Aug. 2020, doi: 10.1016/j.celrep.2020.107985.

[30] Z. Hodáková *et al.*, “Cryo-EM structure of the chain-elongating E3 ubiquitin ligase UBR5,” *EMBO J.*, vol. 42, no. 16, p. e113348, Aug. 2023, doi: 10.15252/embj.2022113348.

[31] J. W. Harper and B. A. Schulman, “Cullin-RING Ubiquitin Ligase Regulatory Circuits: A Quarter Century Beyond the F-Box Hypothesis,” *Annu. Rev. Biochem.*, vol. 90, no. 1, pp. 403–429, June 2021, doi: 10.1146/annurev-biochem-090120-013613.

[32] D. M. Duda, L. A. Borg, D. C. Scott, H. W. Hunt, M. Hammel, and B. A. Schulman, "Structural Insights into NEDD8 Activation of Cullin-RING Ligases: Conformational Control of Conjugation," *Cell*, vol. 134, no. 6, pp. 995–1006, Sept. 2008, doi: 10.1016/j.cell.2008.07.022.

[33] K. Baek *et al.*, "NEDD8 nucleates a multivalent cullin–RING–UBE2D ubiquitin ligation assembly," *Nature*, vol. 578, no. 7795, pp. 461–466, Feb. 2020, doi: 10.1038/s41586-020-2000-y.

[34] G. Dewson, P. J. A. Eichhorn, and D. Komander, "Deubiquitinases in cancer," *Nat. Rev. Cancer*, vol. 23, no. 12, pp. 842–862, Dec. 2023, doi: 10.1038/s41568-023-00633-y.

[35] I. Dikic, S. Wakatsuki, and K. J. Walters, "Ubiquitin-binding domains — from structures to functions," *Nat. Rev. Mol. Cell Biol.*, vol. 10, no. 10, pp. 659–671, Oct. 2009, doi: 10.1038/nrm2767.

[36] K. Husnjak and I. Dikic, "Ubiquitin-Binding Proteins: Decoders of Ubiquitin-Mediated Cellular Functions," *Annu. Rev. Biochem.*, vol. 81, no. 1, pp. 291–322, July 2012, doi: 10.1146/annurev-biochem-051810-094654.

[37] C. Arkinson, K. C. Dong, C. L. Gee, and A. Martin, "Mechanisms and regulation of substrate degradation by the 26S proteasome," *Nat. Rev. Mol. Cell Biol.*, vol. 26, no. 2, pp. 104–122, Feb. 2025, doi: 10.1038/s41580-024-00778-0.

[38] G. Bjørkøy *et al.*, "p62/SQSTM1 forms protein aggregates degraded by autophagy and has a protective effect on huntingtin-induced cell death," *J. Cell Biol.*, vol. 171, no. 4, pp. 603–614, Nov. 2005, doi: 10.1083/jcb.200507002.

[39] S. Pankiv *et al.*, "p62/SQSTM1 Binds Directly to Atg8/LC3 to Facilitate Degradation of Ubiquitinated Protein Aggregates by Autophagy," *J. Biol. Chem.*, vol. 282, no. 33, pp. 24131–24145, Aug. 2007, doi: 10.1074/jbc.M702824200.

[40] N. Fujita *et al.*, "Recruitment of the autophagic machinery to endosomes during infection is mediated by ubiquitin," *J. Cell Biol.*, vol. 203, no. 1, pp. 115–128, Oct. 2013, doi: 10.1083/jcb.201304188.

[41] V. Kirkin *et al.*, "A Role for NBR1 in Autophagosomal Degradation of Ubiquitinated Substrates," *Mol. Cell*, vol. 33, no. 4, pp. 505–516, Feb. 2009, doi: 10.1016/j.molcel.2009.01.020.

[42] A. Ordureau *et al.*, "Defining roles of PARKIN and ubiquitin phosphorylation by PINK1 in mitochondrial quality control using a ubiquitin replacement strategy," *Proc. Natl. Acad. Sci.*, vol. 112, no. 21, pp. 6637–6642, May 2015, doi: 10.1073/pnas.1506593112.

[43] Y. Ye, H. H. Meyer, and T. A. Rapoport, "Function of the p97–Ufd1–Npl4 complex in retrotranslocation from the ER to the cytosol," *J. Cell Biol.*, vol. 162, no. 1, pp. 71–84, July 2003, doi: 10.1083/jcb.200302169.

[44] W. S. Chia, D. X. Chia, F. Rao, S. Bar Nun, and S. Geifman Shochat, "ATP Binding to p97/VCP D1 Domain Regulates Selective Recruitment of Adaptors to Its Proximal N-Domain," *PLoS ONE*, vol. 7, no. 12, p. e50490, Dec. 2012, doi: 10.1371/journal.pone.0050490.

[45] V. E. Pye *et al.*, "Structural insights into the p97-Ufd1-Npl4 complex," *Proc. Natl. Acad. Sci.*, vol. 104, no. 2, pp. 467–472, Jan. 2007, doi: 10.1073/pnas.0603408104.

[46] E. E. Blythe, K. C. Olson, V. Chau, and R. J. Deshaies, "Ubiquitin- and ATP-dependent unfoldase activity of P97/VCP•NPLOC4•UFD1L is enhanced by a mutation that causes multisystem proteinopathy," *Proc. Natl. Acad. Sci.*, vol. 114, no. 22, May 2017, doi: 10.1073/pnas.1706205114.

[47] Q. Wang, L. Li, and Y. Ye, “Regulation of retrotranslocation by p97-associated deubiquitinating enzyme ataxin-3,” *J. Cell Biol.*, vol. 174, no. 7, pp. 963–971, Sept. 2006, doi: 10.1083/jcb.200605100.

[48] N. Tolay and A. Buchberger, “Comparative profiling of stress granule clearance reveals differential contributions of the ubiquitin system,” *Life Sci. Alliance*, vol. 4, no. 5, p. e202000927, May 2021, doi: 10.26508/lsa.202000927.

[49] T. E. Messick and R. A. Greenberg, “The ubiquitin landscape at DNA double-strand breaks,” *J. Cell Biol.*, vol. 187, no. 3, pp. 319–326, Nov. 2009, doi: 10.1083/jcb.200908074.

[50] F. Mattiroli *et al.*, “RNF168 Ubiquitinates K13-15 on H2A/H2AX to Drive DNA Damage Signaling,” *Cell*, vol. 150, no. 6, pp. 1182–1195, Sept. 2012, doi: 10.1016/j.cell.2012.08.005.

[51] Q. Hu *et al.*, “Mechanisms of RNF168 nucleosome recognition and ubiquitylation,” *Mol. Cell*, vol. 84, no. 5, pp. 839-853.e12, Mar. 2024, doi: 10.1016/j.molcel.2023.12.036.

[52] F. Tokunaga *et al.*, “SHARPIN is a component of the NF-κB-activating linear ubiquitin chain assembly complex,” *Nature*, vol. 471, no. 7340, pp. 633–636, Mar. 2011, doi: 10.1038/nature09815.

[53] S. E. Kaiser *et al.*, “Protein standard absolute quantification (PSAQ) method for the measurement of cellular ubiquitin pools,” *Nat. Methods*, vol. 8, no. 8, pp. 691–696, Aug. 2011, doi: 10.1038/nmeth.1649.

[54] K. Watanabe, S. Tateishi, M. Kawasuji, T. Tsurimoto, H. Inoue, and M. Yamaizumi, “Rad18 guides polη to replication stalling sites through physical interaction and PCNA monoubiquitination,” *EMBO J.*, vol. 23, no. 19, pp. 3886–3896, Sept. 2004, doi: 10.1038/sj.emboj.7600383.

[55] P. Alcón, S. Shakeel, Z. A. Chen, J. Rappsilber, K. J. Patel, and L. A. Passmore, "FANCD2–FANCI is a clamp stabilized on DNA by monoubiquitination of FANCD2 during DNA repair," *Nat. Struct. Mol. Biol.*, vol. 27, no. 3, pp. 240–248, Mar. 2020, doi: 10.1038/s41594-020-0380-1.

[56] J. Zhang *et al.*, "The regulation of TGF-β/SMAD signaling by protein deubiquitination," *Protein Cell*, vol. 5, no. 7, pp. 503–517, July 2014, doi: 10.1007/s13238-014-0058-8.

[57] A. Chen, F. E. Kleiman, J. L. Manley, T. Ouchi, and Z.-Q. Pan, "Autoubiquitination of the BRCA1·BARD1 RING Ubiquitin Ligase," *J. Biol. Chem.*, vol. 277, no. 24, pp. 22085–22092, June 2002, doi: 10.1074/jbc.M201252200.

[58] H. Wang *et al.*, "Role of histone H2A ubiquitination in Polycomb silencing," *Nature*, vol. 431, no. 7010, pp. 873–878, Oct. 2004, doi: 10.1038/nature02985.

[59] J. M. Espinosa, "Histone H2B ubiquitination: the cancer connection," *Genes Dev.*, vol. 22, no. 20, pp. 2743–2749, Oct. 2008, doi: 10.1101/gad.1732108.

[60] T. Nakagawa *et al.*, "CRL4VprBP E3 Ligase Promotes Monoubiquitylation and Chromatin Binding of TET Dioxygenases," *Mol. Cell*, vol. 57, no. 2, pp. 247–260, Jan. 2015, doi: 10.1016/j.molcel.2014.12.002.

[61] H. Tsuchiya *et al.*, "Ub-ProT reveals global length and composition of protein ubiquitylation in cells," *Nat. Commun.*, vol. 9, no. 1, p. 524, Feb. 2018, doi: 10.1038/s41467-018-02869-x.

[62] S. Fang, J. P. Jensen, R. L. Ludwig, K. H. Vousden, and A. M. Weissman, "Mdm2 Is a RING Finger-dependent Ubiquitin Protein Ligase for Itself and p53," *J. Biol. Chem.*, vol. 275, no. 12, pp. 8945–8951, Mar. 2000, doi: 10.1074/jbc.275.12.8945.

[63] A. Devin, Y. Lin, S. Yamaoka, Z. Li, M. Karin, and Z.-G. Liu, “The a and b Subunits of IkB Kinase (IKK) Mediate TRAF2- Dependent IKK Recruitment to Tumor Necrosis Factor (TNF) Receptor 1 in Response to TNF”.

[64] National Cancer Institute, “The Distinct Roles of TRAF2 and RIP in IKK Activation by TNF-R1: TRAF2 Recruits IKK to TNF-R1 while RIP Mediates IKK Activation,” in *Definitions*, Qeios, 2020. doi: 10.32388/3SMZOB.

[65] Z. J. Chen, “Ubiquitin signalling in the NF-κB pathway,” *Nat. Cell Biol.*, vol. 7, no. 8, pp. 758–765, Aug. 2005, doi: 10.1038/ncb0805-758.

[66] T. M. Durcan *et al.*, “USP 8 regulates mitophagy by removing K 6-linked ubiquitin conjugates from parkin,” *EMBO J.*, vol. 33, no. 21, pp. 2473–2491, Nov. 2014, doi: 10.15252/embj.201489729.

[67] A. Suryo Rahmanto *et al.*, “K6-linked ubiquitylation marks formaldehyde-induced RNA-protein crosslinks for resolution,” *Mol. Cell*, vol. 83, no. 23, pp. 4272-4289.e10, Dec. 2023, doi: 10.1016/j.molcel.2023.10.011.

[68] J. B. Heidelberger *et al.*, “Proteomic profiling of VCP substrates links VCP to K6-linked ubiquitylation and c-Myc function,” *EMBO Rep.*, vol. 19, no. 4, p. e44754, Apr. 2018, doi: 10.15252/embr.201744754.

[69] L. Jin, A. Williamson, S. Banerjee, I. Philipp, and M. Rape, “Mechanism of Ubiquitin-Chain Formation by the Human Anaphase-Promoting Complex,” *Cell*, vol. 133, no. 4, pp. 653–665, May 2008, doi: 10.1016/j.cell.2008.04.012.

[70] M. L. Matsumoto *et al.*, “K11-Linked Polyubiquitination in Cell Cycle Control Revealed by a K11 Linkage-Specific Antibody,” *Mol. Cell*, vol. 39, no. 3, pp. 477–484, Aug. 2010, doi: 10.1016/j.molcel.2010.07.001.

[71] R. F. Shearer *et al.*, "K27-linked ubiquitylation promotes p97 substrate processing and is essential for cell proliferation," *EMBO J.*, vol. 41, no. 9, p. e110145, May 2022, doi: 10.15252/embj.2021110145.

[72] Q. Yin *et al.*, "K27-linked ubiquitination of BRAF by ITCH engages cytokine response to maintain MEK-ERK signaling," *Nat. Commun.*, vol. 10, no. 1, p. 1870, Apr. 2019, doi: 10.1038/s41467-019-09844-0.

[73] M. Gatti *et al.*, "RNF168 Promotes Noncanonical K27 Ubiquitination to Signal DNA Damage," *Cell Rep.*, vol. 10, no. 2, pp. 226–238, Jan. 2015, doi: 10.1016/j.celrep.2014.12.021.

[74] H. Garadi Suresh *et al.*, "K29-linked free polyubiquitin chains affect ribosome biogenesis and direct ribosomal proteins to the intranuclear quality control compartment," *Mol. Cell*, vol. 84, no. 12, pp. 2337-2352.e9, June 2024, doi: 10.1016/j.molcel.2024.05.018.

[75] W.-C. Yuan *et al.*, "K33-Linked Polyubiquitination of Coronin 7 by Cul3-KLHL20 Ubiquitin E3 Ligase Regulates Protein Trafficking," *Mol. Cell*, vol. 54, no. 4, pp. 586–600, May 2014, doi: 10.1016/j.molcel.2014.03.035.

[76] H. Huang *et al.*, "K33-Linked Polyubiquitination of T Cell Receptor-ζ Regulates Proteolysis-Independent T Cell Signaling," *Immunity*, vol. 33, no. 1, pp. 60–70, July 2010, doi: 10.1016/j.immuni.2010.07.002.

[77] Y. Nibe *et al.*, "Novel polyubiquitin imaging system, PolyUb-FC, reveals that K33-linked polyubiquitin is recruited by SQSTM1/p62," *Autophagy*, vol. 14, no. 2, pp. 347–358, Feb. 2018, doi: 10.1080/15548627.2017.1407889.

[78] T. Kirisako *et al.*, "A ubiquitin ligase complex assembles linear polyubiquitin chains".

[79] J. Niu, Y. Shi, K. Iwai, and Z.-H. Wu, "LUBAC regulates NF-κB activation upon genotoxic stress by promoting linear ubiquitination of NEMO: NEMO linear ubiquitination upon genotoxic stress," *EMBO J.*, vol. 30, no. 18, pp. 3741–3753, Sept. 2011, doi: 10.1038/emboj.2011.264.

[80] T. L. Haas *et al.*, "Recruitment of the Linear Ubiquitin Chain Assembly Complex Stabilizes the TNF-R1 Signaling Complex and Is Required for TNF-Mediated Gene Induction," *Mol. Cell*, vol. 36, no. 5, pp. 831–844, Dec. 2009, doi: 10.1016/j.molcel.2009.10.013.

[81] L. Gao *et al.*, "The mechanism of linear ubiquitination in regulating cell death and correlative diseases," *Cell Death Dis.*, vol. 14, no. 10, p. 659, Oct. 2023, doi: 10.1038/s41419-023-06183-3.

[82] F. Ohtake, H. Tsuchiya, Y. Saeki, and K. Tanaka, "K63 ubiquitylation triggers proteasomal degradation by seeding branched ubiquitin chains," *Proc. Natl. Acad. Sci.*, vol. 115, no. 7, Feb. 2018, doi: 10.1073/pnas.1716673115.

[83] H.-J. Meyer and M. Rape, "Enhanced Protein Degradation by Branched Ubiquitin Chains," *Cell*, vol. 157, no. 4, pp. 910–921, May 2014, doi: 10.1016/j.cell.2014.03.037.

[84] R. G. Yau *et al.*, "Assembly and Function of Heterotypic Ubiquitin Chains in Cell-Cycle and Protein Quality Control," *Cell*, vol. 171, no. 4, pp. 918-933.e20, Nov. 2017, doi: 10.1016/j.cell.2017.09.040.

[85] A. Waltho *et al.*, "K48- and K63-linked ubiquitin chain interactome reveals branch- and length-specific ubiquitin interactors," *Life Sci. Alliance*, vol. 7, no. 8, p. e202402740, Aug. 2024, doi: 10.26508/lsa.202402740.

[86] C. H. Emmerich *et al.*, "Activation of the canonical IKK complex by K63/M1-linked hybrid ubiquitin chains," *Proc. Natl. Acad. Sci.*, vol. 110, no. 38, pp. 15247–15252, Sept. 2013, doi: 10.1073/pnas.1314715110.

[87] M. E. French, C. F. Koehler, and T. Hunter, “Emerging functions of branched ubiquitin chains,” *Cell Discov.*, vol. 7, no. 1, p. 6, Jan. 2021, doi: 10.1038/s41421-020-00237-y.

[88] F. Wang *et al.*, “Structure of the human UBR5 E3 ubiquitin ligase,” *Structure*, vol. 31, no. 5, pp. 541-552.e4, May 2023, doi: 10.1016/j.str.2023.03.010.

[89] F. Ohtake, Y. Saeki, S. Ishido, J. Kanno, and K. Tanaka, “The K48-K63 Branched Ubiquitin Chain Regulates NF-κB Signaling,” *Mol. Cell*, vol. 64, no. 2, pp. 251–266, Oct. 2016, doi: 10.1016/j.molcel.2016.09.014.

[90] F. Ohtake, H. Tsuchiya, Y. Saeki, and K. Tanaka, “K63 ubiquitylation triggers proteasomal degradation by seeding branched ubiquitin chains,” *Proc. Natl. Acad. Sci.*, vol. 115, no. 7, Feb. 2018, doi: 10.1073/pnas.1716673115.

[91] S. M. Lange *et al.*, “VCP/p97-associated proteins are binders and debranching enzymes of K48–K63-branched ubiquitin chains,” *Nat. Struct. Mol. Biol.*, vol. 31, no. 12, pp. 1872–1887, Dec. 2024, doi: 10.1038/s41594-024-01354-y.

[92] D. L. Haakonsen *et al.*, “Stress response silencing by an E3 ligase mutated in neurodegeneration,” *Nature*, vol. 626, no. 8000, pp. 874–880, Feb. 2024, doi: 10.1038/s41586-023-06985-7.

[93] A. Kaiho-Soma *et al.*, “TRIP12 promotes small-molecule-induced degradation through K29/K48-branched ubiquitin chains,” *Mol. Cell*, vol. 81, no. 7, pp. 1411-1424.e7, Apr. 2021, doi: 10.1016/j.molcel.2021.01.023.

[94] C. Liu, W. Liu, Y. Ye, and W. Li, “Ufd2p synthesizes branched ubiquitin chains to promote the degradation of substrates modified with atypical chains,” *Nat. Commun.*, vol. 8, no. 1, p. 14274, Feb. 2017, doi: 10.1038/ncomms14274.

[95] A. Kaiho-Soma *et al.*, "TRIP12 promotes small-molecule-induced degradation through K29/K48-branched ubiquitin chains," *Mol. Cell*, vol. 81, no. 7, pp. 1411-1424.e7, Apr. 2021, doi: 10.1016/j.molcel.2021.01.023.

[96] M. Morita *et al.*, "Combinatorial ubiquitin code degrades deubiquitylation-protected substrates," *Nat. Commun.*, vol. 16, no. 1, p. 2496, Mar. 2025, doi: 10.1038/s41467-025-57873-9.

[97] T. Gudjonsson *et al.*, "TRIP12 and UBR5 Suppress Spreading of Chromatin Ubiquitylation at Damaged Chromosomes," *Cell*, vol. 150, no. 4, pp. 697–709, Aug. 2012, doi: 10.1016/j.cell.2012.06.039.

[98] M. E. Sowa, E. J. Bennett, S. P. Gygi, and J. W. Harper, "Defining the Human Deubiquitinating Enzyme Interaction Landscape," *Cell*, vol. 138, no. 2, pp. 389–403, July 2009, doi: 10.1016/j.cell.2009.04.042.

[99] Y. Sheng *et al.*, "Molecular recognition of p53 and MDM2 by USP7/HAUSP," *Nat. Struct. Mol. Biol.*, vol. 13, no. 3, pp. 285–291, Mar. 2006, doi: 10.1038/nsmb1067.

[100] M. Hu, L. Gu, M. Li, P. D. Jeffrey, W. Gu, and Y. Shi, "Structural Basis of Competitive Recognition of p53 and MDM2 by HAUSP/USP7: Implications for the Regulation of the p53–MDM2 Pathway," *PLoS Biol.*, vol. 4, no. 2, p. e27, Jan. 2006, doi: 10.1371/journal.pbio.0040027.

[101] R. S. Ranaweera and X. Yang, "Auto-ubiquitination of Mdm2 Enhances Its Substrate Ubiquitin Ligase Activity," *J. Biol. Chem.*, vol. 288, no. 26, pp. 18939–18946, June 2013, doi: 10.1074/jbc.M113.454470.

[102] H. M. Magnussen *et al.*, "Structural basis for DNA damage-induced phosphoregulation of MDM2 RING domain," *Nat. Commun.*, vol. 11, no. 1, p. 2094, Apr. 2020, doi: 10.1038/s41467-020-15783-y.

[103] L. F. Stevenson, A. Sparks, N. Allende-Vega, D. P. Xirodimas, D. P. Lane, and M. K. Saville, "The deubiquitinating enzyme USP2a regulates the p53 pathway by targeting Mdm2," *EMBO J.*, vol. 26, no. 4, pp. 976–986, Feb. 2007, doi: 10.1038/sj.emboj.7601567.

[104] S. K. Mungamuri, R. F. Qiao, S. Yao, J. J. Manfredi, W. Gu, and S. A. Aaronson, "USP7 Enforces Heterochromatinization of p53 Target Promoters by Protecting SUV39H1 from MDM2-Mediated Degradation," *Cell Rep.*, vol. 14, no. 11, pp. 2528–2537, Mar. 2016, doi: 10.1016/j.celrep.2016.02.049.

[105] C. Cai *et al.*, "USP25 regulates KEAP1-NRF2 anti-oxidation axis and its inactivation protects acetaminophen-induced liver injury in male mice," *Nat. Commun.*, vol. 14, no. 1, p. 3648, June 2023, doi: 10.1038/s41467-023-39412-6.

[106] C. Schülein-Völk *et al.*, "Dual Regulation of Fbw7 Function and Oncogenic Transformation by Usp28," *Cell Rep.*, vol. 9, no. 3, pp. 1099–1109, Nov. 2014, doi: 10.1016/j.celrep.2014.09.057.

[107] C. Prieto-Garcia *et al.*, "USP28 enables oncogenic transformation of respiratory cells, and its inhibition potentiates molecular therapy targeting mutant EGFR, BRAF and PI3K," *Mol. Oncol.*, vol. 16, no. 17, pp. 3082–3106, Sept. 2022, doi: 10.1002/1878-0261.13217.

[108] K. R. Spencer and G. G. King, "MDM2 as a therapeutic target in advanced biliary tract cancers," *The Oncologist*, vol. 30, no. 5, p. oyaf094, May 2025, doi: 10.1093/oncolo/oyaf094.

[109] R. Pillai, M. Hayashi, A.-M. Zavitsanou, and T. Papagiannakopoulos, "NRF2: KEAPing Tumors Protected," *Cancer Discov.*, vol. 12, no. 3, pp. 625–643, Mar. 2022, doi: 10.1158/2159-8290.CD-21-0922.

[110] Z. Zhang, E. L. Mena, R. T. Timms, I. Koren, and S. J. Elledge, "Degrons: defining the rules of protein degradation," *Nat. Rev. Mol. Cell Biol.*, July 2025, doi: 10.1038/s41580-025-00870-z.

[111] A. Varshavsky, "The N-end rule pathway and regulation by proteolysis," *Protein Sci.*, vol. 20, no. 8, pp. 1298–1345, Aug. 2011, doi: 10.1002/pro.666.

[112] D. Sherpa, J. Chrustowicz, and B. A. Schulman, "How the ends signal the end: Regulation by E3 ubiquitin ligases recognizing protein termini," *Mol. Cell*, vol. 82, no. 8, pp. 1424–1438, Apr. 2022, doi: 10.1016/j.molcel.2022.02.004.

[113] A. Varshavsky, "N-degron pathways," *Proc. Natl. Acad. Sci.*, vol. 121, no. 39, p. e2408697121, Sept. 2024, doi: 10.1073/pnas.2408697121.

[114] H. Cha-Molstad *et al.*, "p62/SQSTM1/Sequestosome-1 is an N-recognin of the N-end rule pathway which modulates autophagosome biogenesis," *Nat. Commun.*, vol. 8, no. 1, p. 102, July 2017, doi: 10.1038/s41467-017-00085-7.

[115] C.-S. Hwang, A. Shemorry, and A. Varshavsky, "N-Terminal Acetylation of Cellular Proteins Creates Specific Degradation Signals," *Science*, vol. 327, no. 5968, pp. 973–977, Feb. 2010, doi: 10.1126/science.1183147.

[116] M. E. R. Maitland, G. A. Lajoie, G. S. Shaw, and C. Schild-Poulter, "Structural and Functional Insights into GID/CTLH E3 Ligase Complexes," *Int. J. Mol. Sci.*, vol. 23, no. 11, p. 5863, May 2022, doi: 10.3390/ijms23115863.

[117] Y. Chun, D. A. Fruman, and G. Lee, "The picky mTORC1 in metabolic enzyme degradation," *Mol. Cell*, vol. 84, no. 11, pp. 2011–2013, June 2024, doi: 10.1016/j.molcel.2024.05.013.

[118] Y. Li *et al.*, "CRL2ZER1/ZYG11B recognizes small N-terminal residues for degradation," *Nat. Commun.*, vol. 13, no. 1, p. 7636, Dec. 2022, doi: 10.1038/s41467-022-35169-6.

[119] B. Dumétier, A. Zadoroznyj, and L. Dubrez, "IAP-Mediated Protein Ubiquitination in Regulating Cell Signaling," *Cells*, vol. 9, no. 5, p. 1118, Apr. 2020, doi: 10.3390/cells9051118.

[120] C. Pla-Prats, S. Cavadini, G. Kempf, and N. H. Thomä, "Recognition of the CCT5 DI-GLU degron by $CRL4^{DCAF12}$ is dependent on TRiC assembly," *EMBO J.*, vol. 42, no. 4, p. e112253, Feb. 2023, doi: 10.15252/embj.2022112253.

[121] M. Ravalin *et al.*, "Specificity for latent C termini links the E3 ubiquitin ligase CHIP to caspases," *Nat. Chem. Biol.*, vol. 15, no. 8, pp. 786–794, Aug. 2019, doi: 10.1038/s41589-019-0322-6.

[122] M. Glotzer, A. W. Murray, and M. W. Kirschner, "Cyclin is degraded by the ubiquitin pathway," *Nature*, vol. 349, no. 6305, pp. 132–138, Jan. 1991, doi: 10.1038/349132a0.

[123] C. Kraft, H. C. Vodermaier, S. Maurer-Stroh, F. Eisenhaber, and J.-M. Peters, "The WD40 Propeller Domain of Cdh1 Functions as a Destruction Box Receptor for APC/C Substrates," *Mol. Cell*, vol. 18, no. 5, pp. 543–553, May 2005, doi: 10.1016/j.molcel.2005.04.023.

[124] H. Xu, "DegronMD: Leveraging Evolutionary and Structural Features for Deciphering Protein-Targeted Degradation, Mutations, and Drug Response to Degrons".

[125] J. He, W. C. H. Chao, Z. Zhang, J. Yang, N. Cronin, and D. Barford, "Insights into Degron Recognition by APC/C Coactivators from the Structure of an Acm1-Cdh1 Complex," *Mol. Cell*, vol. 50, no. 5, pp. 649–660, June 2013, doi: 10.1016/j.molcel.2013.04.024.

[126] B. Hao, S. Oehlmann, M. E. Sowa, J. W. Harper, and N. P. Pavletich, "Structure of a Fbw7-Skp1-Cyclin E Complex: Multisite-Phosphorylated Substrate Recognition by SCF Ubiquitin Ligases," *Mol. Cell*, vol. 26, no. 1, pp. 131–143, Apr. 2007, doi: 10.1016/j.molcel.2007.02.022.

[127] Z. Zhang, E. L. Mena, R. T. Timms, I. Koren, and S. J. Elledge, "Degrons: defining the rules of protein degradation," *Nat. Rev. Mol. Cell Biol.*, July 2025, doi: 10.1038/s41580-025-00870-z.

[128] J. Krönke *et al.*, "Lenalidomide Causes Selective Degradation of IKZF1 and IKZF3 in Multiple Myeloma Cells," *Science*, vol. 343, no. 6168, pp. 301–305, Jan. 2014, doi: 10.1126/science.1244851.

[129] M. Guharoy, P. Bhowmick, M. Sallam, and P. Tompa, "Tripartite degrons confer diversity and specificity on regulated protein degradation in the ubiquitin-proteasome system," *Nat. Commun.*, vol. 7, no. 1, p. 10239, Jan. 2016, doi: 10.1038/ncomms10239.

[130] S. Juszkiewicz and R. S. Hegde, "Quality Control of Orphaned Proteins," *Mol. Cell*, vol. 71, no. 3, pp. 443–457, Aug. 2018, doi: 10.1016/j.molcel.2018.07.001.

[131] M. Heusel *et al.*, "Complex-centric proteome profiling by SEC - SWATH - MS," *Mol. Syst. Biol.*, vol. 15, no. 1, p. e8438, Jan. 2019, doi: 10.15252/msb.20188438.

[132] C. Padovani, P. Jevtić, and M. Rapé, "Quality control of protein complex composition," *Mol. Cell*, vol. 82, no. 8, pp. 1439–1450, Apr. 2022, doi: 10.1016/j.molcel.2022.02.029.

[133] C. Pla-Prats and N. H. Thomä, "Quality control of protein complex assembly by the ubiquitin–proteasome system," *Trends Cell Biol.*, vol. 32, no. 8, pp. 696–706, Aug. 2022, doi: 10.1016/j.tcb.2022.02.005.

[134] M. Pizzinga *et al.*, "Translation factor mRNA granules direct protein synthetic capacity to regions of polarized growth," *J. Cell Biol.*, vol. 218, no. 5, pp. 1564–1581, May 2019, doi: 10.1083/jcb.201704019.

[135] X. Chen and C. Mayr, "A working model for condensate RNA-binding proteins as matchmakers for protein complex assembly," *RNA*, vol. 28, no. 1, pp. 76–87, Jan. 2022, doi: 10.1261/rna.078995.121.

[136] M. Seidel *et al.*, "Co-translational assembly orchestrates competing biogenesis pathways," *Nat. Commun.*, vol. 13, no. 1, p. 1224, Mar. 2022, doi: 10.1038/s41467-022-28878-5.

[137] M. M. Masse *et al.*, "Nascent chains derived from a foldable protein sequence interact with specific ribosomal surface sites near the exit tunnel," *Sci. Rep.*, vol. 14, no. 1, p. 12324, May 2024, doi: 10.1038/s41598-024-61274-1.

[138] H. Zhang, C. Zhou, Z. Mohammad, and J. Zhao, "Structural basis of human 20S proteasome biogenesis," *Nat. Commun.*, vol. 15, no. 1, p. 8184, Sept. 2024, doi: 10.1038/s41467-024-52513-0.

[139] A. Shiber *et al.*, "Cotranslational assembly of protein complexes in eukaryotes revealed by ribosome profiling," *Nature*, vol. 561, no. 7722, pp. 268–272, Sept. 2018, doi: 10.1038/s41586-018-0462-y.

[140] Y. Yagita, E. Zavodszky, S.-Y. Peak-Chew, and R. S. Hegde, "Mechanism of orphan subunit recognition during assembly quality control," *Cell*, vol. 186, no. 16, pp. 3443-3459.e24, Aug. 2023, doi: 10.1016/j.cell.2023.06.016.

[141] K. Yanagitani, S. Juszkiewicz, and R. S. Hegde, "UBE2O is a quality control factor for orphans of multiprotein complexes," *Science*, vol. 357, no. 6350, pp. 472–475, Aug. 2017, doi: 10.1126/science.aan0178.

[142] M.-K. Sung *et al.*, "A conserved quality-control pathway that mediates degradation of unassembled ribosomal proteins," *eLife*, vol. 5, p. e19105, Aug. 2016, doi: 10.7554/eLife.19105.

[143] S. Carrillo Roas *et al.*, "Convergence of orphan quality control pathways at a ubiquitin chain-elongating ligase," *Mol. Cell*, vol. 85, no. 4, pp. 815-828.e10, Feb. 2025, doi: 10.1016/j.molcel.2025.01.002.

[144] D. B. Grabarczyk *et al.*, “HUWE1 employs a giant substrate-binding ring to feed and regulate its HECT E3 domain,” *Nat. Chem. Biol.*, vol. 17, no. 10, pp. 1084–1092, Oct. 2021, doi: 10.1038/s41589-021-00831-5.

[145] Y. Weyer *et al.*, “The Dsc ubiquitin ligase complex identifies transmembrane degrons to degrade orphaned proteins at the Golgi,” *Nat. Commun.*, vol. 15, no. 1, p. 9257, Oct. 2024, doi: 10.1038/s41467-024-53676-6.

[146] S. Mueller *et al.*, “Protein degradation corrects for imbalanced subunit stoichiometry in OST complex assembly,” *Mol. Biol. Cell*, vol. 26, no. 14, pp. 2596–2608, July 2015, doi: 10.1091/mbc.E15-03-0168.

[147] L. Long *et al.*, “CRISPR screens unveil signal hubs for nutrient licensing of T cell immunity,” *Nature*, vol. 600, no. 7888, pp. 308–313, Dec. 2021, doi: 10.1038/s41586-021-04109-7.

[148] L. A. Hehl *et al.*, “Structural snapshots along K48-linked ubiquitin chain formation by the HECT E3 UBR5,” *Nat. Chem. Biol.*, vol. 20, no. 2, pp. 190–200, Feb. 2024, doi: 10.1038/s41589-023-01414-2.

[149] P. Youkharibache, S. Veretnik, Q. Li, K. A. Stanek, C. Mura, and P. E. Bourne, “The Small β-Barrel Domain: A Survey-Based Structural Analysis,” *Structure*, vol. 27, no. 1, pp. 6–26, Jan. 2019, doi: 10.1016/j.str.2018.09.012.

[150] S. Zhang, L. F. Valenzuela, E. Zatulovskiy, L. Mangiante, C. Curtis, and J. M. Skotheim, “The G1-S transition is promoted by Rb degradation via the E3 ligase UBR5,” *Sci. Adv.*, 2024.

[151] L. Cipolla *et al.*, “UBR5 interacts with the replication fork and protects DNA replication from DNA polymerase η toxicity,” *Nucleic Acids Res.*, vol. 47, no. 21, pp. 11268–11283, Dec. 2019, doi: 10.1093/nar/gkz824.

[152] S. Kaisari *et al.*, "Role of ubiquitin-protein ligase UBR5 in the disassembly of mitotic checkpoint complexes," *Proc. Natl. Acad. Sci.*, vol. 119, no. 9, p. e2121478119, Mar. 2022, doi: 10.1073/pnas.2121478119.

[153] K. G. Mark *et al.*, "Orphan quality control shapes network dynamics and gene expression," *Cell*, vol. 186, no. 16, pp. 3460-3475.e23, Aug. 2023, doi: 10.1016/j.cell.2023.06.015.

[154] L. Schukur *et al.*, "Identification of the HECT E3 ligase UBR5 as a regulator of MYC degradation using a CRISPR/Cas9 screen," *Sci. Rep.*, vol. 10, no. 1, p. 20044, Nov. 2020, doi: 10.1038/s41598-020-76960-z.

[155] J. M. Tsai *et al.*, "UBR5 forms ligand-dependent complexes on chromatin to regulate nuclear hormone receptor stability," *Mol. Cell*, vol. 83, no. 15, pp. 2753-2767.e10, Aug. 2023, doi: 10.1016/j.molcel.2023.06.028.

[156] A. de Vivo, A. Sanchez, J. Yegres, J. Kim, S. Emly, and Y. Kee, "The OTUD5–UBR5 complex regulates FACT-mediated transcription at damaged chromatin," *Nucleic Acids Res.*, vol. 47, no. 2, pp. 729–746, Jan. 2019, doi: 10.1093/nar/gky1219.

[157] Z. Xie *et al.*, "Significance of the E3 ubiquitin protein UBR5 as an oncogene and a prognostic biomarker in colorectal cancer," *Oncotarget*, vol. 8, no. 64, pp. 108079–108092, Dec. 2017, doi: 10.18632/oncotarget.22531.

[158] M. Song *et al.*, "Tumor derived UBR5 promotes ovarian cancer growth and metastasis through inducing immunosuppressive macrophages," *Nat. Commun.*, vol. 11, no. 1, p. 6298, Dec. 2020, doi: 10.1038/s41467-020-20140-0.

[159] J. Li *et al.*, "E3 Ubiquitin Ligase UBR5 Promotes the Metastasis of Pancreatic Cancer via Destabilizing F-Actin Capping Protein CAPZA1," *Front. Oncol.*, vol. 11, p. 634167, Mar. 2021, doi: 10.3389/fonc.2021.634167.

[160] S. A. Swenson *et al.*, "UBR5 HECT domain mutations identified in mantle cell lymphoma control maturation of B cells," *Blood*, vol. 136, no. 3, pp. 299–312, July 2020, doi: 10.1182/blood.2019002102.

[161] N. Bansal *et al.*, "Tumor Suppressor Protein p53 Recruits Human Sin3B/HDAC1 Complex for Down-Regulation of Its Target Promoters in Response to Genotoxic Stress," *PLoS ONE*, vol. 6, no. 10, p. e26156, Oct. 2011, doi: 10.1371/journal.pone.0026156.

[162] Y. Xu *et al.*, "Architecture of the RNA polymerase II-Paf1C-TFIIS transcription elongation complex," *Nat. Commun.*, vol. 8, no. 1, p. 15741, June 2017, doi: 10.1038/ncomms15741.

[163] Y. Aoi *et al.*, "SPT5 stabilization of promoter-proximal RNA polymerase II," *Mol. Cell*, vol. 81, no. 21, pp. 4413-4424.e5, Nov. 2021, doi: 10.1016/j.molcel.2021.08.006.

[164] S. Ling and W.-C. Lin, "EDD Inhibits ATM-mediated Phosphorylation of p53," *J. Biol. Chem.*, vol. 286, no. 17, pp. 14972–14982, Apr. 2011, doi: 10.1074/jbc.M110.182527.

[165] S. Sur *et al.*, "A panel of isogenic human cancer cells suggests a therapeutic approach for cancers with inactivated p53," *Proc. Natl. Acad. Sci.*, vol. 106, no. 10, pp. 3964–3969, Mar. 2009, doi: 10.1073/pnas.0813333106.

[166] D. S. Laman Trip *et al.*, "A tissue-specific atlas of protein–protein associations enables prioritization of candidate disease genes," *Nat. Biotechnol.*, May 2025, doi: 10.1038/s41587-025-02659-z.

[167] I. De *et al.*, "The RNA helicase Aquarius exhibits structural adaptations mediating its recruitment to spliceosomes," *Nat. Struct. Mol. Biol.*, vol. 22, no. 2, pp. 138–144, Feb. 2015, doi: 10.1038/nsmb.2951.

[168] M. Zhang, J. M. Berk, A. B. Mehrtash, J. Kanyo, and M. Hochstrasser, "A versatile new tool derived from a bacterial deubiquitylase to detect and purify ubiquitylated

substrates and their interacting proteins," *PLOS Biol.*, vol. 20, no. 6, p. e3001501, June 2022, doi: 10.1371/journal.pbio.3001501.

[169] L. Comai, J. E. Katz, and P. Mallick, Eds., *Proteomics: Methods and Protocols*, vol. 1550. in Methods in Molecular Biology, vol. 1550. New York, NY: Springer New York, 2017. doi: 10.1007/978-1-4939-6747-6.

[170] J. Li *et al.*, "TMTpro reagents: a set of isobaric labeling mass tags enables simultaneous proteome-wide measurements across 16 samples," *Nat. Methods*, vol. 17, no. 4, pp. 399–404, Apr. 2020, doi: 10.1038/s41592-020-0781-4.

[171] S. A. Wagner *et al.*, "A Proteome-wide, Quantitative Survey of In Vivo Ubiquitylation Sites Reveals Widespread Regulatory Roles," *Mol. Cell. Proteomics*, vol. 10, no. 10, p. M111.013284, Oct. 2011, doi: 10.1074/mcp.M111.013284.

[172] J. Cox and M. Mann, "MaxQuant enables high peptide identification rates, individualized p.p.b.-range mass accuracies and proteome-wide protein quantification," *Nat. Biotechnol.*, vol. 26, no. 12, pp. 1367–1372, Dec. 2008, doi: 10.1038/nbt.1511.

[173] J. Cox, N. Neuhauser, A. Michalski, R. A. Scheltema, J. V. Olsen, and M. Mann, "Andromeda: A Peptide Search Engine Integrated into the MaxQuant Environment," *J. Proteome Res.*, vol. 10, no. 4, pp. 1794–1805, Apr. 2011, doi: 10.1021/pr101065j.

[174] A. T. Kong, F. V. Leprevost, D. M. Avtonomov, D. Mellacheruvu, and A. I. Nesvizhskii, "MSFragger: ultrafast and comprehensive peptide identification in mass spectrometry–based proteomics," *Nat. Methods*, vol. 14, no. 5, pp. 513–520, May 2017, doi: 10.1038/nmeth.4256.

[175] V. Demichev, C. B. Messner, S. I. Vernardis, K. S. Lilley, and M. Ralser, "DIA-NN: neural networks and interference correction enable deep proteome coverage in high throughput," *Nat. Methods*, vol. 17, no. 1, pp. 41–44, Jan. 2020, doi: 10.1038/s41592-019-0638-x.

[176] M. E. Ritchie *et al.*, “limma powers differential expression analyses for RNA-sequencing and microarray studies,” *Nucleic Acids Res.*, vol. 43, no. 7, pp. e47–e47, Apr. 2015, doi: 10.1093/nar/gkv007.

[177] S. Xu *et al.*, “Using clusterProfiler to characterize multiomics data,” *Nat. Protoc.*, vol. 19, no. 11, pp. 3292–3320, Nov. 2024, doi: 10.1038/s41596-024-01020-z.

[178] J. Jumper *et al.*, “Highly accurate protein structure prediction with AlphaFold,” *Nature*, vol. 596, no. 7873, pp. 583–589, Aug. 2021, doi: 10.1038/s41586-021-03819-2.

[179] Y. Takei and T. Ishida, “How to select the best model from AlphaFold2 structures?,” Apr. 05, 2022, *Bioinformatics*. doi: 10.1101/2022.04.05.487218.

[180] K. M. Ruff and R. V. Pappu, “AlphaFold and Implications for Intrinsically Disordered Proteins,” *J. Mol. Biol.*, vol. 433, no. 20, p. 167208, Oct. 2021, doi: 10.1016/j.jmb.2021.167208.

[181] R. Evans *et al.*, “Protein complex prediction with AlphaFold-Multimer,” Oct. 04, 2021, *Bioinformatics*. doi: 10.1101/2021.10.04.463034.

Acknowledgments

Redacted for data protection reasons.

Curriculum vitae

Redacted for data protection reasons.